Combining Similarity Transformed Equation of Motion Coupled Cluster (STEOM-CC), Vibronic Coupling models, and Spin-Orbit Coupling: Towards a First Principle Description of Intersystem Crossing

by

John Sous

A thesis

presented to the University of Waterloo

in fulfillment of the

thesis requirement for the degree of

Master of Science

in

Chemistry

Waterloo, Ontario, Canada, 2013

Author's Declaration

I hereby declare that I am the sole author of this thesis (with the exception of Chapter 3). This is a true copy of the thesis, including any required final revisions, as accepted by my examiners.

I understand that my thesis may be made electronically available to the public.

Abstract

Electronic Structure Theory has led to a variety of developments and applications. In the Nooijen group the focus is on the development and use of Coupled Cluster based approaches. Coupled Cluster is a very strong and accurate approach to the quantum mechanical problem. The research results presented in the thesis testify to the Similarity Transformed Equation of Motion Coupled Cluster (STEOM-CC) for being a very accurate and yet computationally inexpensive approach for excited states. This study reveals new features about STEOM and provides promise regarding future improvement in the methodology. STEOM can be used as the first step in the construction of the Vibronic model, which is a strong tool to move to paradigms beyond the Born-Oppenheimer approximation. Spin-Orbit Coupling (SOC) is a very important ingredient required to study relativistic phenomena and its quantum mechanical implementation for many body systems is not straightforward. The most widely used SOC operator in Chemical Physics is the Breit-Pauli operator, which requires employing non-trivial approximations to the Dirac equation to adapt the theory to many body systems. The integration of electronic structure approaches, Vibronic Coupling, and SOC is essential to study the phenomenon of intersystem crossing (transition between spin states) in fine detail. In this thesis a computational benchmark of STEOM is discussed, while the frameworks of Vibronic Coupling and Spin-Orbit Coupling (SOC) are considered on a theoretical level.

Acknowledgments

I would like to thank all the people who made this work possible. In particular, I am grateful to Professor Marcel Nooijen for being my academic advisor and mentor during the time I spent in Waterloo. Professor Nooijen offered me a unique opportunity to move to the field of Chemical Physics and supported my admission to the graduate program despite of all the obstacles and hurdles pertaining to not having an undergraduate education in Chemical Physics.

Professor Nooijen invested many hours mentoring me. I cannot enumerate the number of hours (probably in the order of hundreds), we spent discussing Quantum Mechanics and other interesting topics. I will always come to his office with a pile of questions and we will discuss for few hours. This happened almost every day.

I am also grateful to Professor Nooijen's approach to research. At several instances during my studies, Marcel would not respond to my questions, suggesting that I should 'toil with the problem' for a while until I figure it out. I came to appreciate this mentality as I bore its fruit.

I would like to acknowledge other members of the theory group for providing a stimulating environment for research and discussion. In particular, I would like to thank Professor Pierre-Nicholas Roy, Professor Robert LeRoy, Professor Frederick McCourt, Dr. Toby Zeng, Professor Scott Hopkins and Professor Mikko Karttunen. I am also thankful to Dr. Grégoire Guillon for the time we spent discussing interesting problems in Chemical physics as well as advanced Linear Algebra of Hilbert Spaces.

Table of Contents

Glossary

Abbreviations

CC-related abbreviations:

CC **C**oupled **C**luster: Exponential ansatz solution to the Schrödinger equation: $e^{\hat{T}}\Phi_0$, associated with the transformed Hamiltonian $\overline{H} = e^{-\hat{T}}\hat{H}e^{\hat{T}}$.

CCSD **C**oupled **C**luster **S**ingles and **D**oubles: CC approach including single and double excitations in the CC operator $\hat{T}$.

CCD **C**oupled **C**luster **D**oubles: CC approach including double excitations in the CC operator $\hat{T}$.

CCSDT **C**oupled **C**luster **S**ingles **D**oubles and **T**riples: CC approach including single, double, and triple excitations in the CC operator $\hat{T}$.

CCSD(T) A CC approach that includes single and double excitations with a perturbative triple correction in the CC operator $\hat{T}$.

CC-LRT **C**oupled **C**luster **L**inear **R**esponse **T**heory

CC2 A second order CC response approach including $e^{\hat{T}_1}$ completely.

CC3 An iterative triple correction to CCSD for both ground and excited states.

CC(*P*;*Q*) An approach that merges renormalized and active-space CC approaches to account for static and dynamic correlation.

FSCC **F**ock **S**pace **C**oupled **C**luster: An approach that is closely related to STEOM-CC.

CI-related abbreviations:

CI **C**onfiguration **I**nteraction: A scheme to diagonalize the Hamiltonian matrix over manifold of electronic states.

CIS **C**onfiguration **I**nteraction **S**ingles: refers to the inclusion of single excitations in the CI manifold.

CID **C**onfiguration **I**nteraction **D**oubles: refers to the inclusion of double excitations in the CI manifold.

CISD **C**onfiguration **I**nteraction **S**ingles and **D**oubles: refers to the inclusion of single and double excitations in the CI manifold.

Full CI **Full C**onfiguration **I**nteraction: CI approach over manifold of all possible electronic excitations.

MRCI **M**ulti**R**eference **C**onfiguration **I**nteraction: The reference function in CI consists of multiple configurations.

SAC-CI **S**ymmetry **A**dapted **C**luster **C**onfiguration **I**nteraction: similar to EOM-CC (refer to ***EOM-CC***).

EOM-CC-related abbreviations:

EOM-CC **E**quation **o**f **M**otion **C**oupled **C**luster: First one solves the CC equations (for $\hat{T}$), then diagonalizes the transformed Hamiltonian $\overline{H} = e^{-\hat{T}}\hat{H}e^{\hat{T}}$ to get other eigenstates.

EOM-CCSD **E**quation **o**f **M**otion **C**oupled **C**luster **S**ingles and **D**oubles: The EOM-CC approach applied to the CCSD cluster operator (refer to ***CCSD***).
EOM-CCSDT **E**quation **o**f **M**otion **C**oupled **C**luster **S**ingles **D**oubles and **T**riples: The EOM-CC approach applied to the CCSDT cluster operator (refer to ***CCSDT***).
EOM-CCSDT-3 **E**quation **o**f **M**otion **C**oupled **C**luster **S**ingles **D**oubles and **T**riples: An iterative inclusion of perturbative triples correction.
IP-EOM-CC **I**onization **P**otential **E**quation **o**f **M**otion **C**oupled **C**luster: The final diagonalization of $\overline{H}$ in EOM-CC is over states that have one less electron than the parent CC state.
EA-EOM-CC **E**lectron **A**ttached **E**quation **o**f **M**otion **C**oupled **C**luster: The final diagonalization of $\overline{H}$ in EOM-CC is over states that have one more electron than the parent CC state.
MR-EOM-CC **M**ulti**R**eference **E**quation **o**f **M**otion **C**oupled **C**luster: The EOM-CC approach to the electronic structure problem using a reference wave function composed of multiple determinants.

STEOM-related abbreviations:
STEOM-CC **S**imilarity **T**ransformed **E**quation **o**f **M**otion **C**oupled **C**luster: An approach to calculate excited states based on a doubly transformed Hamiltonian. Final diagonalization space consists of single excitations only.
DIP-STEOM-CC **D**ouble **I**onization **P**otential **S**imilarity **T**ransformed **E**quation **o**f **M**otion **C**oupled **C**luster: Final diagonalization is over states having two less electrons than the reference state.
DEA-STEOM-CC **D**ouble **E**lectron **A**ttachment **S**imilarity **T**ransformed **E**quation **o**f **M**otion **C**oupled **C**luster: Final diagonalization is over states having two more electrons than the reference state.
STEOM-PT The CCSD step in STEOM-CC is replaced by an MB**PT**(2) calculation (see ***MBPT(2)***).
STEOM-H (ω) The final transformed Hamiltonian is symmetrized or **h**ermitized.
EXT-STEOM **E**xtended **S**imilarity **T**ransformed **E**quation **o**f **M**otion **C**oupled **C**luster: Diagonalize double-transformed STEOM Hamiltonian over singles and doubles; can describe doubly excited states.
STEOM-D A perturbative **d**oubles correction on top of STEOM.
STEOM-ORB A STEOM approach to optimize the active **orb**itals such that they span a space that captures the majority of the excitation character.

Miscellaneous abbreviations:
AMFI **A**tomic **M**ean-**F**ield **I**ntegral method: An approximate mean-field atom-based treatment of spin-orbit operators.
AO **A**tomic **O**rbital: AOs are atom-centered orbitals employed as one-electron basis functions.
CAS-SCF **C**omplete **A**ctive **S**pace **S**elf-**C**onsistent **F**ield: Full CI in a small set of active orbitals followed by orbital optimization.
CASPT2 **C**omplete **A**ctive **S**pace second order **P**erturbation **T**heory: A second order perturbation theory on top of CAS-SCF.

DFT **D**ensity **F**unctional **T**heory: A semi-empirical solution to the Schrödinger equation that typically includes optimizing an energy functional of molecular orbitals.
TDDFT **T**ime **D**ependent **D**ensity **F**unctional **T**heory: Time-dependent DFT response approach to calculate exited states using DFT.
FMS **F**ull **M**ultiple **S**pawning: Gaussian wave packet approach to non-adiabatic nuclear dynamics.
HF **H**artree-**F**ock: An approximation to the Schrödinger equation that yields a minimum energy single determinant wave function.
ISC **I**nter**S**ystem **C**rossing: A term that refers to population transfer between electronic states of different spin multiplicity, mediated by spin-orbit coupling and nuclear dynamics.
MBPT **M**any **B**ody **P**erturbation **T**heory: A perturbative expansion based on linked cluster theorem.
MBPT(2) **M**any **B**ody second order **P**erturbation **T**heory: MBPT to second order.
NEVPT2 **N**-**E**lectron **V**alence second order **P**erturbation **T**heory: A variant of the second order multireference perturbation theory (Compare ***CASPT2***).
OSV **O**rbital-**S**pecific **V**irtual approximation: Associates a compact set of correlating virtual orbitals with each occupied orbital; used in local correlation.
PNO **P**air **N**atural **O**rbital: Associates a compact set of correlating virtual orbitals with each *pair* of occupied orbital; used in local correlation.
SCF **S**elf-**C**onsistent **F**ield
SO **S**pin-**O**rbit: Shorthand to Spin-Orbit, usually used in the context of the Spin-Orbit Breit-Pauli operator.
SOC **S**pin-**O**rbit **C**oupling: The relativistic effect that couples orbital angular momentum to spin angular momentum.
TDH **T**ime-**D**ependent **H**artree: An approach to nuclear dynamics employing a single product of one-dimensional functions (Hartree product).
MCTDH **M**ulti**C**onfigurational **T**ime-Dependent **H**artree: An approach to non-adiabatic nuclear dynamics employing multiple Hartree products (see ***TDH***).

Terms

Adiabatic states: Electronic states that satisfy the electronic Schrödinger Equation at each nuclear geometry.
Diabatic states: Linear combination of adiabatic states such that the diabatic states change little with nuclear geometry (not unique).
Derivative coupling: Contributions to the nuclear kinetic energy operator, which couple different electronic states. It is small in the diabatic basis.
Non-adiabatic dynamics: describes coupled electronic and nuclear motion. Population transfer occurs through kinetic energy elements in the adiabatic basis, through off-diagonal potential energy elements in the diabatic basis.
Configuration: Spin- and symmetry-adapted combination of Slater determinants, corresponding to single set of 'spatial' orbitals.

Orbital: One electron function, typically linear combination of atom-centered basis function (AOs).
Slater determinant: An anti-symmetrical product of one-electron functions.

Chapter 1

Introduction

One might arguably describe this era as being one of great scientific blossom. The fact is that we are witnessing scientific development in numerous fields, ranging from better understanding of physical reality to the implementation of advanced technology that makes what used to be intractable and even impossible possible. It is the discovery of Quantum Mechanics [1] almost a century ago that changed our world, in my opinion. Quantum Mechanics provided a very deep understanding of the physics of microscopic systems. As Quantum Mechanics matured, more applications became into fruition, from developments in Particle Physics and Cosmology to new discoveries in Condensed Matter Physics, Atomic and Molecular Physics and Chemical Physics. We witnessed major events like the discovery of laser [2] and transistors [3], we understood bizarre phenomena like superfluidity [4, 5] and superconductivity [6], and we managed not only to understand complex chemical reactions, but also manipulate them. This latter statement relating to chemistry is the subject of the field of Chemical Physics, which attempts to explain chemistry better and influence its evolution in unforeseen ways. Chemical Physics is a very rich field that encompasses both theory and experiment. It has many different theoretical applications ranging from modeling chemical reactions and dynamics of complex reactions to investigating the electronic structure of atoms and molecules and simulating spectroscopy of interesting systems. It also has numerous experimental applications, for example some experimentalists are concerned with the behavior of atoms in the cold and ultra cold regime. A famous experiment is to cool

atoms and allow them to fall under gravity acceleration and observe their behavior. It is also worth mentioning that, about twenty years ago, experimentalists were successful in attaining the first Bose-Einstein condensate.

The collaboration of theorists with experimentalists is one of the reasons behind the development of science and in our case Chemical Physics. Experimentalists provide theorists with experimental *data* about physical systems and chemical reactions, while theorists aim to suggest possible *interpretations* pertaining to the meaning of the experimental data provided by experimentalists. Theorists go further and propose theoretical models that can provide qualitative *rationalization* to the phenomenon under study. The insight gained is picked up by experimentalists to design new experiments and approach similar problems in different ways.

The contribution goes the other way as well, as in some cases theorists propose experiments that can provide insight and in other cases they go far attempting to provide theoretical and foundational reasons as to why some experiments do not make sense. Computational scientists represent another group, situated on the interface between theory and experiment. Computational science aims to apply theories to reproduce experimental results by means of numerical *calculations*. This way the circle is complete.

In the Nooijen group, our interest in Chemical Physics relates more to *Electronic Structure Theory* and methodology as well as to the development of accurate models to incorporate nuclear dynamics to simulate spectroscopy. Our target is to develop very accurate models based on accurate Electronic Structure Theory including relativistic

effects, and treating nuclear dynamics beyond the Born-Oppenheimer approximation. Our ultimate goal is to reproduce experiment.

The focus of my work is mainly on Electronic Structure Theory, in particular a research contribution regarding the Similarity Transformed Equation of Motion Coupled Cluster (STEOM-CC) is presented in this thesis. The beautiful STEOM-CC has the ability to provide an accurate and efficient description of excited states. It is this analysis of excited states that comprises the first step in the construction of models that go beyond the Born-Oppenheimer approximation, one of which is the Vibronic model developed in the Nooijen group. Incorporating Spin-Orbit Coupling (SOC) effects allow for the accurate modeling of forbidden transitions and Intersystem Crossings (ISC) normally not described with the non-relativistic Born-Oppenheimer approximation.

In this thesis, I survey the above topics that are of interest in the Nooijen group. I start in chapter 2 by an introduction to Coupled Cluster theory, which is the theory we use to study electronic structure. I then proceed to present my research contribution in the group in chapter 3, which is a study that testifies to the success of STEOM-CC for capturing excited states. In chapter 4 I review the theory behind the construction of the Vibronic model, which allows the study of nuclear dynamics beyond the Born-Oppenheimer approximation. Then, I review the theory underlying the implementation of SOC for chemical physics and quantum chemistry applications in chapter 5. Chapters 4 and 5 are concerned with ingredients that are needed to describe Intersystem Crossing (ISC) and include a concise summary of the relevant literature. I conclude by a section I name “The

Full Picture", which connects the different chapters and provides a global picture to the research concerning simulating ISC and spin-forbidden transitions.

Chapter 2

Introduction to Coupled Cluster Theory

I. Introduction

The last 60 years have witnessed a vast development in the field of Electronic Structure Theory. Electronic structure theory provides a base for a wealth of applications in Chemistry and Physics, for example in spectroscopy. Two major theories represent the forefront in research in the field: Coupled Cluster (CC) theory [1-4] and Density Functional Theory (DFT) [5, 6]. CC theory has a reputation for being a physical theory. It is an ab initio method, rooted in Quantum Mechanics. From a reductionist's point of view, this method is capable of providing physical insight. Unlike DFT methods [7], CC is a definite theory in the sense that it provides approximate yet systematically improvable solutions to the Schrödinger equation and does not include optimizing a semi-empirical functional.

Initially, the quantum chemistry community was slow to accept CC theory, probably because the earliest researchers in the field used elegant but unfamiliar mathematical tools such as Feynman-like diagrams and second quantization to derive working equations. It took around 10 years before Hurley [8] re-derived the equations in terms, which are more familiar to quantum chemists. By the end of 1970s, computer implementations of the theory for realistic systems began to appear in the groups of Pople [9] and Bartlett [10]. Since then, CC became very popular among quantum chemists.

In this chapter, we aim to introduce the basics of CC theory. We follow to a great extent the theoretical development as presented by Isaiah Shavitt and Rodney J. Bartlett in their book "Many-Body Methods in Chemistry and Physics: MBPT and Coupled-Cluster Theory" [2].

We start by explaining the foundations of the CC approach. We then proceed to discuss the Equation of Motion Coupled Cluster (EOM-CC) approach, which has the power to describe excited, ionized, and electron-attached states.

II. The Physical Basis of CC Theory

In this section, we present an intuitive idea about CC theory without using elegant and detailed mathematics. Let us start by considering a two-electron system, for which the exact wave function can be written as a linear combination of a *reference* function ϕ_0 and all double excitations relative to it [11]. The orbitals are obtained by transforming the orbitals in such a way to diagonalize the one particle density matrix of the correlated wave function (Configuration Interaction (CI) wave function). The unnormalized wave function can be written as

$$\psi = \phi_0 + c\chi \tag{2.1}$$

where ϕ_0 and χ are the orthonormal two-electron functions for each atom and c is a coefficient. We suppress electronic coordinate in the above equation. More generally for a system with more than two electrons in Hartree-Fock (HF) orbitals, the contribution of single excitations tends to be very small [2].

Let us consider a system of N non-interacting He atoms, with Hamiltonian

$$\hat{H} = \sum_{i=1}^{N} \hat{h}(i) \tag{2.2}$$

It follows that for the N non-interacting He atoms, one writes

$$\Phi_0 = \mathcal{A}\phi_0(1)\phi_0(2) \dots \phi_0(N) \tag{2.3}$$

where the arguments 1, 2, …, N label the atoms. Again the electronic coordinates are suppressed. $\mathcal{A}$ is the antisymmetrizer, which acts by exchanging electrons between different two-electron factors ϕ_0. Due to lack of interaction, it can be ignored. The double-excitation functions are of the form

$$\Phi_i = \mathcal{A}\phi_0(1)\phi_0(2) \dots \phi_0(i-1)\chi(i)\phi_0(i+1) \dots \phi_0(N) \tag{2.4}$$

$\chi(i)$ is the basis function for the ith double excitation relative to ϕ_0 There is no need to consider mixed double excitations, or single excitations, because of the lack of interaction among the atoms and between ϕ_0 and any single excitation from it. The CI Doubles (CID) wave function reads

$$\Psi_{\text{CID}} = \Phi_0 + \sum_{i=1}^{N} C_i \Phi_i \tag{2.5}$$

Following Shavitt and Bartlett [2], we define a single-atom two-electron excitation operator $\hat{t}_i$ for the ith atom in the space spanned by $\{\phi_0(i),\ \chi(i)\}$ by

$$\hat{t}_i\phi_0(i) = \tau\chi(i), \qquad \hat{t}_i\,\chi(i) = 0 \tag{2.6}$$

where τ is a constant to be determined. The $\hat{t}_i$ operator has no effect on the basis functions for the other atoms:

$$\hat{t}_i\phi_0(j) = \phi_0(j), \quad \hat{t}_i\chi(j) = \chi(j) \qquad i \neq j \tag{2.7}$$

In bra-ket notation, the operator can be represented as

$$\hat{t}_i = |\chi(i)\rangle\langle\phi_0(i)| + \sum_{j\neq i} \hat{1}_j \tag{2.8}$$

Note that $\phi_0(i)$ and $\chi(i)$ are the orthonormal two-electron functions for each atom. Since atoms are non-interacting, the functions on one atom are orthogonal to those on any other atom.

For the N-atom wave function we define the operator

$$\hat{T}_2 = \sum_i \hat{t}_i \tag{2.9}$$

The subscript 2 on $\hat{T}_2$ indicates that it is a sum of operators that excite two electrons at a time.

Let us compute the effect of different powers of $\hat{T}_2$ on Φ_0 and Φ_i:

$$\begin{aligned}
\hat{T}_2\Phi_0 &= \sum_i \hat{t}_i\,\Phi_0 = \tau \sum_i \Phi_i \\
\hat{T}_2\Phi_i &= \sum_j \hat{t}_j\,\Phi_i = \tau \sum_{j\,(j\neq i)} \Phi_{ij} = \tau \sum_{ij} \Phi_{ij} \qquad (\Phi_{ii} = 0) \\
\hat{T}_2{}^2\Phi_0 &= \tau \sum_i \hat{T}_2\Phi_i = \tau^2 \sum_{ij} \Phi_{ij} \\
\hat{T}_2{}^3\Phi_0 &= \tau^2 \sum_{ij} \hat{T}_2\Phi_{ij} = \tau^3 \sum_{ijk} \Phi_{ijk}\,, \quad \text{etc.}
\end{aligned} \tag{2.10}$$

It turns out that the exact solution (full CI) for the N non-interacting He atoms [2] is

$$\Psi = \Phi_0 + \sum_i \tau\Phi_i + \frac{1}{2!}\sum_{ij} \tau^2\Phi_{ij} + \frac{1}{3!}\sum_{ijk} \tau^3\Phi_{ijk} + \cdots \tag{2.11}$$

which is the same as

$$\Psi = \Phi_0 + \hat{T}_2\Phi_0 + \frac{1}{2!}\hat{T}_2{}^2\Phi_0 + \frac{1}{3!}\hat{T}_2{}^3\Phi_0 + \cdots = e^{\hat{T}_2}\Phi_0 \qquad (2.12)$$

The $\frac{1}{n!}$ is to prevent over-counting. It can be shown that the CC solution is equivalent to the full-CI solution. The details of the full CI solution are left out for brevity and it suffices to layout the result for our purposes. For details refer to reference [2].

We note that the exponential Ansatz $\Psi = e^{\hat{T}_2}\Phi_0$, which is the basis for the formulation of CC theory, automatically accounts for correct relationship between the coefficients τ, τ^2, … of the various excitation levels.

To obtain equations for τ and the corresponding energy E we project the Schrödinger equation onto $\langle\Phi_i|$:

$$\begin{aligned} \langle\Phi_0|\big(\hat{H} - E\big)e^{\hat{T}_2}|\Phi_0\rangle &= 0 \\ \langle\Phi_i|\big(\hat{H} - E\big)e^{\hat{T}_2}|\Phi_0\rangle &= 0 \end{aligned} \qquad (2.13)$$

and solve for τ and E.

The above analysis shows that one double-excitation operator suffices to describe an arbitrary number of non-interacting two-electron systems. The exponential ansatz is crucial to the approach.

III. CC in Second Quantization

In this section, we aim to provide a rigorous mathematical description of CC theory. We start by reviewing the notions of second quantization, which is the tool to mathematically account for the theory. We associate a creation operator denoted with a dagger (†) with each orbital, for example $\hat{a}^\dagger$ with φ_a, and also an annihilation operator with each orbital, for example $\hat{\imath}$ with φ_i. In our notation, a and b label virtual orbitals, while i and j label occupied orbitals. Let us demonstrate the action of creation and annihilation operators respectively on a reference wave function $|\Phi_0\rangle$

$$\begin{aligned} \hat{a}^\dagger|\Phi_0\rangle = \hat{a}^\dagger|\varphi_i \dots \varphi_l\rangle = |\varphi_a\varphi_i \dots \varphi_l\rangle = |\Phi^a\rangle \\ \hat{\imath}|\Phi_0\rangle = \hat{\imath}|\varphi_i \dots \varphi_l\rangle = |\varphi_j \dots \varphi_l\rangle = |\Phi_i\rangle \end{aligned} \tag{2.14}$$

The creation operator $\hat{a}^\dagger$ creates an electron in orbital φ_a, while the annihilation operator $\hat{\imath}$ annihilates an electron from orbital φ_i.

If we act with two consecutive creation operators in different order:

$$\begin{aligned} \hat{a}^\dagger\hat{b}^\dagger|\Phi_0\rangle = \hat{a}^\dagger\hat{b}^\dagger|\varphi_i \dots \varphi_l\rangle = |\varphi_a\varphi_b\varphi_i \dots \varphi_l\rangle = |\Phi^{ab}\rangle \\ \hat{b}^\dagger\hat{a}^\dagger|\Phi_0\rangle = \hat{b}^\dagger\hat{a}^\dagger|\varphi_i \dots \varphi_l\rangle = |\varphi_b\varphi_a\varphi_i \dots \varphi_l\rangle \\ = -|\varphi_a\varphi_b\varphi_i \dots \varphi_l\rangle = -|\Phi^{ab}\rangle = |\Phi^{ba}\rangle, \end{aligned} \tag{2.15}$$

we derive the anticommutation relations for creation operators: $\{\hat{a}^\dagger, \hat{b}^\dagger\} = 0$. Note the minus sign satisfies the Pauli principle for fermions.

Using similar procedures (omitted for briefness), one can derive the following anitcommution relations: $\{\hat{\imath}, \hat{\jmath}\} = 0$ and $\{\hat{\imath}, \hat{a}^\dagger\} = \delta_{ia}$. For more details the reader is referred to reference [11].

In the context of CC we define single and double excitations respectively in the following way:

$$|\Phi_i^a\rangle = \hat{a}^\dagger \hat{\imath}|\Phi_0\rangle$$
$$\left|\Phi_{ij}^{ab}\right\rangle = \hat{a}^\dagger \hat{b}^\dagger \hat{\jmath}\hat{\imath}|\Phi_0\rangle \tag{2.16}$$

where the reference wave function $|\Phi_0\rangle$ in this context is the HF wave function.

Now one can consider the structure of the double excitation operator $\hat{T}_2$ in second quantization:

$$\hat{T}_2 \equiv \sum_{\substack{i<j \\ a<b}} t_{ij}^{ab} \hat{a}^\dagger \hat{b}^\dagger \hat{\jmath}\,\hat{\imath} \tag{2.17}$$

Note that this $\hat{T}_2$ operator is different from the one mentioned in section II. Up to this point we were considering operators of the type of $\hat{T}_2$, which excites two electrons at a time. To be complete the cluster operator should be written as

$$\hat{T} = \hat{T}_1 + \hat{T}_2 + \hat{T}_3 + \cdots \tag{2.18}$$

with the coupled-cluster wave function in the form

$$\Psi = e^{\hat{T}}\Phi_0 \tag{2.19}$$

Taking the Taylor series of $e^{\hat{T}}$ and expanding $\hat{T}$ in terms of one-body ($\hat{T}_1$), two-body ($\hat{T}_2$) cluster operators etc., one obtains

$$\begin{aligned}\Psi \;=\; & \Phi_0 + \hat{T}_1\Phi_0 + \hat{T}_2\Phi_0 + \cdots \\ & + \frac{1}{2}\hat{T}_1{}^2\Phi_0 + \hat{T}_1\hat{T}_2\Phi_0 + \frac{1}{2}\hat{T}_2{}^2\Phi_0 + \cdots \\ & + \frac{1}{3!}\hat{T}_1{}^3\Phi_0 + \frac{1}{2}\hat{T}_1{}^2\hat{T}_2\Phi_0 + \frac{1}{2}\hat{T}_1\hat{T}_2{}^2\Phi_0 + \frac{1}{3!}\hat{T}_2{}^3\Phi_0 + \cdots \\ & + \cdots\end{aligned} \tag{2.20}$$

If one chooses Φ_0 to be the Hartree-Fock wave function, the contribution of $\hat{T}_1\Phi_0$ is quite small as a result of the fact that $\langle \Phi_i^a | \hat{H} | \Phi_0 \rangle = 0$.

As a result and for other involved arguments [2], one can approximate the exponential cluster operator. The simplest CC approach is what is referred to as Coupled Cluster Doubles (CCD) [3]: $\hat{T}_{CCD} = \hat{T}_2$. An extension to this approach is Coupled Cluster Singles and Doubles (CCSD) [3]: $\hat{T}_{CCSD} = \hat{T}_1 + \hat{T}_2$. An excellent approximation is the Coupled Cluster Singles Doubles and Triples (CCSDT) [3]: $\hat{T}_{CCSDT} = \hat{T}_1 + \hat{T}_2 + \hat{T}_3$. A very good approach is the one developed by Ragavachari et al. [12] which is referred to as CCSD(T). CCSD(T) is a perturbative approximation to CCSDT, in which triples are obtained in a non-iterative fashion upon solving the CCSD equations.

We would like to point out the specific feature of the CC approach that it avoids having an eigenvalue problem and instead one has a set of simultaneous algebraic equations, which need to be solved iteratively.

CC also has a very important characteristic that makes it very interesting. Due to the nature of the (total) exponential operator, which can be written as the sum of cluster operators, one can write the CC wave function as a product of independent CC wave functions, each for a fragment of the molecule in study. As a result, the sum of the CC energies computed for each fragment is equal to the energy computed for the full molecule. This property is referred to as “size consistency” [4].

IV. Excited, Ionic and Electron-Attached States

The conventional CC approach is very effective for electronic states dominated by a single determinant, such as molecular ground states near their equilibrium geometry. Most excited, ionized and electron-attached states are open-shell states, which are not always dominated by single determinants.

This requires resorting to multireference methods, which do not make use of single determinant wave functions. Another possibility is the Equation of Motion Coupled Cluster (EOM-CC) method [13-16], which is based on the conventional single reference CC approach.

V. The EOM-CC Ansatz

In the EOM-CC method one considers the two Schrödinger-equation eigenstates simultaneously, an *initial state* Ψ_0 and a *target state* Ψ_k

$$\widehat{H}\Psi_0 = E_0\Psi_0, \qquad \widehat{H}\Psi_k = E_k\Psi_k \tag{2.21}$$

The initial state is usually an appropriately chosen closed-shell state, most commonly the ground state. The target state is an excited or ionic state. The goal of the method is to compute the energy difference

$$\omega_k = E_k - E_0 \tag{2.22}$$

and other properties of the target state. This is done by an efficient procedure that cancels common terms in the solutions for the two states before the actual calculation.

The initial-state coupled-cluster wave function and the target-state coupled-cluster wave function are defined as:

$$|\Psi_0\rangle = e^{\hat{T}}|0\rangle$$
$$|\Psi_k\rangle = \hat{R}_k|\Psi_0\rangle = \hat{R}_k e^{\hat{T}}|0\rangle \tag{2.23}$$

where $\hat{R}_k$ is the excitation operator.

Now the Schrödinger equation for the target state reads

$$\hat{H}\hat{R}_k e^{\hat{T}}|0\rangle = E_k \hat{R}_k e^{\hat{T}}|0\rangle. \tag{2.24}$$

Multiplying on the left with $e^{-\hat{T}}$ and using that $\hat{R}_k$ and $\hat{T}$ commute, we get

$$\overline{H}\hat{R}_k|0\rangle = E_k \hat{R}_k|0\rangle \tag{2.25}$$

with $\overline{H} = e^{-\hat{T}}\hat{H}e^{\hat{T}}$. This is a right eigenfunction equation.

Realizing that $\hat{R}_0 = \hat{1}$, this right eigenfunction equation for the initial state reads

$$\overline{H}|0\rangle = E_0|0\rangle \tag{2.26}$$

Multiplying this equation on the left by $\hat{R}_k$ and subtracting from the preceding one, we get

$$\left[\overline{H}, \hat{R}_k\right]|0\rangle = (E_k - E_0)\hat{R}_k|0\rangle = \omega_k \hat{R}_k|0\rangle \tag{2.27}$$

One projects this equation on the subspace of singles and doubles to get the EOM-CC equation. Using the iterative Davidson algorithm [17] one can solve this eigenvalue equation for $\hat{R}_k$ and ω_k. This technique avoids the explicit evaluation of the matrix and requires instead direct calculation of the matrix-vector product, using the current estimate of the solution vector, in each iteration.

VI. IP-EOM-CC and EA-EOM-CC

The EOM-CC formalism involves operators in second quantization. Formally the operators span a Fock space and hence are not restricted to a specific number of electrons. This is the reason why the EOM-CC approach can be used for processes involving changes in the number of electrons. EOM-CC can be used to calculate ionized states and electron-attached states. These methods are referred to as Ionization Potential Equation of Motion Coupled Cluster (IP-EOM-CC) and Electron Attachment Equation of Motion Coupled Cluster (EA-EOM-CC) respectively.

The $\hat{R}$ operator takes the form of an operator that reduces the number of electrons by one for ionization processes. In second quantization, $\hat{R}$ is

$$\hat{R} = \sum_{i} r_i \hat{\imath} + \sum_{b,\ j>i} r_{ji}^{b} \hat{b}^{\dagger} \hat{\jmath} \hat{\imath} + \sum_{b>c,\ j>k>i} r_{jki}^{bc} \hat{b}^{\dagger} \hat{\jmath} \hat{c}^{\dagger} \hat{k} \hat{\imath} + \cdots. \tag{2.28}$$

For electron attachment processes, the operator $\hat{R}$ takes the form of an operator that increases the number of electrons by one:

$$\hat{R} = \sum_{a} r^{a} \hat{a}^{\dagger} + \sum_{a>b,\ j} r_{j}^{ba} \hat{b}^{\dagger} \hat{\jmath} \hat{a}^{\dagger} + \sum_{a>b>c,\ j>i} r_{ji}^{bac} \hat{b}^{\dagger} \hat{\jmath} \hat{a}^{\dagger} \hat{\imath}\, \hat{c}^{\dagger} + \cdots. \tag{2.29}$$

The EOM-CC methodology is very powerful and is the basis for the Similarity Transformed Equation of Motion Coupled Cluster (STEOM-CC), which is described in the next chapter.

VII. The Essence

We conclude by emphasizing the strengths of the CC approach. The approach is a descendent of Quantum Mechanics and can give a very good description of the physics of the electronic structure for a specific system. For instance, one gains knowledge about the nature of the problem when studying whether a single reference or a multireference methodology can provide more accurate results. The other advantage is the computational power. The algorithms developed in the context of CC tend to make the problem computationally cheaper than employing the full CI or MultiReference CI (MRCI) approach. One might argue that CC approaches cannot compete with other methodologies when it comes to computational time. Namely, DFT tends to be much faster and widely applicable to larger systems. It suffices to state that in recent years, through the development of ideas (and computer implementations) in local correlation [18-24], explicit correlation approaches (for review see references [25-29]), and most recently the use of a compact set of virtual orbitals associated with each pair of (localized) occupied orbitals in the Pair Natural Orbital (PNO) approach [30-32] or the Orbital-Specific Virtual (OSV) approximation [33], CC calculations of much larger systems (100's of atoms) are routinely feasible. At the current progress in the field, it is not unrealistic to expect to have very accurate and yet computationally efficient CC approaches that can be applied to very large systems in the near future.

Chapter 3

Similarity Transformed Equation of Motion Coupled Cluster Theory Revisited: A Benchmark Study of Valence Excited States

J. Sous, P. Goel, and M. Nooijen

Department of Chemistry, University of Waterloo, Waterloo, Ontario, Canada N2L 3G1

The Similarity Transformed Equation of Motion Coupled Cluster (STEOM-CC) method is benchmarked against CC3 and EOM-CCSDT-3 for a large test set of valence excited states of organic molecules studied by Schreiber et al. [M. Schreiber, M.R. Silva-Junior, S.P. Sauer, and W. Thiel, J. Chem. Phys. **128**, 134110 (2008)]. STEOM-CC is found to behave quite satisfactorily and provides significant improvement over EOM-CCSD, CASPT2, and NEVPT2 for singlet excited states; lowering standard deviations of these methods by almost a factor of two. Triplet excited states are found to be described less accurately, however. Besides the parent version of STEOM-CC additional variations are considered. STEOM-D includes a perturbative correction from doubly excited determinants. The novel STEOM-H (ω) approach presents a sophisticated technique to render

the STEOM-CC transformed Hamiltonian hermitian. In STEOM-PT the expensive CCSD step is replaced by MBPT(2), while Extended STEOM (EXT-STEOM) provides access to doubly excited states. To study orbital invariance in STEOM, we investigate orbital rotation in the STEOM-ORB approach. Comparison of theses variations of STEOM for the large test set provides a comprehensive statistical basis to gauge the usefulness of these approaches.

I. Introduction

Coupled Cluster (CC) theory has been a very fruitful pursuit in electronic structure theory for many years now, see for example references [1-3]. It has long been recognized as a highly accurate, systematic and computationally attractive approach for accurate thermochemistry calculations of small molecules [4-6], using primarily the CC approach that includes single and double excitations with a connected perturbative correction for triples, known as CCSD(T) [7]. In recent years, through the development of ideas (and computer implementations) in local correlation [8-14], explicit correlation approaches (for review see references [15-19]), and most recently the use of a compact set of virtual orbitals associated with each pair of (localized) occupied orbitals in the Pair Natural Orbital (PNO) approach [20-22] or the Orbital-Specific Virtual (OSV) approximation [23], CC calculations of much larger systems (100's of atoms) are routinely feasible.

The coupled cluster treatment of excited states has also seen a systematic development using primarily the Equation of Motion Coupled Cluster (EOM-CC) [24-29], Coupled Cluster Linear Response Theory (CC-LRT) [30-32], and the Symmetry Adapted Cluster Configuration Interaction method (SAC-CI) [33, 34]. Also here, connected triple excitation effects, for example in CC3 [35] and EOM-CCSDT-3 [36] approaches, are important to gain sufficiently high accuracy [35-38]. The most commonly used methods include EOM-CCSD/ CCSD-LRT and SAC-CI. The most recent promising variation is the newly developed CC(P;Q) approach [39, 40], which is obtained by merging the renormalized [41] and active-space coupled cluster [42] methods. At present all

implementations of CC excited state methods (except CC2) are currently based on canonical orbitals, although much progress has been made in creating efficient parallel implementations for example in packages like NWCHEM [43] and ACES III [44]. Viable local versions of EOM-CC/ CCLRT are still under development. One of the issues that arise is that excited states (in particular of the charge-transfer type) are not readily localized, i.e. any singly excited state $\hat{a}^{\dagger}\hat{i}\left|0\right\rangle$ is in principle present, regardless of localization of the particle-hole pair. The use of excited state pair natural orbitals to limit the number of included excitations for a particular state is a possible entrance to the problem, even if one has to give up on the locality of such orbitals. Some work in the CC2 context [45, 46] has been pursued in this direction, but it is not obvious that such an approach will work as well as it does for ground states. Currently, canonical orbital based EOM-CC and CCLRT approaches are still the state of the art, and these methods are computationally demanding.

One of the authors has long advocated a somewhat different approach to excited states: the Similarity Transformed Equation of Motion Coupled Cluster (STEOM-CC) method [47-50]. This method was developed in the late 1990's and its design was strongly influenced by the work on Fock Space Coupled Cluster (FSCC) Theory [51-57], in particular by the beautiful paper by Leszek Stolarczyk and Henk Monkhorst on their version of Fock Space Coupled Cluster [58], which was based on the use of similarity transformations in second quantization (or Fock space). This idea is also referred to as the use of many-body similarity transformations. The idea behind the similarity transform is conceptually straightforward. In second quantization one can perform a sequence of

exponential similarity transformations, which we might somewhat schematically indicate as

$$\hat{G} = ...e^{-\hat{S}}e^{-\hat{T}}\hat{H}e^{\hat{T}}e^{\hat{S}}... \qquad (3.1)$$

One can then use the freedom in the choice of amplitudes in the operators $\hat{S},\hat{T}$ to equate second quantized elements of the transformed Hamiltonian $\hat{G}$ to zero, in particular those operators that promote electrons from occupied into virtual orbitals. A crucial concept that enters this construction is the concept of normal ordering which follows the rules of the generalized Wick theorem [59]: the definition / action of the second quantized operator depends on the ordering convention of the elementary creation and annihilation operators, or, on the precise definition of normal ordering. In the STEOM approach, as in single reference CC or EOM-CC, the normal order is defined with respect to a single determinant vacuum state. This is the easiest possibility. More than a decade ago Mukherjee and Kutzelnigg [60, 61] defined a generalization of the concept of normal ordering to the multireference situation (see also references [62, 63]), and this has led to a very rich set of developments (canonical transformation theory [64-66], antihermitian contracted Schrödinger equation [67, 68], internally contracted multireference coupled cluster [69, 70]). This generalization has also allowed the development of a promising multireference equation of motion coupled cluster theory [71, 72], which uses both the many-body transformation concept, and the generalized normal ordering. For an early paper that forecasts some of these developments we refer to ref. [73]. The advantage of the many-body similarity transform strategy is that the vanishing matrix elements in the second quantized operator can enter many Hilbert-space matrix elements $\left\langle \Phi_\lambda \middle| \hat{G} \middle| \Phi_\mu \right\rangle$ and this leads in general to an approximate block structure in the transformed Hamiltonian.

As a result the transformed Hamiltonian can be diagonalized over a compact subspace, while yielding accurate results. Another advantage is that the transformed Hamiltonian remains a connected operator under a broad range of conditions. Therefore any scaling or size-consistency issues are related to the final diagonalization procedure. In the context of local correlation these methods also have a clear built in localization criterion: all of the (connected) transformation operators are near-sighted: their amplitudes vanish (rapidly) when they involve distant localized orbitals. This locality is lacking in the final diagonalization, and this is the origin of non-locality in the EOM-CC approach. In the STEOM-CC approach the final diagonalization is over singly excited states only, and this can be pushed to quite large systems, even when lacking locality.

STEOM has a number of virtues and some of them are listed below (see also ref. [74]):

1) The main virtue is the computational efficiency. After the similarity transformation one can diagonalize over very compact subspaces. For the excitation energy variant of STEOM one needs to solve for $\hat{T}, \hat{S}^{IP}, \hat{S}^{EA}$ amplitudes (see section II), and one diagonalizes the transformed Hamiltonian over singly excited states only. Solving for the transformation amplitudes is about twice as expensive as a closed shell CCSD calculation. The remaining computational cost is minor, and one can get tens of excited states for the price of twice a CCSD calculation.
2) The method has nice theoretical scaling properties, and it satisfies the notion of generalized extensivity [75]. This implies it is size-intensive, such that excitation energies on a chromophore are unaffected by a distant fragment. Moreover STEOM satisfies charge transfer separability, meaning that it follows the proper limit of

$\mathrm{IP} + \mathrm{EA} - \frac{1}{\mathrm{R}}$ for a separated particle-hole pair excitation [49]. This property is violated by EOM-CCSD, and this likely affects the accuracy of the EOM-CC approach for valence excitations.

3) While the final diagonalization manifold in STEOM is over singly excited states only, the approach implicitly includes the effects of 'connected' triple excitations (viewed from an EOM-CC perspective). These effects are responsible for charge-transfer separability, but they also are responsible for the fact that valence excited states (of singlet type) tend to be more accurate in STEOM-CC than in (the more expensive) EOM-CC [49, 50]. This will be demonstrated also in this chapter.

Besides these advantages there are also some limitations to STEOM:

1) One has to make a selection of so-called 'active' occupied and virtual orbitals, associated with the *S*-type operators that are included in the second transformation. This is a somewhat non-trivial choice and this makes the method not completely black box. In practice this choice is often not so hard or critical, and certainly it is very different (and much easier) than choosing active spaces in a Complete Active Space second order Perturbation Theory (CASPT2) [76-78] or second order N-Electron Valence Perturbation Theory (NEVPT2) [79-82] calculation. Moreover, STEOM is not fully invariant to rotations of the occupied and virtual orbitals in their respective subspaces. This non-invariance issue has never been assessed before, and it will be discussed in this chapter.
2) The method can break down if a molecule has important ionized or attached states that acquire a large double excitation component. In comparison, any single reference CC

method breaks down if large double excitation amplitudes occur. STEOM is more sensitive as also the *S*-amplitudes should be small for the method to work well. This is very often the case for organic molecules at their equilibrium geometry, but not always. A redeeming feature is that this situation can be diagnosed quite readily, and only few excited states may be affected. One bad apple does not necessarily spoil the rest, but it is a bit of a delicate issue.

3) Like in EOM-CC, the final transformed Hamiltonian in STEOM is not hermitian. Because one uses quite compact diagonalization spaces in STEOM, one finds on occasion that eigenvalues become complex. This happens primarily if two states have the same symmetry and are nearly degenerate. This can happen readily for example if one makes slight distortions of a molecule with a degenerate point group symmetry (e.g., benzene). This is mainly a computational inconvenience, as there is nothing inherently bad about small imaginary parts of approximate excitation energies.
4) The method is only available in the ACES II program [83] and has been implemented only once as far as we know. There have not been many efficiency features in this implementation, e.g. as treating the 4-virtual terms in the Atomic Orbital (AO) basis set, or that parallelization have not been implemented. In some sense the implementation of the method has always remained in a pilot stage of development. This is a somewhat unusual situation in quantum chemistry, where promising methodologies are often briskly taken up by the community. As a result STEOM has never (or not yet) become a mainstream method.

The latter point is one of the reasons to pursue this study. We think STEOM is quite competitive with many approaches used widely in the community today. This includes both CC based approaches and also more efficient Time Dependent Density Functional Theory (TDDFT) like methods. For a review on TDDFT, we refer the reader to ref. [84, 85]. It would be very worthwhile to combine STEOM with local correlation and in particular PNO like approaches, and to incorporate into a state of the art electronic structure program. Much of the work regarding STEOM in the past has been exploratory. The method has been used in the Double Ionization Potential (DIP) [86-88] and Double Electron Attachment (DEA) [89] variants to explore multireference situations. It has been extended to investigate doubly excited states [90, 91]. Analytical gradients for the method have been derived and implemented in the ACES II program [92, 74], but used little. Despite all of these developments, relatively few applications of the method have appeared, and the merits of the approach and general applicability have not been all that well established. Anticipating this may change in the near future, we wish to help this development along and provide more insight into the performance of the approach.

In this chapter we will first summarize, in section II, the theoretical details of the STEOM-CC approach. In addition we will consider a few other variations. The CCSD calculation can be replaced by its Many Body second order Perturbation Theory (MBPT(2)) counterpart, to yield the STEOM-PT approach. We will consider the Extended STEOM (EXT-STEOM) approach [90, 91], in which the doubly transformed Hamiltonian is diagonalized over singles and double excitations. We will also consider a perturbative doubles correction to STEOM, denoted STEOM-D first reported in ref. [75].

This approach is still computationally efficient and is expected to include the main effects from Extended STEOM. We will also consider the issue of orbital invariance in STEOM using the novel STEOM-ORB approach, and explore a new approach, STEOM-H (ω) to hermitize the Hamiltonian and in this way ensure the reality of eigenvalues and orthogonality of eigenvectors.

To benchmark the results for STEOM-CC calculations and its cousins we will compare to Coupled Cluster response and EOM-CC approaches that include iterative triples corrections, notably the CC3 [35] and EOM-CCSDT-3 [36] approaches. We will also include comparisons to EOM-CCSD, CASPT2 [76-78] and NEVPT2 [79-82] results. All the molecules we consider are essentially single reference molecules, and the above methods are suitable in principle to accurately evaluate excitation energies, provided that they are dominated by single excitations. Somewhat to our surprise the two methods, CC3 and EOM-CCSDT-3, can easily deviate by up to about 0.1 eV for excitation energies. This is somewhat large for methodology that is used as a benchmark. Unfortunately this is the best that we can do at present. We will compare these benchmarks and hope to inspire work on a future more accurate benchmark calculation. The test set of molecules we use, has become popular in recent years [93-96]. It concerns a number of valence excited states for organic molecules of various character. The test set and computational details along with the results of the analysis and the discussion will be presented in section III.

II. Theory

Similarity Transformed Equation of Motion Coupled Cluster (STEOM-CC) theory dates back more than 15 years. The scheme is based on a two-fold many-body similarity transformation of the Hamiltonian and a subsequent diagonalization over a compact subspace. We will assume the ground state of the system is qualitatively well described by a closed-shell Hartree-Fock (HF) single determinant, which also serves as the vacuum state of the many-body theory. Orbitals occupied in the Hartree-Fock determinant are denoted with indices i,j,k,l, while virtual orbitals are denoted a,b,c,d. The STEOM-CC scheme proceeds in the following fashion.

In the first step the CCSD equations

$$\left\langle {}^{a}_{i} \middle| e^{-\hat{T}} \hat{H} e^{\hat{T}} \middle| 0 \right\rangle = \left\langle {}^{ab}_{ij} \middle| e^{-\hat{T}} \hat{H} e^{\hat{T}} \middle| 0 \right\rangle = 0 \tag{3.2}$$

are solved, with the Hamiltonian expressed in second quantization, and normal ordering with respect to the closed-shell Hartree-Fock state as

$$H = h_0 + h_p^r \left\{ E_r^p \right\} + \frac{1}{2} h_{pq}^{rs} \left\{ E_{rs}^{pq} \right\} \tag{3.3}$$

in which h_0 is the Hartree-Fock energy, h_p^r are the elements of the Fock matrix and h_{pq}^{rs} are non-antisymmetrized two-electron integrals. $\hat{E}_r^p$, $\hat{E}_{rs}^{pq}$ denote generators of the unitary group and braces are used to denote normal ordering with respect to the reference state.

The cluster operator is expressed as

$$\hat{T} = t_a^i \hat{E}_i^a + \frac{1}{2} t_{ab}^{ij} \hat{E}_{ij}^{ab} \tag{3.4}$$

Throughout the paper we will use the Einstein summation convention and a tensorial notation. Following the solution of the CCSD equations, second quantized matrix elements of the first similarity transformed Hamiltonian are constructed

$$\hat{\bar{H}} = e^{-\hat{T}} \hat{H} e^{\hat{T}} = \bar{h}_0 + \bar{h}_p^r \left\{ E_r^p \right\} + \frac{1}{2} \bar{h}_{pq}^{rs} \left\{ E_{rs}^{pq} \right\} + \ldots \; \hat{T} = t_a^i \hat{E}_i^a + \frac{1}{2} t_{ab}^{ij} \hat{E}_{ij}^{ab}, \qquad (3.5)$$

again expressed in normal order with respect to the closed-shell Hartree-Fock state. Using the $\hat{\bar{H}}$ matrix elements the CCSD equations can be represented as

$$\bar{h}_a^i = \bar{h}_{ab}^{ij} = 0, \;\; E(CCSD) = \bar{h}_0 \qquad (3.6)$$

In the next step of a STEOM-CC calculation one defines a second transformation operator

$$\begin{aligned} \hat{S} &= \hat{S}^{IP} + \hat{S}^{EA} \\ \hat{S}^{IP} &= s_m^{i'} \left\{ \hat{E}_{i'}^m \right\} + \frac{1}{2} s_{mb}^{ij} \left\{ \hat{E}_{ij}^{mb} \right\} \\ \hat{S}^{EA} &= s_{a'}^e \left\{ \hat{E}_e^{a'} \right\} + \frac{1}{2} s_{ab}^{ej} \left\{ \hat{E}_{ej}^{ab} \right\} \end{aligned} \qquad (3.7)$$

The index *m* denotes a subset of the occupied orbitals, while the index *e* similarly labels a subset of virtual orbitals. We refer to these orbitals as active, but they play a very different role than in for example Complete Active Space Self-Consistent field (CAS-SCF) calculations, and the selection of active spaces in STEOM is relatively straightforward, and usually not that critical. No optimization of active orbitals is involved beyond HF. The primed indices (both *i'* and *a'*) refer to explicitly inactive labels. The operator $\hat{S}$ is used to define a second similarity transformation

$$\hat{G} = \left\{ e^{\hat{S}} \right\}^{-1} \hat{\bar{H}} \left\{ e^{\hat{S}} \right\} \qquad (3.8)$$

A normal ordered exponential is used to simplify the details of equations as the components of $\hat{S}$ do not commute. The inverse of the normal ordered exponential is not known explicitly, and in practice one defines the transformed Hamiltonian in an iterative fashion

$$\hat{G} = \hat{\bar{H}}\left\{e^{\hat{S}}\right\} - \left\{e^{\hat{S}} - 1\right\}\hat{G} \tag{3.9}$$

This can be reduced to a connected form, and rather than iteration one can use backwards substitution [97, 73] to define the transformed Hamiltonian

$$\hat{G} = (\hat{\bar{H}}\left\{e^{\hat{S}}\right\})_C - (\left\{e^{\hat{S}} - 1\right\}\hat{G})_C \,, \tag{3.10}$$

where as usual the subscripts *C* (for connected) implies that the expression is written in normal order. The transformed Hamiltonian is represented as

$$\hat{G} = g_0 + g_p^r \left\{\hat{E}_r^p\right\} + \frac{1}{2} g_{pq}^{rs} \left\{\hat{E}_{rs}^{pq}\right\} + \ldots \tag{3.11}$$

The amplitudes of the operator $\hat{S}$ are defined such that second quantized matrix elements of the transformed Hamiltonian are equated to zero:

$$g_m^{i'} = g_{mb}^{ij} = g_{a'}^{e} = g_{ab}^{ej} = 0 \tag{3.12}$$

In addition the pre-existing zeros in $\bar{H}$ after solving the CCSD equations are preserved:

$$g_a^i = g_{ab}^{ij} = 0 \tag{3.13}$$

As a result of the transformations the structure of the doubly transformed Hamiltonian in the space of N-particle states is

$$\begin{pmatrix} G & 0 & S & D & T \\ 0 & g_0 & X & X & X \\ S & 0 & X & X & X \\ D & 0 & \sim & X & X \\ T & \sim & \sim & \sim & X \end{pmatrix} \tag{3.14}$$

Here 0, *S*, *D*, *T* indicate the reference state and single, double, triple excited determinants respectively. The ~ elements indicate smallish matrix elements, due to remaining 2-body terms in $\hat{G}$ that involve inactive orbitals, and 3-body and higher-body matrix elements that are introduced by the transformations. If the ~ elements are assumed to be rigorously zero it is seen that ***G*** attains a block form, and the eigenvalues of such a matrix can be found by diagonalizing each diagonal subblock individually. In practice this is only true to good approximation. In particular, in the original STEOM-CCSD approach the transformed Hamiltonian matrix is diagonalized over single excitations only. The computational cost of this final step is very minor in the context of the preceding CCSD calculation. The approach provides access to both singlet and triplet excited states that are dominated by singly excited configurations.

In practice the *S*-amplitudes are not solved directly from the defining non-linear equations, which can sometimes be cumbersome to converge. Rather one solves for a large number of roots of the IP-EOM-CCSD and EA-EOM-CCSD equations corresponding to the active space in STEOM. Finding roots of IP-EOM-CCSD equations amounts to a diagonalization of $(\hat{\bar{H}} - \bar{h}_0)$ over the ionized *1h, 2h1p* determinants

$$\hat{i}|0\rangle, \hat{a}^\dagger \hat{i}\, \hat{j}|0\rangle \tag{3.15}$$

and searching for eigenvectors corresponding to principal IP's that are dominated by *1h* configurations. We refer to the fraction of *1h* configurations in each eigenvector as the %singles for the ionized state. Likewise in the EA-EOM-CCSD step $(\hat{\bar{H}} - \bar{h}_0)$ is diagonalized over the *1p, 2p1h* configurations

$$\hat{a}^\dagger|0\rangle, \hat{a}^\dagger\hat{b}^\dagger\hat{j}|0\rangle \tag{3.16}$$

Again one searches for eigenvectors corresponding to the principal EA's that are dominated by the *1p* configurations. From the right hand eigenvectors of the IP-EOM-CCSD and EA-EOM-CCSD equations (denoted $\boldsymbol{C}$) one can extract the *S*-amplitudes using a renormalization, i.e.

$$\begin{aligned} s_m^i &= C_\lambda^i U_m^\lambda;\ s_{mb}^{ij} = C_{\lambda b}^{ij} U_m^\lambda;\ s_m^n = -\delta_m^n \\ s_a^e &= C_a^\mu W_\mu^e; s_{ab}^{ej} = C_{ab}^{\mu j} W_\mu^e;\ \ s_f^e = \delta_f^e \end{aligned} \tag{3.17}$$

The transformation coefficients $\boldsymbol{U}$, $\boldsymbol{W}$ are chosen such that the active-active components of $\hat{S}$ are signed unit matrices. This requires an inversion of the IP-EOM and EA-EOM eigenvectors within the occupied and virtual active spaces to obtain the $\boldsymbol{U}$ and $\boldsymbol{W}$ matrices. In our implementation of STEOM we equate the complete singles components of the $\hat{S}$ operators to zero after renormalization. These amplitudes can only effect occupied-occupied or virtual-virtual orbital rotations. As the final doubly transformed Hamiltonian is diagonalized over the full singles space, the eigenvalues are invariant in regards to inclusion of the $\hat{S}_1$ operator in the transformation. The solution of the CCSD and IP- and / or EA-amplitudes are standard ingredients in the STEOM approach. In practice the number of active virtuals is typically between 20 and 30 orbitals, comparable to the total number of occupied orbitals for our typical molecule. Solution of *all* desired

S^{EA} amplitudes is comparable in expense therefore to solving the CCSD equations. Solution of the IP-EOM-CCSD equations has negligible expense in comparison. The final diagonalization step in STEOM-CCSD is comparable to a Configuration Interaction Singles (CIS) calculation with modified matrix elements, and also has a very modest expense for the molecules we consider. Therefore, solving for a large number of STEOM excitation energies in practice is about twice as expensive as a ground state CCSD calculation.

Since the similarity transformations act at the level of second quantization, similar simplifications occur for other sectors of the Fock space. In particular, diagonalizing the single particle g_i^j; g_a^b matrices would yield IP-EOM-CCSD and EA-EOM-CCSD eigenvalues. This aspect is the reason one can solve the non-linear equations defining the *S*-amplitudes by using a stable diagonalization procedure instead [49]. In DIP-STEOM one diagonalizes over *2h* configurations, while in DEA-STEOM one diagonalizes over *2p* determinants. Both of these approaches can describe certain multireference problems. The STEOM approach is closely related to Fock Space Coupled Cluster (FSCC) Theory [58]. The basic steps of solving CCSD and IP/ EA sector amplitudes are identical. In STEOM these equations are derived using the strategy of many-body (second quantized) similarity transformations. In FSCC one invokes the so-called subsystem embedding conditions. The diagrammatic equations presented originally by Lindgren [51, 52] are very much in the spirit of the STEOM many-body philosophy. In STEOM the final step is a simple diagonalization procedure, and one can obtain as many states as desired (within the subspace of single excited states). In contrast, in the original Fock-Space

Coupled Cluster approach one had to solve a final non-linear equation and obtain all the roots in a predefined active space. This was often a very cumbersome step and the problem was often referred to as the intruder state problem. For the active orbital spaces used in this work (e.g. 20 occupied and 20 virtual orbitals) one would have to somehow avoid this intruder state problem for all 400 excited states in the active space. In practice this would lead to insurmountable convergence issues and typical active spaces in the original FSCC approach would have to be chosen carefully. These kinds of issues are absent in STEOM, and there are few limitations on the choice of active space. STEOM is robust in this respect. The issue has been solved in an alternative manner in the intermediate Hamiltonian formulation of Meissner [98], and this procedure is equally robust. In recent times the IP-EOM-CC and EA-EOM-CC amplitudes have been used in additional intermediate Hamiltonian approaches designed by Musial and Bartlett [99, 100].

It is pertinent to indicate the limitations of the STEOM-CCSD approach itself. Most importantly, the reference state is assumed to be well described by the single reference CCSD approach. The reason is that otherwise one obtains large *T*-amplitudes and the three-body and higher-rank operators in $\bar{H}$ and $\hat{G}$ can be expected to become important. As a result the block-diagonal form of $\hat{G}$ (indicated by the ~) is violated to a large extent, and a loss in accuracy results. The same is true for the IP-EOM-CCSD and EA-EOM-CCSD eigenvectors. Three-body contributions to $\hat{G}$ are again important if these eigenvectors have too much double excitation character (and consequently a low %singles). In principle one would prefer to include only ionized and attached states in the

transformation with a high %singles (e.g. higher than about 90%). On the other hand it is desirable that the character of the final STEOM excited states consists almost exclusively of active orbitals (e.g. %active > 98% or so). This is a conflicting condition as in practice high energy ionized or attached states tend to acquire significant double excitation character, and one should not choose too many orbitals in the active space therefore. This is usually not a serious issue, and hence it is not difficult to choose adequate active spaces. It may happen that low-lying ionized or attached states have a low %singles. If the corresponding principle orbital is important in the excited state one can expect such a state to be poorly described, whether the violating orbital is included in the active space or not. The STEOM-CC approach breaks down for such states. Fortunately the %active and %singles criteria combined provide a reasonable a posteriori guide as to the quality of results. All of the above considerations apply to all variants of STEOM-CCSD.

In this work we will focus on excitation energies only. We will consider the following variations of STEOM-CCSD

1. STEOM-CCSD itself as described above. We resort to the use of the short-hand notation: STEOM-CC.
2. STEOM-PT in which the CCSD step is replaced by an MBPT(2) calculation.
3. STEOM-H (ω) in which the final transformed Hamiltonian is symmetrized (or hermitized). In the section below we will discuss the details of the hermitization scheme we use, which depends on a continuous parameter ω. If this parameter tends to infinity one obtains the simplest version $\tilde{G}_{\lambda\mu} = \frac{1}{2}(G_{\lambda\mu} + G_{\mu\lambda})$. In all cases the hermitized version yields orthonormal eigenvectors, while the eigenvalues are

guaranteed to be real-valued. This is not always the case in non-hermitian variants of STEOM. The problem of complex eigenvalues can occur in particular if states having the same symmetry are close in energy, e.g. near a conical intersection. For this reason we are interested in a hermitized version of STEOM.

4. Extended STEOM (EXT-STEOM): In this approach the matrix $\boldsymbol{G}$ is diagonalized over both singly and doubly excited configurations. In addition the operator $\hat{G}$ is truncated to up to 3-body operators. This approach is suitable to describe states with significant double excitation character. In a previous work [90] it has been shown that EXT-STEOM states that are dominated by single excitations usually change relatively little from the STEOM-CCSD values. The approach is only implemented for singlet states. This approach is more expensive than the EOM-CCSD approach.
5. STEOM-D: rather than diagonalizing $\boldsymbol{G}$ over singles and doubles completely, as in EXT-STEOM, the doubles-doubles block is assumed to be diagonal (we use the bare Fock matrix elements on the diagonal), and one solves a Brillouin-Wigner type of perturbation expression. If the transformed Hamiltonian is presented in a block form

$$\boldsymbol{G} = \begin{pmatrix} \boldsymbol{A} & \boldsymbol{B} \\ \boldsymbol{C} & \boldsymbol{D} \end{pmatrix} \rightarrow \begin{pmatrix} \boldsymbol{A} & \boldsymbol{B} \\ \boldsymbol{C} & \boldsymbol{d} \end{pmatrix} \tag{3.18}$$

then the STEOM-D eigenvalues ω are solved self-consistently from

$$\boldsymbol{A}\boldsymbol{x} = \boldsymbol{x}\varepsilon; \boldsymbol{x}^{\dagger}\boldsymbol{x} = 1; \;\; \omega = \boldsymbol{x}^{\dagger}\boldsymbol{A}\boldsymbol{x} + \boldsymbol{x}^{\dagger}\boldsymbol{B}(\omega - \boldsymbol{d})^{-1}\boldsymbol{C}\boldsymbol{x} \tag{3.19}$$

This approach can be viewed as an approximation to EXT-STEOM. One might anticipate slightly improved eigenvalues compared to STEOM-CCSD. Morever, the STEOM-D eigenvalues can serve as a diagnostic to indicate if a more extended

treatment is desired. This approach is only slightly more expensive than STEOM-CCSD itself.

6. STEOM-ORB: in this approach the active orbitals are optimized, such that they span a space that captures the majority of the excitation character. The purpose of the approach is to monitor how sensitive STEOM eigenvalues are to the precise nature of the active space. In this procedure one first performs a traditional STEOM calculation, and uses the (Schmidt orthogonalized) set of STEOM eigenvectors, denoted $\boldsymbol{C}$ below, to define an ensemble density matrix in both the occupied and virtual orbital subspaces:

$$D_{ij} = \sum_{\lambda,a} C_a^i(\lambda) C_a^j(\lambda); \quad D_{ab} = \sum_{\lambda,i} C_a^i(\lambda) C_b^i(\lambda); \tag{3.20}$$

These density matrices are subsequently diagonalized, yielding occupation numbers. The corresponding eigenvectors or natural orbitals define an orbital space that is most suitable to expand the excited states. We select those orbitals above an occupation threshold (on the order of 0.05) to lie in the active space, and obtain the remaining active occupied and active virtual orbitals by diagonalizing the Fock matrix over the complementary (occupied or virtual) subspace. In our experience, well over 99.5% of the STEOM-CCSD eigenvectors lies within the thusly-constructed active space. Moreover the states tend to have a very pure excitation character only involving a single pair of orbitals, or a limited linear combination, each having large coefficients. These orbitals are hence quite suitable for interpreting the excitation character. Once the new active orbitals are obtained, a new reorthonormalization of the canonical IP-EOM-CC and EA-EOM-CC eigenvectors is performed, i.e. new matrices $\boldsymbol{U}$ and $\boldsymbol{W}$ are obtained. It is this step that is responsible for subsequent changes in the excitation

energies. The actual orbitals remain the canonical Hartree-Fock orbitals. It is not necessary to rotate all amplitudes and integrals. Only the active labels *m* and *e* are affected. The transformed Hamiltonian ***G*** is obtained using the new *S*-amplitudes and the final STEOM-ORB eigenvalues are obtained from the Configuration Interaction Singles (CIS) diagonalization procedure. In this approach only the final transformation and the final STEOM diagonalization are performed twice, and the approach is therefore computationally efficient. As will be demonstrated in the results section, none of this seems to matter much. Our chief goal is therefore to demonstrate that STEOM is rather insensitive to the precise definition of the orbitals. We consider this a desirable feature.

Hermitization Schemes

The STEOM similarity transformed Hamiltonian is not hermitian. If this transformed Hamiltonian would be diagonalized over the complete Hilbert space, the eigenvalues are still guaranteed to be real (as they would be identical to the original eigenvalues). The virtue of the STEOM approach is of course that accurate results can be obtained by diagonalizing over a compact subspace. However, in that case the eigenvalues and eigenvectors can become complex. The issue of potential complex eigenvalues is most acute when states of the same symmetry are close in energy. Consider for example the 2×2 Hamiltonian

$$\begin{pmatrix} D & a+b \\ a-b & D \end{pmatrix} \tag{3.21}$$

which leads to a secular equation

$$(D-E)^2 = (a^2 - b^2) \qquad (3.22)$$

This gives rise to complex eigenvalues when $(a^2 - b^2) < 0$. An easy way to define a symmetric (or hermitian) Hamiltonian is to simply average: $\tilde{H} = \frac{1}{2}(H + H^\dagger)$. In the above 2×2 example this amounts to simply neglecting the asymmetry parameter *b*. Another possibility is to replace the off-diagonal elements by a multiplicative average value, $\tilde{H}_{ij} = \tilde{H}_{ji} = \pm\sqrt{\left|H_{ij}H_{ji}\right|}$. This leads to a sign ambiguity if the off-diagonal elements have different signs (precisely when complex eigenvalues occur in the 2x2 case). Our experience with this multiplicative hermitization scheme is not all that promising, and we will not consider it further.

Here we will discuss a rather different procedure. Our goal is to define a hermitian Hamiltonian while changing the resulting eigenvalues only in a minor way. We think the scheme below may be of some general interest in related contexts. Let us assume $\boldsymbol{H}$ below is a non-hermitian matrix. In STEOM this matrix would be the matrix $\boldsymbol{G}$ defined over singly excited states, but the analysis applies to any matrix. We define a transformed (i.e. modified) Hamiltonian

$$\tilde{\boldsymbol{H}} = \boldsymbol{e}^{\boldsymbol{S}/2}\boldsymbol{H}\boldsymbol{e}^{\boldsymbol{S}/2} = \boldsymbol{H} + \left\{\boldsymbol{H},\boldsymbol{S}/2\right\} + 1/2\left\{\left\{\boldsymbol{H},\boldsymbol{S}/2\right\},\boldsymbol{S}/2\right\} + \ldots \quad (3.23)$$

The braces indicate anticommutators. The matrix $\boldsymbol{S}$ is antihermitian (i.e. antisymmetric for the real matrices we discuss here), such that the transformation $\boldsymbol{U} = \boldsymbol{e}^{\boldsymbol{S}/2}$ is unitary. The coefficients in the transformation matrix $S_{ij} = -S_{ji}$ are to be solved such that the resulting transformed Hamiltonian is symmetric. The above transformation is not a

similarity transformation, however, and can be expected to change the eigenvalues. The above transformation has another peculiarity. It is not invariant if we shift the Hamiltonian by a constant on the diagonal, $\omega\mathbf{1}$ and then shift the resulting eigenvalues back by $-\omega\mathbf{1}$. We will exploit this feature to define a family of transformed Hamiltonians,

$$\tilde{\boldsymbol{H}}(\omega) = \boldsymbol{e}^{\boldsymbol{S}/2}(\boldsymbol{H} + \omega\mathbf{1})\boldsymbol{e}^{\boldsymbol{S}/2} - \omega\mathbf{1},\ \tilde{\boldsymbol{H}}(\omega) = \tilde{\boldsymbol{H}}(\omega)^{\dagger},\ \boldsymbol{S}^{\dagger} = -\boldsymbol{S} \quad (3.24)$$

We will use the freedom in ω by choosing ω such that eigenvalues tend to change little. Let us consider the iterative solution of the above hermitization equation, changing $\boldsymbol{S}$ by a small amount $\Delta\boldsymbol{S}$:

$$\begin{aligned} \tilde{\boldsymbol{H}}(\omega)_{\boldsymbol{S}+\Delta\boldsymbol{S}} &= \boldsymbol{e}^{(\boldsymbol{S}+\Delta\boldsymbol{S})/2}(\boldsymbol{H} + \omega\mathbf{1})\boldsymbol{e}^{(\boldsymbol{S}+\Delta\boldsymbol{S})/2} - \omega\mathbf{1} \\ &\approx \tilde{\boldsymbol{H}}(\omega)_{\boldsymbol{S}} + \frac{1}{2}\left\{\boldsymbol{H} + \omega\mathbf{1}, \Delta\boldsymbol{S}\right\} \\ &\approx \tilde{\boldsymbol{H}}(\omega)_{\boldsymbol{S}} + \frac{1}{2}\left\{\boldsymbol{H}_0 + \omega\mathbf{1}, \Delta\boldsymbol{S}\right\} \end{aligned} \quad (3.25)$$

Here $\boldsymbol{H}_0$ denotes a diagonal approximation to $\boldsymbol{H}$. If we consider the (*ij*) and (*ji*) components of $\tilde{\boldsymbol{H}}$, denote the diagonal elements of $\boldsymbol{H}$ by *D*, and suppress the ω dependence, then

$$\begin{aligned} (\tilde{H}_{ij})_{S+\Delta S} &\approx (\tilde{H}_{ij})_S + \frac{1}{2}(D_i + D_j + \omega)\Delta S_{ij} \\ (\tilde{H}_{ji})_{S+\Delta S} &\approx (\tilde{H}_{ji})_S + \frac{1}{2}(D_i + D_j + \omega)\Delta S_{ji} \\ &= (\tilde{H}_{ji})_S - \frac{1}{2}(D_i + D_j + \omega)\Delta S_{ij}, \end{aligned} \quad (3.26)$$

where we used the antisymmetry of $\boldsymbol{S}$ in the last line. Subtracting the two equations and equating the difference to zero yields for the correction:

$$\Delta S_{ij} = -\frac{(\tilde{H}_{ij} - \tilde{H}_{ji})}{(D_i + D_j + \omega)} \tag{3.27}$$

Let us note that in the case of STEOM in which $\boldsymbol{H}$ (i.e. $\boldsymbol{G}$) represents a Hamiltonian over excited states all diagonal elements are positive. This simplifies the analysis, but is probably not all that crucial. The above iteration scheme in practice rapidly converges as long as the denominators are not too small. The scheme has an interesting limit. In the case that $\omega \to \infty$:

$$S_{ij}\left(\infty\right) = \lim_{\omega\to\infty} -\frac{(H_{ij} - H_{ji})}{(D_i + D_j + \omega)} = -\frac{(H_{ij} - H_{ji})}{\omega} \tag{3.28}$$

Since the components of $\boldsymbol{S}$ tend to zero, only first order terms in $\boldsymbol{S}$ survive, and hence

$$\begin{aligned} \tilde{H}_{ij}(\infty) &= (H_{ij} + \omega\delta_{ij}) + \left\{\omega, \boldsymbol{S}/2\right\}_{ij} - \omega\delta_{ij} \\ &= H_{ij} - \omega\frac{(H_{ij} - H_{ji})}{2\omega} = \frac{1}{2}(H_{ij} + H_{ji}) \end{aligned} \tag{3.29}$$

Hence in the limit of very large ω the *S*-amplitudes become very small, and the Taylor series converges very rapidly. The transformed Hamiltonian reduces to the averaged sum. As one reduces the values of ω the values of the *S*-amplitudes increase, and the Taylor series expansion has to be carried to higher order to achieve the same accuracy. As the value of ω reaches the negative of the smallest value of an off-diagonal element $(D_i + D_j)$ the iteration scheme starts to diverge. As we will demonstrate in the results section, the eigenvalues of the symmetrized $\tilde{H}(\omega)$ are smooth functions of ω. Most importantly, they seem to deviate less and less from the original eigenvalues as ω starting from positive values, first approaches zero and then negative values. To preserve stability in the scheme, ω shouldn't become too negative. In our default scheme of this

$\omega-$ hermitization scheme we selected the "close to" optimal value as

$\omega_{opt} = -\frac{1}{4}\min[D_i + D_j]$ after some trial and error. Our implementation of the scheme proceeds through a recursive calculation of an anticommutator $\left\{\boldsymbol{A},\boldsymbol{S}/2\right\} = \frac{1}{2}(\boldsymbol{AS}+\boldsymbol{SA})$. This allows us to calculate the transformed Hamiltonian to arbitrary high order. Typically 6-10 recursions are needed to assemble the transformed Hamiltonian to sufficient accuracy. The size of the matrices in the STEOM approach ranges over the space of single excitations. For the current type of applications this type of matrix is easily held in the core memory of the computer. Our aim here is to explore how this $\omega-$ hermitization scheme works, and our measure is the closeness of the eigenvalues of the original and transformed Hamiltonian.

III. Results and Discussion

III.A. Test Set and Computational Details

Let us discuss the details of the test set we use to benchmark the electronic structure methodologies of interest. We investigate excitation spectra of a large set of organic molecules involving $\pi\rightarrow\pi^*$ and $n\rightarrow\pi^*$ excitations, first studied by Schreiber and co-workers [93]. The test set of 28 organic molecules includes unsaturated aliphatic hydrocarbons (including polyenes and cyclic compounds), aromatic hydrocarbons and heterocylces, carbonyl compounds and nucleobases.

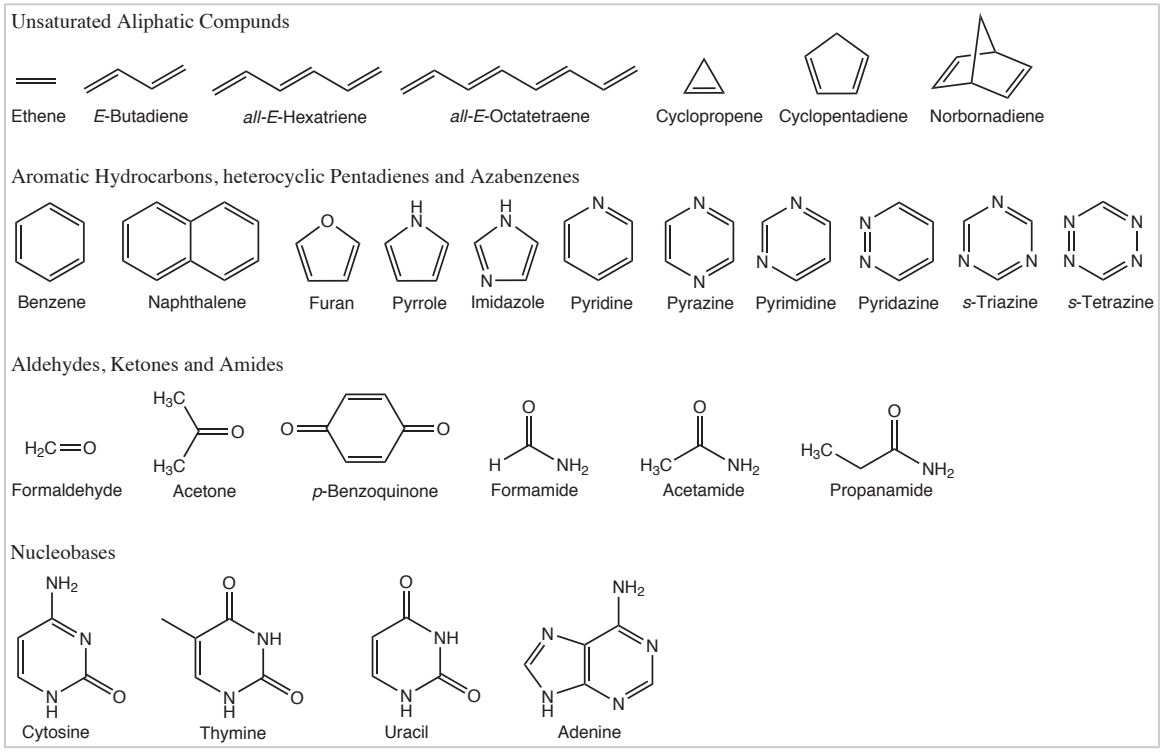

Figure 3.1: Benchmark of test set considered in the study.

Reprinted with permission from [M. Schreiber, M.R. Silva-Junior, S.P. Sauer, and W. Thiel, J. Chem. Phys. **128**, 134110 (2008)]. Copyright [2008], AIP Publishing LLC

We share Schreiber's intention to cover the most important chromophores in organic photochemistry. The ground-state geometries of these molecules were optimized at the MP2 level (Møller-Plesset second-order perturbation theory) with 6-31G* basis [101] using the GAUSSIAN program package [102]. Our calculations as well as results taken from the Schreiber paper [93] and Schapiro paper [96] were performed in the TZVP basis set [103] and with dropped core.

As mentioned before in the introduction, a STEOM calculation requires an appropriate choice of active orbitals. In table 3.1 we document the number of active orbitals chosen for the STEOM calculations we performed, along with the threshold energies used to yield the respective choices. Let us explain the acronyms in Table 3.1: N_IP and N_EA refer to the number of ionized states and electron-attached states respectively; orbitals with canonical HF orbital energies above the IP_low threshold are included in the $\hat{S}^{IP}$ active space, while orbitals with orbital energies below the EA_high threshold are included in the $\hat{S}^{EA}$ active space.

Table 3.1: Documentation of the choice of active orbitals in STEOM calculations performed for the test set. Number of ionized states is denoted N_IP, number of electron-attached states is denoted N_EA. IP_low and EA_high are threshold energies in eV used to obtain the respective choice of orbitals.

Molecule	N_IP	N_EA	IP_low	EA_high
Ethene	4	8	-20.00	10.00
E-Butadiene	7	18	-20.00	14.00
E-Hexatriene	12	22	-22.00	13.00
E-Octatetreane	13	26	-20.00	11.97
Cyclopropene	5	14	-20.00	12.90
Cyclopentadiene	9	14	-20.00	10.00
Norbornadiene	12	23	-20.00	13.00
Benzene	12	21	-25.00	13.50
Naphthalene	16	25	-20.00	11.50
Furan	10	16	-25.00	14.05
Pyrrole	10	17	-23.00	14.00
Imidazole	7	16	-20.00	14.10
Pyridine	10	18	-20.00	13.00
Pyrazine	10	17	-20.00	12.90

Pyrimidine	9	18	-20.00	13.70
Pyridazine	10	16	-20.00	12.20
Triazine	10	13	-23.00	11.50
Tetrazine	10	19	-22.00	15.00
Formaldehyde	5	7	-25.00	13.00
Acetone	8	13	-20.00	10.00
Benzoquinone	6	17	-16.00	10.62
Formamide	5	9	-20.00	14.00
Acetamide	8	14	-20.00	15.00
Propanamide	11	16	-23.00	12.00
Cytosine	12	17	-20.00	11.00
Thymine	14	25	-20.00	13.72
Uracil	12	23	-20.00	14.10
Adenine	6	16	-13.53	10.00

III.B. Discussion of Benchmarks

We briefly outline the general approach here before we discuss in detail. We investigate six variations of STEOM methodologies in this study: STEOM-CC, STEOM-D, STEOM-ORB, STEOM-PT, STEOM-H (ω) and EXT-STEOM methods. We benchmark these methods for the test set and compare to NEVPT2, CASPT2, CC3 and EOM- CCSDT-3 methods. The CASPT2 and CC3 results are obtained from the Schreiber benchmark paper [93]. We obtain the NEVPT2 results from the benchmark paper by Schapiro [96]. However, we perform EOM-CCSDT-3 calculations using the CFOUR program [104]. We exclude the DNA bases from the analysis involving CC3 and EOM-CCSDT-3 as these calculations are computationally expensive.

We present below Tables 3.2a and 3.2b, which include our benchmark results for the excitation energies in eV for singlet and triplets excitations, respectively. In these tables we focus on CC3, EOM-CCSDT-3, NEVPT2, CASPT2, STEOM-CC, STEOM-D, EXT-STEOM, and EOM-CCSD methods. We note that STEOM-D and EXT-STEOM methods have not been implemented for triplets. We also point out that we did not benchmark EOM-CCSDT-3 for triplets for reasons discussed in subsection III.B.1. below. Therefore, Table 3.2b does not include STEOM-D, EXT-STEOM, and EOM-CCSDT-3 results. STEOM-ORB, STEOM-PT, and STEOM-H (ω) methods will be considered separately and are omitted from the Tables.

We would like to make several remarks about the CC3 and CASPT2 results we obtain from the Schreiber paper. First, we note that the singlet state 3 $^1A_1$ ($\pi \rightarrow \pi^*$) of

Cyclopentadiene should have a CC3 excitation energy of 8.69 not 6.69 eV. We think this is probably a typographical error. Second, the singlet state 2 $^1A_1$ ($\pi \rightarrow \pi^*$) of Formaldehyde has a CASPT2 result with a very large deviation from the CC3 result, and which likely corresponds to a different state. We confirm this by comparing the Schreiber's paper result for that state with our benchmarked STEOM results to find that the CC3 result is in good agreement to STEOM unlike the CASPT2. We have excluded this state from statistics involving CASPT2. Finally, we note that we performed CC3 calculations for the singlet states 2 $^1A'$ ($\pi \rightarrow \pi^*$) and 3 $^1A'$ ($\pi \rightarrow \pi^*$) of both Acetamide and Propanamide. We find that our results deviate from the CC3 results in the Schreiber's paper by a deviation that ranges between 0.02 eV and 0.04 eV. The source of error in the Schreiber paper is not clear.

Table 3.2a: Vertical singlet excitation energies in eV for all statistically evaluated molecules.

Molecule	State	CC3 (%T1)	EOM-CCSDT-3 (%T1)	NEVPT2	CASPT2	STEOM-CC	STEOM-D	EXT-STEOM	EOM-CCSD
Ethene	$1\ ^1B_{1u}$ ($\pi\rightarrow\pi^*$)	8.37 (96.9)	8.40 (96.26)	8.69	8.62	8.34	8.33	8.32	8.51
E-Butadiene	$1\ ^1B_{u}$ ($\pi\rightarrow\pi^*$)	6.58 (93.7)	6.61 (92.7)	6.31	6.47	6.66	6.59	6.55	6.73
	$2\ ^1A_{g}$ ($\pi\rightarrow\pi^*$)	6.77 (72.8)	6.89 (61.64)	6.82	6.83	7.38	7.44	6.71	7.42
E-Hexatriene	$1\ ^1B_{u}$ ($\pi\rightarrow\pi^*$)	5.58 (92.6)	5.61 (91.31)	4.96	5.31	5.66	5.59	5.54	5.73
	$2\ ^1A_{g}$ ($\pi\rightarrow\pi^*$)	5.72 (65.8)	5.88 (54.79)	5.59	5.42	6.60	6.57	5.73	6.61
E-Octatetraene	$1\ ^1B_{u}$ ($\pi\rightarrow\pi^*$)	4.94 (91.9)	4.97 (90.42)	4.17	4.70	5.00	4.93	4.86	5.08
	$2\ ^1A_{g}$ ($\pi\rightarrow\pi^*$)	4.97 (62.9)	5.17 (52.37)	4.74	4.64	5.90	5.89	4.93	5.98
Cyclopropene	$1\ ^1B_{1}$ ($\sigma\rightarrow\pi^*$)	6.90 (93)	6.92 (91.94)	6.85	6.76	6.76	6.72	6.69	6.97
	$1\ ^1B_{2}$ ($\pi\rightarrow\pi^*$)	7.10 (95.5)	7.14 (94.27)	7.18	7.06	7.06	7.03	6.99	7.25
Cyclopentadiene	$1\ ^1B_{2}$ ($\pi\rightarrow\pi^*$)	5.73 (94.3)	5.75 (93.13)	5.30	5.51	5.71	5.66	5.65	5.87
	$2\ ^1A_{1}$ ($\pi\rightarrow\pi^*$)	6.61 (79.3)	6.71 (71.75)	6.74	6.31	6.96	6.93	6.63	7.05
	$3\ ^1A_{1}$ ($\pi\rightarrow\pi^*$)	8.69 (93.1)	8.76 (91.25)	8.51	8.52	8.64	8.68	8.69	8.96
Norbornadiene	$1\ ^1A_{2}$ ($\pi\rightarrow\pi^*$)	5.64 (93.4)	5.68 (91.65)	5.07	5.34	5.55	5.52	5.49	5.80
	$1\ ^1B_{2}$ ($\pi\rightarrow\pi^*$)	6.49 (91.9)	6.55 (89.62)	5.84	6.11	6.51	6.43	6.39	6.69
	$2\ ^1B_{2}$ ($\pi\rightarrow\pi^*$)	7.64 (93.8)	7.68 (92.12)	7.10	7.32	7.64	7.60	7.57	7.85
	$2\ ^1A_{2}$ ($\pi\rightarrow\pi^*$)	7.71 (93)	7.74 (91.16)	7.07	7.44	7.67	7.58	7.54	7.86
Benzene	$1\ ^1B_{2u}$ ($\pi\rightarrow\pi^*$)	5.07 (85.8)	5.10 (85.38)	5.24	5.05	4.68	4.88	4.87	5.19
	$1\ ^1B_{1u}$ ($\pi\rightarrow\pi^*$)	6.68 (93.6)	6.69 (92.98)	6.47	6.45	6.70	6.56	6.49	6.75
	$1\ ^1E_{1u}$ ($\pi\rightarrow\pi^*$)	7.45 (92.2)	7.52 (90.84)	7.28	7.07	7.42	7.44	7.45	7.66
	$2\ ^1E_{2g}$ ($\pi\rightarrow\pi^*$)	8.43 (65.6)	8.60 (66.26)	8.45	8.21	8.81	8.93	8.70	9.21
Naphthalene	$1\ ^1B_{3u}$ ($\pi\rightarrow\pi^*$)	4.27 (85.2)	4.30 (84.23)	4.39	4.24	3.99	4.07	4.03	4.41
	$1\ ^1B_{2u}$ ($\pi\rightarrow\pi^*$)	5.03 (90.6)	5.09 (89.05)	4.47	4.77	5.10	5.01	4.96	5.22
	$2\ ^1A_{g}$ ($\pi\rightarrow\pi^*$)	5.98 (82.2)	6.05 (80.23)	6.27	5.90	5.88	5.92	5.77	6.23
	$2\ ^1B_{3u}$ ($\pi\rightarrow\pi^*$)	6.33 (90.7)	6.41 (88.79)	5.85	6.07	6.34	6.33	6.33	6.55
	$1\ ^1B_{1g}$ ($\pi\rightarrow\pi^*$)	6.07 (79.6)	6.22 (78.84)	6.20	6.00	6.37	6.31	6.12	6.53
	$2\ ^1B_{2u}$ ($\pi\rightarrow\pi^*$)	6.57 (90.5)	6.64 (88.76)	6.17	6.33	6.61	6.53	6.50	6.77
	$2\ ^1B_{1g}$ ($\pi\rightarrow\pi^*$)	6.79 (91.3)	6.84 (89.98)	6.41	6.48	6.76	6.70	6.64	6.98
	$3\ ^1A_{g}$ ($\pi\rightarrow\pi^*$)	6.90 (70)	7.14 (65.54)	6.90	6.71	7.42	7.49	7.14	7.77
	$3\ ^1B_{2u}$ ($\pi\rightarrow\pi^*$)	8.44 (87.9)	8.56 (86.41)	8.09	8.18	8.53	8.49	8.47	8.78
	$3\ ^1B_{3u}$ ($\pi\rightarrow\pi^*$)	8.12 (53.7)	8.33 (59.83)	7.98	7.76	8.62	8.69	8.43	9.03
Furan	$2\ ^1A_{1}$ ($\pi\rightarrow\pi^*$)	6.62 (84.9)	6.69 (81.46)	6.79	6.52	6.48	6.64	6.56	6.89
	$1\ ^1B_{2}$ ($\pi\rightarrow\pi^*$)	6.60 (92.6)	6.64 (92.05)	6.59	6.43	6.66	6.63	6.58	6.80
	$3\ ^1A_{1}$ ($\pi\rightarrow\pi^*$)	8.53 (90.7)	8.61 (87.8)	8.62	8.22	8.53	8.57	8.51	8.83
Pyrrole	$2\ ^1A_{1}$ ($\pi\rightarrow\pi^*$)	6.40 (86)	6.46 (83.83)	6.60	6.31	6.26	6.35	6.29	6.61
	$1\ ^1B_{2}$ ($\pi\rightarrow\pi^*$)	6.71 (91.6)	6.75 (90.95)	6.90	6.33	6.73	6.68	6.63	6.88
	$3\ ^1A_{1}$ ($\pi\rightarrow\pi^*$)	8.17 (90.2)	8.24 (87.34)	8.44	8.17	8.19	8.21	8.15	8.44

Imidazole	2 ^{1}A' ($\pi\rightarrow\pi^*$)	6.58 (87.2)	6.64 (86.03)	6.85	6.19	6.49	6.59	6.51	6.80
	1 ^{1}A" ($n\rightarrow\pi^*$)	6.82 (87.6)	6.89 (86.71)	7.00	6.81	6.74	6.66	6.62	7.01
	3 ^{1}A' ($\pi\rightarrow\pi^*$)	7.10 (89.8)	7.14 (88.41)	6.99	6.93	7.05	7.03	6.98	7.27
	2 ^{1}A" ($n\rightarrow\pi^*$)	7.93 (89.4)	8.01 (87.76)	8.06	7.91	7.90	7.81	7.73	8.16
	4 ^{1}A' ($\pi\rightarrow\pi^*$)	8.45 (88.6)	8.51 (86.68)	8.68	8.15	8.46	8.46	8.40	8.69
Pyridine	1 $^1B_2$ ($\pi\rightarrow\pi^*$)	5.15 (85.9)	5.18 (85.44)	5.36	5.02	4.80	4.97	4.95	5.27
	1 $^1B_1$ ($n\rightarrow\pi^*$)	5.05 (88.1)	5.12 (86.65)	5.28	5.14	5.01	4.89	4.79	5.26
	1 $^1A_2$ ($n\rightarrow\pi^*$)	5.50 (87.7)	5.59 (85.77)	5.50	5.47	5.40	5.38	5.34	5.73
	2 $^1A_1$ ($\pi\rightarrow\pi^*$)	6.85 (92.8)	6.87 (91.93)	7.17	6.39	6.90	6.77	6.70	6.94
	2 $^1B_2$ ($\pi\rightarrow\pi^*$)	7.59 (89.7)	7.66 (88.56)	7.38	7.29	7.57	7.59	7.57	7.81
	3 $^1A_1$ ($\pi\rightarrow\pi^*$)	7.70 (91.5)	7.78 (89.94)	7.50	7.46	7.66	7.70	7.70	7.94
	4 $^1A_1$ ($\pi\rightarrow\pi^*$)	8.68 (74.1)	8.86 (67.59)	8.11	8.70	9.07	9.16	8.97	9.45
	3 $^1B_2$ ($\pi\rightarrow\pi^*$)	8.77 (65.2)	8.97 (65.61)	8.58	8.62	9.21	9.38	9.13	9.64
Pyrazine	1 $^1B_{3u}$ ($n\rightarrow\pi^*$)	4.24 (89.9)	4.30 (88.42)	4.25	4.12	4.20	4.06	3.97	4.42
	1 $^1B_{2u}$ ($\pi\rightarrow\pi^*$)	5.02 (86.2)	5.05 (85.77)	5.34	4.85	4.69	4.87	4.85	5.14
	1 ^1A_u ($n\rightarrow\pi^*$)	5.05 (88.4)	5.13 (86.4)	4.99	4.70	4.99	4.96	4.92	5.29
	1 $^1B_{2g}$ ($n\rightarrow\pi^*$)	5.74 (85)	5.83 (84.09)	5.91	5.68	5.75	5.60	5.46	6.03
	1 $^1B_{1g}$ ($n\rightarrow\pi^*$)	6.75 (85.8)	6.89 (81.72)	6.83	6.41	6.81	6.79	6.71	7.14
	1 $^1B_{1u}$ ($\pi\rightarrow\pi^*$)	7.07 (93.3)	7.09 (92.71)	6.85	6.89	7.17	7.03	6.96	7.18
	2 $^1B_{2u}$ ($\pi\rightarrow\pi^*$)	8.05 (89.7)	8.12 (88.44)	7.69	7.65	8.00	8.03	8.02	8.29
	2 $^1B_{1u}$ ($\pi\rightarrow\pi^*$)	8.06 (90.9)	8.15 (89.6)	8.01	7.79	8.04	8.06	8.08	8.35
	2 ^1A_g ($\pi\rightarrow\pi^*$)	8.69 (74.2)	8.90 (67.01)	8.92	8.61	9.07	9.22	8.25	9.54
	1 $^1B_{3g}$ ($\pi\rightarrow\pi^*$)	8.77 (61.1)	9.00 (62.27)	8.76	8.47	9.16	9.51	9.36	9.74
Pyrimidine	1 $^1B_1$ ($n\rightarrow\pi^*$)	4.50 (88.4)	4.57 (86.68)	4.57	4.44	4.45	4.35	4.27	4.71
	1 $^1A_2$ ($n\rightarrow\pi^*$)	4.93 (88.2)	5.00 (86.44)	4.87	4.81	4.78	4.76	4.72	5.13
	1 $^1B_2$ ($\pi\rightarrow\pi^*$)	5.36 (85.7)	5.39 (85.23)	5.63	5.24	4.95	5.17	5.16	5.49
	2 $^1A_1$ ($\pi\rightarrow\pi^*$)	7.06 (92.2)	7.09 (90.44)	7.51	6.64	7.13	7.01	6.92	7.17
	3 $^1A_1$ ($\pi\rightarrow\pi^*$)	7.74 (89.7)	7.81 (87.44)	8.00	7.21	7.70	7.72	7.68	7.97
	2 $^1B_2$ ($\pi\rightarrow\pi^*$)	8.01 (90.7)	8.08 (88.98)	7.80	7.64	7.92	7.96	7.96	8.23
Pyridazine	1 $^1B_1$ ($n\rightarrow\pi^*$)	3.92 (89)	4.00 (87.42)	3.96	3.78	3.86	3.73	3.64	4.12
	1 $^1A_2$ ($n\rightarrow\pi^*$)	4.49 (86.6)	4.59 (84.94)	4.61	4.32	4.47	4.41	4.35	4.76
	2 $^1A_1$ ($\pi\rightarrow\pi^*$)	5.22 (85.2)	5.25 (84.54)	5.48	5.18	4.89	5.07	5.02	5.35
	2 $^1A_2$ ($n\rightarrow\pi^*$)	5.74 (86.6)	5.82 (84.37)	5.95	5.77	5.73	5.63	5.52	6.00
	2 $^1B_1$ ($n\rightarrow\pi^*$)	6.41 (86.6)	6.51 (84.75)	6.74	6.52	6.41	6.35	6.30	6.70
	1 $^1B_2$ ($\pi\rightarrow\pi^*$)	6.93 (90.7)	6.96 (90.6)	7.47	6.31	7.00	6.90	6.82	7.09
	2 $^1B_2$ ($\pi\rightarrow\pi^*$)	7.55 (90.2)	7.61 (87.9)	7.50	7.29	7.59	7.57	7.55	7.78
	3 $^1A_1$ ($\pi\rightarrow\pi^*$)	7.82 (90.5)	7.91 (88.34)	7.70	7.62	7.84	7.88	7.84	8.11
Triazine	1 $^1A_1$" ($n\rightarrow\pi^*$)	4.78 (88)	4.85 (86.28)	4.77	4.60	4.63	4.60	4.61	4.97
	1 ^{1}E" ($n\rightarrow\pi^*$)	4.81 (88.1)	4.89 (86.39)	4.94	4.71	4.71	4.66	4.56	5.02
	1 $^1A_2$" ($n\rightarrow\pi^*$)	4.76 (88)	4.84 (86.18)	4.94	4.68	4.77	4.65	4.61	4.99
	1 $^1A_2$' ($\pi\rightarrow\pi^*$)	5.71 (85.1)	5.74 (84.7)	5.94	5.79	5.24	5.50	5.48	5.84
	2 $^1A_1$' ($\pi\rightarrow\pi^*$)	7.41 (90.8)	7.44 (88.52)	7.36	7.25	7.45	7.34	7.23	7.51
	2 ^{1}E" ($n\rightarrow\pi^*$)	7.80 (88.1)	7.95 (80.54)	8.06	7.72	7.85	7.81	7.66	8.21

	$1\ ^1E'$ ($\pi\rightarrow\pi^*$)	8.04 (88.8)	8.13 (87.6)	8.25	7.49	7.99	8.02	8.00	8.28
	$2\ ^1E'$ ($\pi\rightarrow\pi^*$)	9.44 (74.3)	9.64 (69.23)	9.08	8.99	9.80	9.99	9.79	10.28
Tetrazine	$1\ ^1B_{3u}$ ($n\rightarrow\pi^*$)	2.53 (89.6)	2.60 (88.05)	2.47	2.24	2.49	2.34	2.24	2.72
	$1\ ^1A_u$ ($\pi\rightarrow\pi^*$)	3.79 (87.5)	3.90 (85.63)	3.82	3.48	3.80	3.74	3.68	4.08
	$1\ ^1B_{2u}$ ($\pi\rightarrow\pi^*$)	5.12 (84.6)	5.16 (84.23)	5.50	4.91	4.75	4.97	4.93	5.27
	$1\ ^1B_{1g}$ ($n\rightarrow\pi^*$)	4.97 (82.5)	5.11 (82.75)	5.22	4.73	5.03	4.90	4.76	5.34
	$1\ ^1B_{2g}$ ($n\rightarrow\pi^*$)	5.34 (80.7)	5.44 (80.3)	5.57	5.18	5.41	5.28	5.08	5.71
	$2\ ^1A_u$ ($\pi\rightarrow\pi^*$)	5.46 (87.4)	5.54 (86.08)	5.77	5.47	5.46	5.34	5.23	5.70
	$2\ ^1B_{2g}$ ($n\rightarrow\pi^*$)	6.23 (79.2)	6.43 (77.75)	6.35	6.07	6.49	6.44	6.24	6.77
	$2\ ^1B_{3u}$ ($n\rightarrow\pi^*$)	6.67 (86.7)	6.79 (84.87)	7.18	6.77	6.74	6.67	6.59	7.00
	$2\ ^1B_{1g}$ ($n\rightarrow\pi^*$)	6.87 (84.7)	7.00 (82.74)	6.89	6.38	6.91	6.86	6.80	7.25
	$1\ ^1B_{1u}$ ($\pi\rightarrow\pi^*$)	7.45 (91)	7.49 (90.93)	6.93	6.96	7.61	7.44	7.38	7.66
	$2\ ^1B_{1u}$ ($\pi\rightarrow\pi^*$)	7.79 (90.2)	7.87 (88.8)	7.24	7.43	7.83	7.81	7.78	8.06
	$3\ ^1B_{1g}$ ($n\rightarrow\pi^*$)	7.08 (63.2)	7.43 (62.55)	7.09	6.74	8.00	7.96	7.23	8.36
	$1\ ^1B_{3g}$ ($n\rightarrow\pi^*$)		8.43 (83.63)			8.42	8.40	6.38	8.57
	$2\ ^1B_{2u}$ ($\pi\rightarrow\pi^*$)	8.51 (87.7)	8.62 (87.27)	8.40	8.15	8.51	8.56	8.57	8.88
	$2\ ^1B_{3g}$ ($\pi\rightarrow\pi^*$)	8.47 (63.6)	8.72 (63.06)	8.24	8.32	8.85	9.11	7.98	9.43
Formaldehyde	$1\ ^1A_2$ ($n\rightarrow\pi^*$)	3.95 (91.2)	3.96 (90.49)	4.22	3.98	3.82	3.72	3.65	3.97
	$1\ ^1B_1$ ($\sigma\rightarrow\pi^*$)	9.18 (90.9)	9.20 (90.23)	9.40	9.14	9.03	8.95	8.89	9.26
	$2\ ^1A_1$ ($\pi\rightarrow\pi^*$)	10.45 (91.3)	10.49 (88.29)			10.33	10.40	10.42	10.54
Acetone	$1\ ^1A_2$ ($n\rightarrow\pi^*$)	4.40 (90.8)	4.41 (90.01)	4.49	4.42	4.27	4.12	4.04	4.44
	$1\ ^1B_1$ ($\sigma\rightarrow\pi^*$)	9.17 (91.5)	9.19 (90.4)	9.59	9.27	9.07	8.94	8.87	9.26
	$2\ ^1A_1$ ($\pi\rightarrow\pi^*$)	9.65 (90.1)	9.73 (86.77)	9.58	9.31	9.70	9.68	9.63	9.88
Benzoquinone	$1\ ^1B_{1g}$ ($n\rightarrow\pi^*$)	2.75 (84.1)	2.85 (83.34)	3.06	2.78	2.92	2.70	2.53	3.07
	$1\ ^1A_u$ ($n\rightarrow\pi^*$)	2.85 (83)	2.95 (82.44)	3.04	2.8	3.03	2.81	2.61	3.19
	$1\ ^1B_{3g}$ ($\pi\rightarrow\pi^*$)	4.59 (87.9)	4.68 (86.14)	4.43	4.25	4.70	4.68	4.56	4.93
	$1\ ^1B_{1u}$ ($\pi\rightarrow\pi^*$)	5.62 (88.4)	5.69 (86.51)	5.02	5.29	5.70	5.60	5.54	5.90
	$1\ ^1B_{3u}$ ($n\rightarrow\pi^*$)	5.82 (75.2)	6.05 (73.06)	5.96	5.6	6.31	6.25	5.74	6.55
	$2\ ^1B_{3g}$ ($\pi\rightarrow\pi^*$)	7.27 (88.8)	7.37 (82.04)	6.82	6.98	7.41	7.37	7.18	7.63
	$2\ ^1B_{1u}$ ($\pi\rightarrow\pi^*$)	7.82 (68.6)	7.98 (68.77)	7.78	7.91	8.38	8.34	7.52	8.47
Formamide	$1\ ^1A''$ ($n\rightarrow\pi^*$)	5.65 (90.7)	5.66 (90.01)	5.93	5.63	5.48	5.37	5.32	5.66
	$2\ ^1A'$ ($\pi\rightarrow\pi^*$)	8.27 (87.9)	8.35 (85.2)	7.81	7.44	8.32	8.36	8.35	8.51
	$3\ ^1A'$ ($\pi\rightarrow\pi^*$)	10.93 (86.6)	11.09 (82.33)	10.97	10.54	11.05	11.13	11.11	11.40
Acetamide	$1\ ^1A''$ ($n\rightarrow\pi^*$)	5.69 (90.6)	5.71 (89.78)	5.96	5.8	5.49	5.38	5.33	5.71
	$2\ ^1A'$ ($\pi\rightarrow\pi^*$)	7.69 (86.6)	7.76 (87.09)	7.69	7.27	7.61	7.65	7.66	7.88
	$3\ ^1A'$ ($\pi\rightarrow\pi^*$)	10.53 (84.9)	10.60 (85.88)	10.5	10.09	10.50	10.54	10.54	10.79
Propanamide	$1\ ^1A''$ ($n\rightarrow\pi^*$)	5.72 (90.6)	5.73 (89.76)	5.99	5.72	5.50	5.40	5.35	5.74
	$2\ ^1A'$ ($\pi\rightarrow\pi^*$)	7.67 (86.2)	7.74 (86.75)	7.61	7.2	7.66	7.67	7.67	7.87
	$3\ ^1A'$ ($\pi\rightarrow\pi^*$)	10.08 (85.6)	10.15 (86.19)	10.37	9.94	10.02	10.07	10.04	10.35
Cytosine	$1\ ^1A'$ ($\pi\rightarrow\pi^*$)					4.46	4.61	4.60	
	$1\ ^1A''$ ($n\rightarrow\pi^*$)					5.12	5.07	5.02	

	$2\ ^1A'\ (\pi\rightarrow\pi^*)$	5.54	5.64	5.58
	$2\ ^1A''\ (n\rightarrow\pi^*)$	5.66	5.59	5.53
	$3\ ^1A'\ (\pi\rightarrow\pi^*)$	6.43	6.50	6.51
	$4\ ^1A'\ (\pi\rightarrow\pi^*)$	6.86	6.91	6.85
	$5\ ^1A'\ (\pi\rightarrow\pi^*)$	7.73	7.71	7.68
	$6\ ^1A'\ (\pi\rightarrow\pi^*)$	8.18	8.16	8.12
Thymine	$1\ ^1A''\ (n\rightarrow\pi^*)$	4.87	4.75	4.67
	$1\ ^1A'\ (\pi\rightarrow\pi^*)$	5.13	5.24	5.24
	$2\ ^1A''\ (n\rightarrow\pi^*)$	6.28	6.19	6.14
	$2\ ^1A'\ (\pi\rightarrow\pi^*)$	6.37	6.44	6.36
	$3\ ^1A'\ (\pi\rightarrow\pi^*)$	6.67	6.76	6.71
	$3\ ^1A''\ (n\rightarrow\pi^*)$	6.70	6.67	6.63
	$4\ ^1A''\ (n\rightarrow\pi^*)$	7.25	7.25	7.21
	$4\ ^1A'\ (\pi\rightarrow\pi^*)$	7.40	7.51	7.50
	$5\ ^1A'\ (\pi\rightarrow\pi^*)$	8.33	8.33	8.30
Uracil	$1\ ^1A''\ (n\rightarrow\pi^*)$	4.87	4.74	4.66
	$1\ ^1A'\ (\pi\rightarrow\pi^*)$	5.18	5.33	5.34
	$2\ ^1A''\ (n\rightarrow\pi^*)$	6.19	6.11	6.08
	$2\ ^1A'\ (\pi\rightarrow\pi^*)$	6.37	6.43	6.34
	$3\ ^1A'\ (\pi\rightarrow\pi^*)$	6.82	6.91	6.86
	$3\ ^1A''\ (n\rightarrow\pi^*)$	6.87	6.84	6.80
	$4\ ^1A'\ (\pi\rightarrow\pi^*)$	7.26	7.43	7.44
	$4\ ^1A''\ (n\rightarrow\pi^*)$	7.26	7.27	7.22
	$5\ ^1A'\ (\pi\rightarrow\pi^*)$	8.29	8.28	8.26
Adenine	$1\ ^1A'\ (\pi\rightarrow\pi^*)$	4.87	5.02	4.98
	$1\ ^1A''\ (n\rightarrow\pi^*)$	5.24	5.18	5.15
	$2\ ^1A'\ (\pi\rightarrow\pi^*)$	5.39	5.36	5.29
	$2\ ^1A''\ (n\rightarrow\pi^*)$	5.86	5.78	5.73
	$3\ ^1A'\ (\pi\rightarrow\pi^*)$	6.56	6.55	6.49
	$4\ ^1A'\ (\pi\rightarrow\pi^*)$	6.68	6.77	6.68
	$5\ ^1A'\ (\pi\rightarrow\pi^*)$	6.85	6.84	6.73
	$6\ ^1A'\ (\pi\rightarrow\pi^*)$	7.42	7.40	7.31
	$7\ ^1A'\ (\pi\rightarrow\pi^*)$	7.81	7.78	7.68

Table 3.2b: Vertical triplet excitation energies in eV for all statistically evaluated molecules.

Molecule	State	CC3 (%T1)	NEVPT2	CASPT2	STEOM-CC	EOM-CCSD (%T1)
Ethene	$1\ ^3B_{1u}$ ($\pi\rightarrow\pi^*$)	4.48 (99.30)	4.60	4.60	4.42	4.42 (99.4)
E-Butadiene	$1\ ^3B_u$ ($\pi\rightarrow\pi^*$)	3.32 (98.50)	3.39	3.44	3.13	3.25 (98.9)
	$1\ ^3A_g$ ($\pi\rightarrow\pi^*$)	5.17 (98.90)	5.28	5.16	4.99	5.15 (99.1)
E-Hexatriene	$1\ ^3B_u$ ($\pi\rightarrow\pi^*$)	2.69 (98.00)	2.74	2.71	2.46	2.62 (98.6)
	$1\ ^3A_g$ ($\pi\rightarrow\pi^*$)	4.32 (98.40)	4.40	4.31	4.18	4.28 (98.9)
E-Octatetraene	$1\ ^3B_u$ ($\pi\rightarrow\pi^*$)	2.30 (97.60)	2.33	2.33	2.06	2.23 (98.5)
	$1\ ^3A_g$ ($\pi\rightarrow\pi^*$)	3.67 (98.10)	3.73	3.69	3.51	3.62 (98.7)
Cyclopropene	$1\ ^3B_2$ ($\pi\rightarrow\pi^*$)	4.34 (99.10)	4.56	4.35	4.08	4.30 (99.2)
	$1\ ^3B_1$ ($\sigma\rightarrow\pi^*$)	6.62 (98.10)	6.58	6.51	6.55	6.66 (98.5)
Cyclopentadiene	$1\ ^3B_2$ ($\pi\rightarrow\pi^*$)	3.25 (98.50)	3.33	3.28	3.07	3.18 (98.9)
	$1\ ^3A_1$ ($\pi\rightarrow\pi^*$)	5.09 (98.70)	5.23	5.10	5.02	5.07 (99)
Norbornadiene	$1\ ^3A_2$ ($\pi\rightarrow\pi^*$)	3.72 (98.70)	3.81	3.75	3.49	3.67 (99)
	$1\ ^3B_2$ ($\pi\rightarrow\pi^*$)	4.16 (99.00)	4.31	4.22	3.89	4.09 (99.2)
Benzene	$1\ ^3B_{1u}$ ($\pi\rightarrow\pi^*$)	4.12 (98.70)	4.33	4.17	3.52	3.94 (99)
	$1\ ^3E_{1u}$ ($\pi\rightarrow\pi^*$)	4.90 (97.00)	5.00	4.90	4.80	4.97 (97.9)
	$1\ ^3B_{2u}$ ($\pi\rightarrow\pi^*$)	6.04 (98.20)	5.54	5.76	5.97	6.00 (98.6)
	$1\ ^3E_{2g}$ ($\pi\rightarrow\pi^*$)	7.49 (94.90)	7.61	7.41	7.53	7.73 (97.6)
Naphthalene	$1\ ^3B_{2u}$ ($\pi\rightarrow\pi^*$)	3.11 (97.30)	3.28	3.20	2.71	2.99 (98.2)
	$1\ ^3B_{3u}$ ($\pi\rightarrow\pi^*$)	4.18 (93.20)	4.27	4.29	4.13	4.27 (97.9)
	$1\ ^3B_{1g}$ ($\pi\rightarrow\pi^*$)	4.47 (96.90)	4.59	4.55	4.22	4.44 (97.4)
	$2\ ^3B_{2u}$ ($\pi\rightarrow\pi^*$)	4.64 (97.80)	4.73	4.71	4.46	4.67 (98.6)
	$2\ ^3B_{3u}$ ($\pi\rightarrow\pi^*$)	5.11 (96.80)	4.53	5.00	5.03	5.10 (97.8)
	$1\ ^3A_g$ ($\pi\rightarrow\pi^*$)	5.52 (96.50)	5.62	5.57	5.42	5.57 (97.7)
	$2\ ^3B_{1g}$ ($\pi\rightarrow\pi^*$)	6.48 (97.60)	5.95	6.25	6.64	6.79 (98.3)
	$2\ ^3A_g$ ($\pi\rightarrow\pi^*$)	6.47 (97.90)	6.25	6.42	6.66	6.81 (98.5)
	$3\ ^3A_g$ ($\pi\rightarrow\pi^*$)	6.79 (95.00)	6.56	6.63	6.77	6.96 (97.3)
	$3\ ^3B_{1g}$ ($\pi\rightarrow\pi^*$)	6.76 (94.00)	6.83	6.67	6.83	7.04 (97.3)
Furan	$1\ ^3B_2$ ($\pi\rightarrow\pi^*$)	4.17 (98.50)	4.36	4.17	3.84	4.10 (98.9)
	$1\ ^3A_1$ ($\pi\rightarrow\pi^*$)	5.48 (98.20)	5.67	5.49	5.28	5.48 (98.7)
Pyrrole	$1\ ^3B_2$ ($\pi\rightarrow\pi^*$)	4.48 (98.40)	4.74	4.52	4.18	4.41 (98.8)
	$1\ ^3A_1$ ($\pi\rightarrow\pi^*$)	5.51 (97.80)	5.70	5.53	5.46	5.54 (98.4)
Imidazole	$1\ ^3A'$ ($\pi\rightarrow\pi^*$)	4.69 (98.40)	4.80	4.65	4.40	4.62 (98.8)
	$2\ ^3A'$ ($\pi\rightarrow\pi^*$)	5.79 (97.90)	5.93	5.74	5.68	5.83 (98.5)
	$1\ ^3A''$ ($n\rightarrow\pi^*$)	6.37 (97.40)	6.49	6.36	6.23	6.43 (98.3)
	$3\ ^3A'$ ($\pi\rightarrow\pi^*$)	6.55 (97.90)	6.67	6.44	6.40	6.56 (98.4)

	$4\ ^3A'$ ($\pi\rightarrow\pi^*$)	7.42 (97.10)	7.15	7.43	7.32	7.54 (98)
	$2\ ^3A''$ ($n\rightarrow\pi^*$)	7.51 (96.00)	7.61	7.51	7.56	7.76 (97.6)
Pyridine	$1\ ^3A_1$ ($\pi\rightarrow\pi^*$)	4.25 (98.60)	4.48	4.27	3.69	4.07 (99)
	$1\ ^3B_1$ ($n\rightarrow\pi^*$)	4.50 (97.10)	4.60	4.55	4.39	4.61 (98.1)
	$1\ ^3B_2$ ($\pi\rightarrow\pi^*$)	4.86 (97.20)	4.97	4.72	4.82	4.91 (98)
	$2\ ^3A_1$ ($\pi\rightarrow\pi^*$)	5.05 (97.00)	5.16	5.03	5.00	5.13 (97.9)
	$1\ ^3A_2$ ($n\rightarrow\pi^*$)	5.46 (95.80)	5.49	5.48	5.43	5.67 (97.5)
	$2\ ^3B_2$ ($\pi\rightarrow\pi^*$)	6.40 (97.80)	6.49	6.02	6.34	6.41 (98.3)
	$3\ ^3A_1$ ($\pi\rightarrow\pi^*$)	7.66 (95.30)	7.87	7.56	7.73	7.90 (97.7)
	$3\ ^3B_2$ ($\pi\rightarrow\pi^*$)	7.83 (94.40)	7.28	7.88	7.94	8.12 (97.4)
Tetrazine	$1\ ^3B_{3u}$ ($n\rightarrow\pi^*$)	1.89 (97.20)	1.69	1.56	1.79	1.99 (98.1)
	$1\ ^3A_u$ ($n\rightarrow\pi^*$)	3.52 (96.30)	3.46	3.26	3.55	3.74 (97.7)
	$1\ ^3B_{1u}$ ($\pi\rightarrow\pi^*$)	4.33 (98.50)	4.56	4.36	3.67	4.05 (99)
	$1\ ^3B_{1g}$ ($n\rightarrow\pi^*$)	4.21 (97.10)	4.37	4.14	4.04	4.31 (98.2)
	$1\ ^3B_{2u}$ ($\pi\rightarrow\pi^*$)	4.54 (97.40)	4.76	4.56	4.53	4.57 (98.1)
	$1\ ^3B_{2g}$ ($n\rightarrow\pi^*$)	4.93 (96.40)	5.22	4.93	4.87	5.09 (98)
	$2\ ^3A_u$ ($n\rightarrow\pi^*$)	5.03 (96.60)	5.11	5.02	5.01	5.20 (97.8)
	$2\ ^3B_{1u}$ ($\pi\rightarrow\pi^*$)	5.38 (96.50)	5.54	5.40	5.42	5.48 (97.5)
	$2\ ^3B_{2g}$ ($n\rightarrow\pi^*$)	6.04 (93.00)	6.18	5.97	6.29	6.51 (96.8)
	$2\ ^3B_{3u}$ ($n\rightarrow\pi^*$)	6.53 (95.80)	6.78	6.54	6.63	6.80 (97.5)
	$2\ ^3B_{1g}$ ($n\rightarrow\pi^*$)	6.60 (92.30)	6.62	6.31	6.86	7.11 (96.9)
	$2\ ^3B_{2u}$ ($\pi\rightarrow\pi^*$)	7.36 (96.80)	6.54	7.10	7.52	7.46 (97.7)
Formaldehyde	$1\ ^3A_2$ ($n\rightarrow\pi^*$)	3.55 (98.10)	3.75	3.58	3.50	3.52 (98.6)
	$1\ ^3A_1$ ($\pi\rightarrow\pi^*$)	5.83 (99.20)	6.05	5.84	5.65	5.78 (99.3)
Acetone	$1\ ^3A_2$ ($n\rightarrow\pi^*$)	4.05 (97.90)	4.13	4.08	3.95	4.03 (98.4)
	$1\ ^3A_1$ ($\pi\rightarrow\pi^*$)	6.03 (98.90)	6.04	6.03	5.81	5.94 (99.1)
Benzoquinone	$1\ ^3B_{1g}$ ($n\rightarrow\pi^*$)	2.51 (95.90)	2.88	2.63	2.54	2.71 (97.9)
	$1\ ^3B_{1u}$ ($\pi\rightarrow\pi^*$)	2.96 (97.80)	2.94	2.99	2.64	2.89 (98.5)
	$1\ ^3A_u$ ($n\rightarrow\pi^*$)	2.62 (95.70)	2.89	2.68	2.65	2.83 (97.8)
	$1\ ^3B_{3g}$ ($\pi\rightarrow\pi^*$)	3.41 (98.00)	3.43	3.31	3.20	3.42 (98.6)
Formamide	$1\ ^3A''$ ($n\rightarrow\pi^*$)	5.36 (97.80)	5.65	5.40	5.23	5.32 (98.4)
	$1\ ^3A'$ ($\pi\rightarrow\pi^*$)	5.74 (98.40)	5.87	5.58	5.63	5.67 (98.7)
Acetamide	$1\ ^3A''$ ($n\rightarrow\pi^*$)	5.42 (98.30)	5.54	5.53	5.26	5.39 (98.4)
	$1\ ^3A'$ ($\pi\rightarrow\pi^*$)	5.88 (98.30)	5.67	5.75	5.73	5.83 (98.7)
Propanamide	$1\ ^3A''$ ($n\rightarrow\pi^*$)	5.45 (97.70)	5.60	5.44	5.27	5.41 (98.4)
	$1\ ^3A'$ ($\pi\rightarrow\pi^*$)	5.90 (98.30)	5.90	5.79	5.74	5.84 (98.7)

In the following sections, we analyze our benchmark results and draw conclusions regarding STEOM methods.

III.B.1. CC3 against EOM-CCSDT-3

In this subsection we analyze the benchmark results for CC3 and EOM-CCSDT-3 methods for the singlet excitations. For the triplet excitations, as reported by Schreiber et al., EOM-CCSD results are very close to CC3 results. This reflects that electron correlation effects are less pronounced for triplet excited states. For this reason one can expect also EOM-CCSDT-3 results to be very close for the triplet states, and no further analysis was attempted. A critical parameter that is used to gauge the reliability of CC3 calculations is the %T1 diagnostic. If this parameter becomes too small, double excitations are important, and correspondingly the perturbative treatment of triples corrections in CC3 or EOM-CCSDT-3 becomes suspect. We use a %T1 threshold value 87%, meaning that only states that have %T1 larger than or equal to this value are included in the statistical analysis. All excitation energies are reported in Tables 3.2a and 3.2b regardless of %T1. Our %T1 threshold is somewhat conservative probably, and 85% has been used also in the literature [72].

We present our statistical data for the comparison between CC3 and EOM-CCSDT-3 in Table 3.3.

Statistics	EOM-CCSDT-3 − CC3
Minimum Error	0.006
Maximum Error	0.113
Mean Error	0.049
Mean Absolute Error	0.049
Root Mean Square Error	0.056
Standard Deviation	0.027

Table 3.3: Statistical analysis of the benchmark set excitation energy deviations in eV of EOM-CCSDT-3 from CC3 for singlet states with T1≥87%.

We also perform a histogram bar chart analysis for our results (Figure 3.2a). In such a chart one counts the number of occurrences (errors or deviations here) in given equally spaced intervals. The bin size determines our distribution as the central interval is always centered around zero. This bin size is reported in the figure caption. To get a qualitative picture of the distribution, we also construct continuous plots. This is a more convenient representation if a number of distributions are examined in a single graph. We emphasize that continuous plots (using 3-point spline extrapolation) are not an entirely accurate representation of our results, as our results are constituted of discrete data points. In all following subsections, we use continuous plots to represent our data as they provide significant ease and insight of the distribution studied. We also note that the distribution is sensitive to the bin size chosen. We always attempt to choose a convenient bin size that will provide a suitable representation of the data.

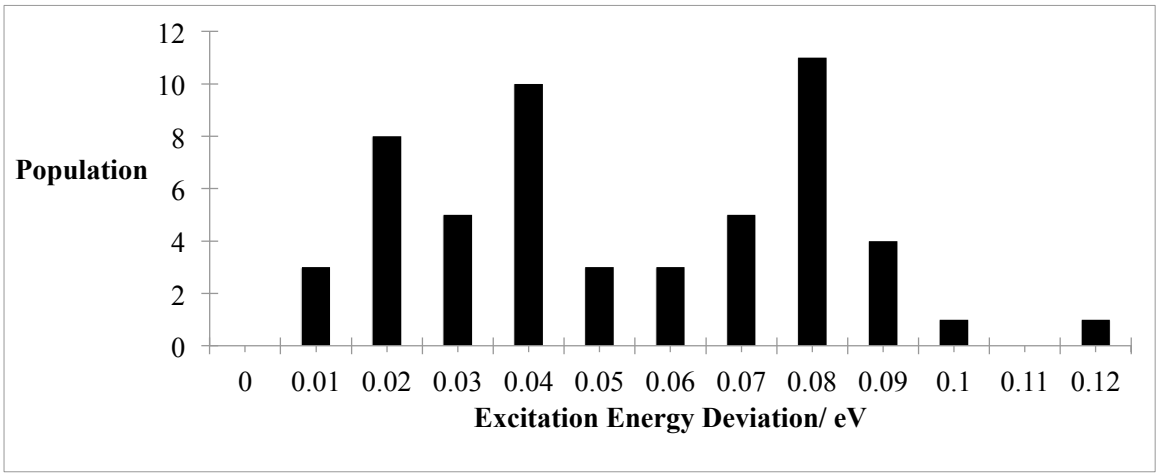

Figure 3.2a: Histogram bar chart (bin size 0.01), showing distribution of the benchmark set excitation energy deviations of EOM-CCSDT-3 from CC3 for singlet states with %T1≥87%.

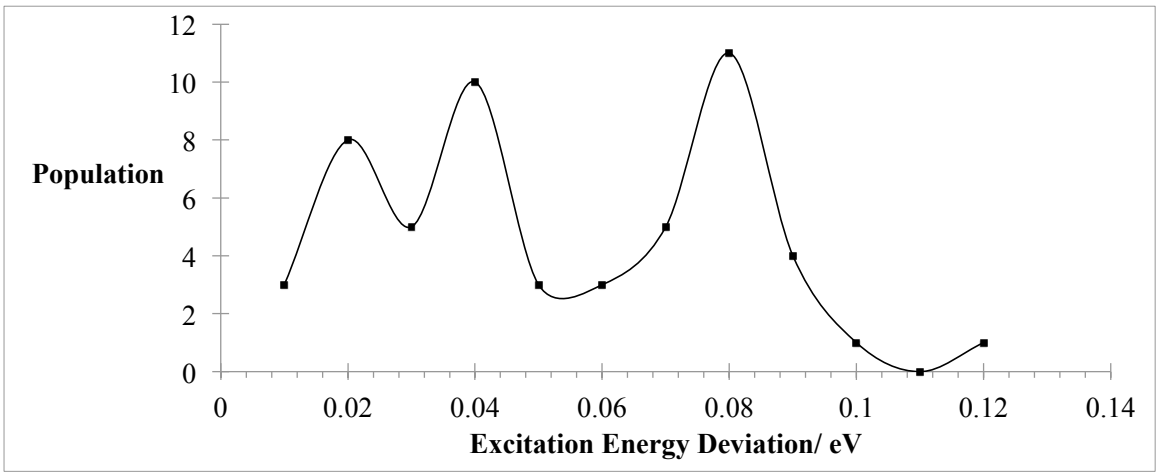

Figure 3.2b: Continuous curves as a representation for the distribution of the benchmark set excitation energy deviations of EOM-CCSDT-3 from CC3 for singlet states with T1≥87%.

The results presented here are somewhat surprising. From previous CC3 benchmark studies on small molecules it has been established that CC3 results can be expected to be quite close to the full Configuration Interaction (CI) solution, within a mean absolute error of only 0.016 eV for singles dominated singlet as well as triplet excitation energies

[105]. From a formal theoretical perspective the EOM-CCSDT-3 approach is slightly more complete than CC3, and is likewise expected to be close to the full CI. Nonetheless, for the present test set of larger molecules, we find somewhat significant deviations of around 0.08 eV, quite frequently. We note that all deviations greater than 0.07 eV are $\pi \rightarrow \pi^*$ excitations with the exception of two deep lying states for pyridazine and tetrazine, which are $n \rightarrow \pi^*$ excitations. Since these methods serve to benchmark our STEOM results, and other approaches in the literature, e.g. [93, 96], these deviations are larger than we would like. These results are indicative that a future more accurate benchmark is desired. A possible candidate for such a future benchmark might be the CC(P;Q) approach developed by Shen and Piecuch [39, 40] or the full EOM-CCSDT approach [106, 107].

III.B.2. STEOM-H (ω) Methods

As discussed in section II., a hermitized version of STEOM is of interest, and we discussed a continuous family of approaches denoted STEOM-H (ω), with the $\omega \rightarrow \infty$ limit representing the simplest averaging of the transformed Hamiltonian and its transpose. Here we present the results of the statistical analysis of the benchmarks of different STEOM-H (ω) methods compared to STEOM-CC in Tables 3.4a and 3.4b for singlet excitations and triplet excitations respectively.

Statistics	**STEOM-H (ω*)**	**STEOM-H (0)**	**STEOM-H (0.5)**	**STEOM-H (∞)**
Minimum Error	-0.103	-0.073	-0.098	-0.124
Maximum Error	0.000	-0.003	-0.004	-0.012
Mean Error	-0.016	-0.023	-0.033	-0.048
Mean Absolute Error	0.016	0.023	0.033	0.048
Root Mean Square Error	0.020	0.025	0.037	0.052
Standard Deviation	0.012	0.012	0.016	0.020

Table 3.4a: Statistical analysis of the benchmark set excitation energy deviations in eV of STEOM-H (ω) methods from STEOM-CC for singlet states.

Statistics	**STEOM-H (ω*)**	**STEOM-H (0)**	**STEOM-H (0.5)**	**STEOM-H (∞)**
Minimum Error	-0.026	-0.036	-0.053	-0.071
Maximum Error	0.004	-0.002	-0.005	-0.010
Mean Error	-0.006	-0.013	-0.023	-0.037
Mean Absolute Error	0.007	0.013	0.023	0.037
Root Mean Square Error	0.009	0.014	0.025	0.039
Standard Deviation	0.006	0.006	0.010	0.014

Table 3.4b: Statistical analysis of the benchmark set excitation energy deviations in eV of STEOM-H (ω) methods from STEOM-CC for triplet states.

As in the previous section, we perform a histogram analysis for the results and we represent the distributions as continuous curves (Figures 3.3a and 3.3b).

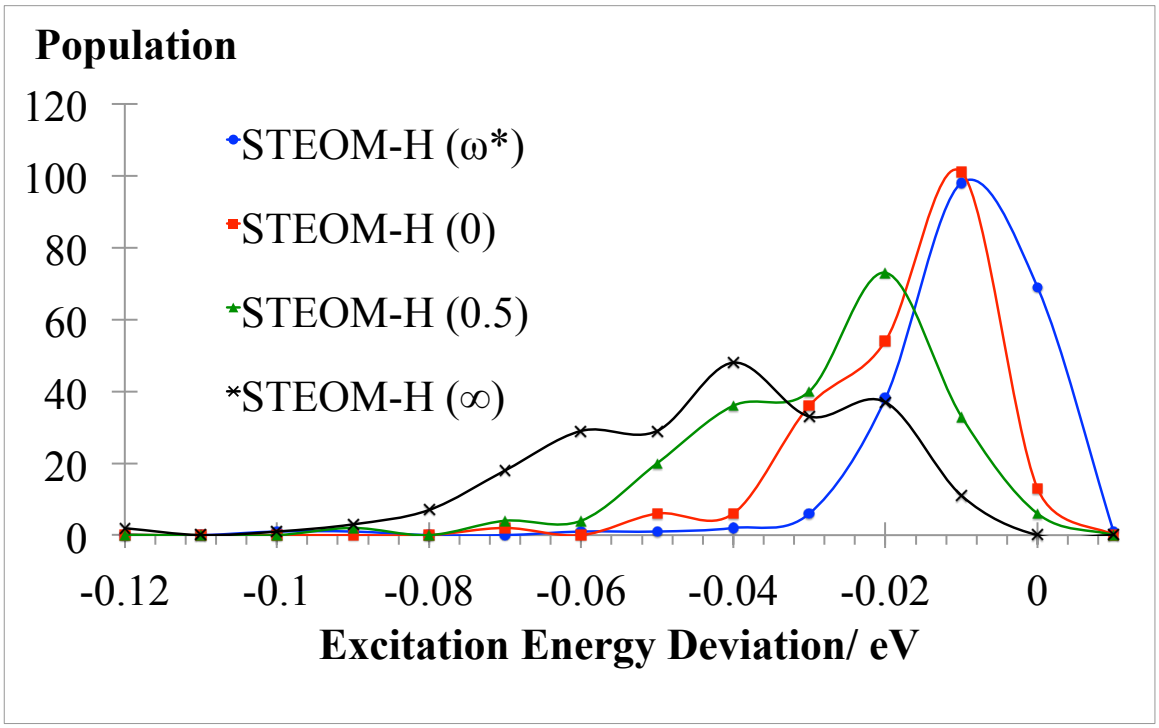

Figure 3.3a: Distribution of the benchmark set excitation energy deviations of STEOM-H (ω) methods from STEOM-CC for singlet states. Bin size: 0.01.

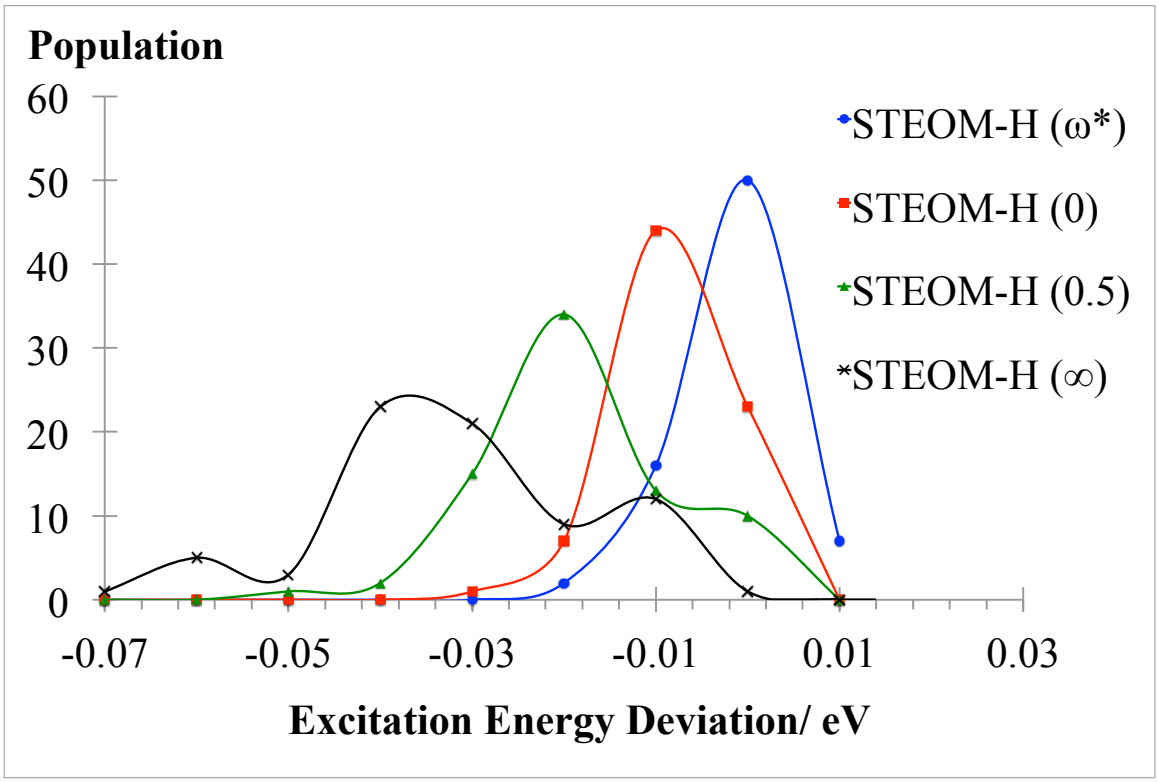

Figure 3.3b: Distribution of the benchmark set excitation energy deviations of STEOM-H (ω) methods from STEOM-CC for triplet states. Bin size: 0.01.

The best STEOM-H method is unambiguously the STEOM-H (ω*) approach. Let us recall that in this approach the ω parameter is determined for each symmetry block of excitation energies separately from the diagonal elements of the sector of the transformed Hamiltonian. In practice the value of ω* is between -0.1 a.u. or -2.7 eV and -0.2 a.u. or -5.4 eV. The deviation from STEOM-CC monotonically increases as ω increases with greatest deviation for $\omega \rightarrow \infty$ as is evident from Figures 3.3a and 3.3b. Since these results are quite close to STEOM-CC in general, no further analysis of the hermitized approaches is needed. Their trends will clearly follow the parent STEOM-CC approach.

III.B.3. STEOM-ORB

Next we investigate another minor issue: the dependence of STEOM-CC results on the precise choice of active orbitals. In the STEOM-ORB approach a set of "natural orbitals" is introduced within the subspaces of occupied and virtual Hartree-Fock orbitals, as discussed in section II. We present the results of the statistical analysis of the benchmarks of STEOM-ORB compared to STEOM-CC in Table 3.5 for singlet excitations and triplet excitations.

Statistics	Singlets	Triplets
Minimum Error	-0.055	-0.043
Maximum Error	0.004	0.002
Mean Error	-0.008	-0.014
Mean Absolute Error	0.008	0.014
Root Mean Square Error	0.011	0.018
Standard Deviation	0.008	0.011

Table 3.5: Statistical analysis of the benchmark set excitation energy deviations in eV of STEOM-ORB from STEOM-CC for singlet states and triplet states.

The distributions are represented as continuous curves in Figures 3.4a and 3.4b below.

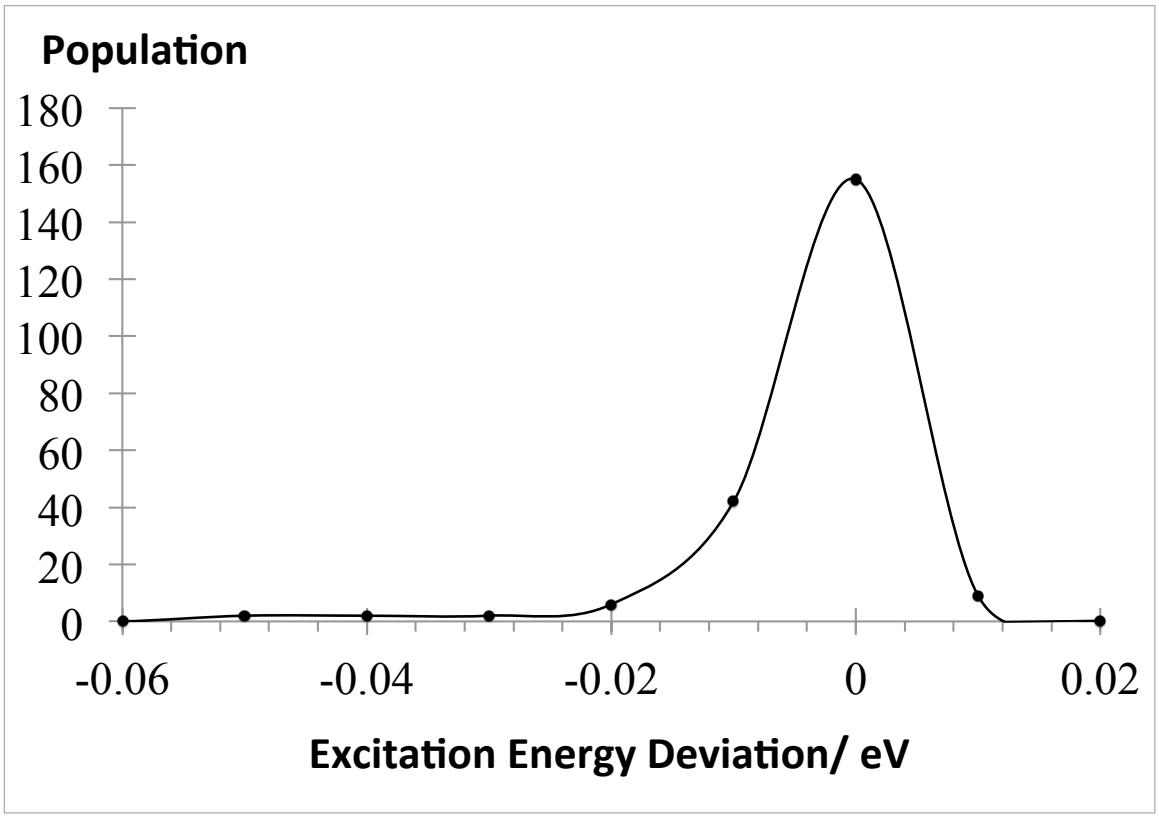

Figure 3.4a: Distribution of the benchmark set excitation energy deviations of STEOM-ORB from STEOM-CC for singlet states. Bin size: 0.01.

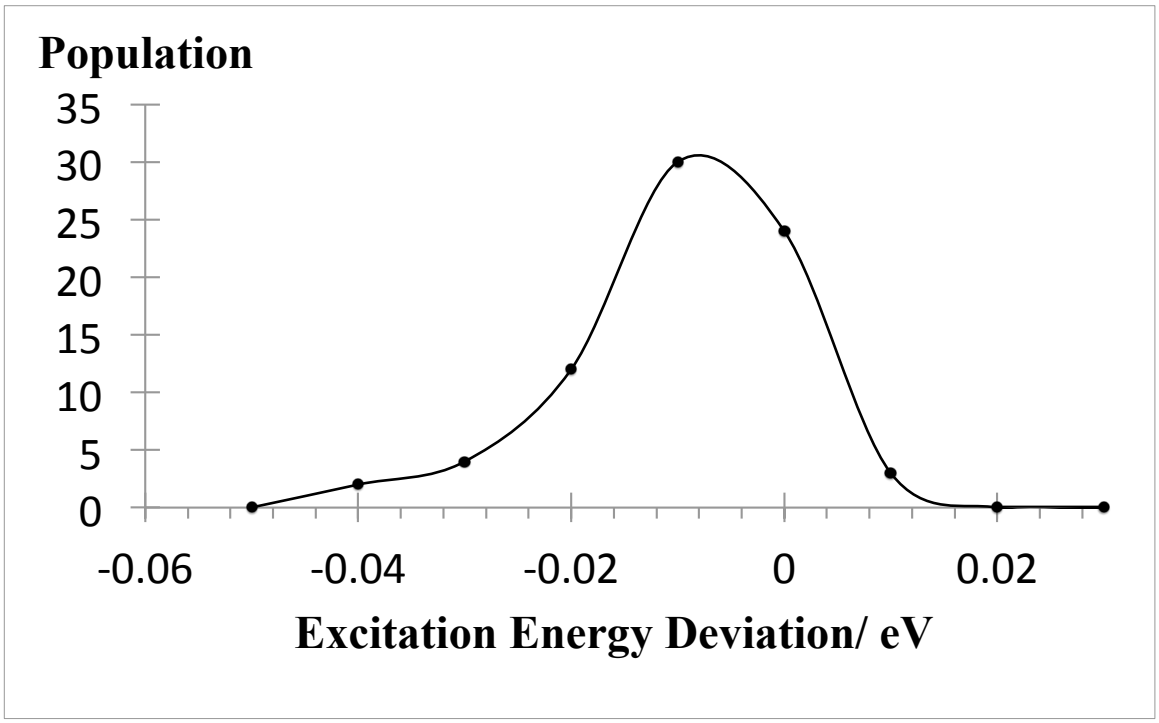

Figure 3.4b: Distribution of the benchmark set excitation energy deviations of STEOM-ORB from STEOM-CC for triplet states. Bin size: 0.01.

These results clearly indicate that STEOM-CC results are quite insensitive to the precise definition of active orbitals. This is a redeeming feature of the approach. Results are clear-cut again, and there is no need to make additional analysis of the STEOM-ORB approach. They closely follow the parent STEOM-CC results.

III.B.4. STEOM-PT

We study the results of the statistical analysis of the benchmarks of STEOM-PT compared to STEOM-CC in Table 3.6 for singlet excitations and triplet excitations.

Statistics	Singlets	Triplets
Minimum Error	-0.265	-0.188
Maximum Error	0.264	0.442
Mean Error	0.056	0.064
Mean Absolute Error	0.099	0.093
Root Mean Square Error	0.121	0.120
Standard Deviation	0.107	0.102

Table 3.6: Statistical analysis of the benchmark set excitation energy deviations in eV of STEOM-PT from STEOM-CC for singlet states and triplet states.

We demonstrate the distributions as continuous curves (Figures 3.5a and 3.5b) to provide insight about the STEOM-PT methodology.

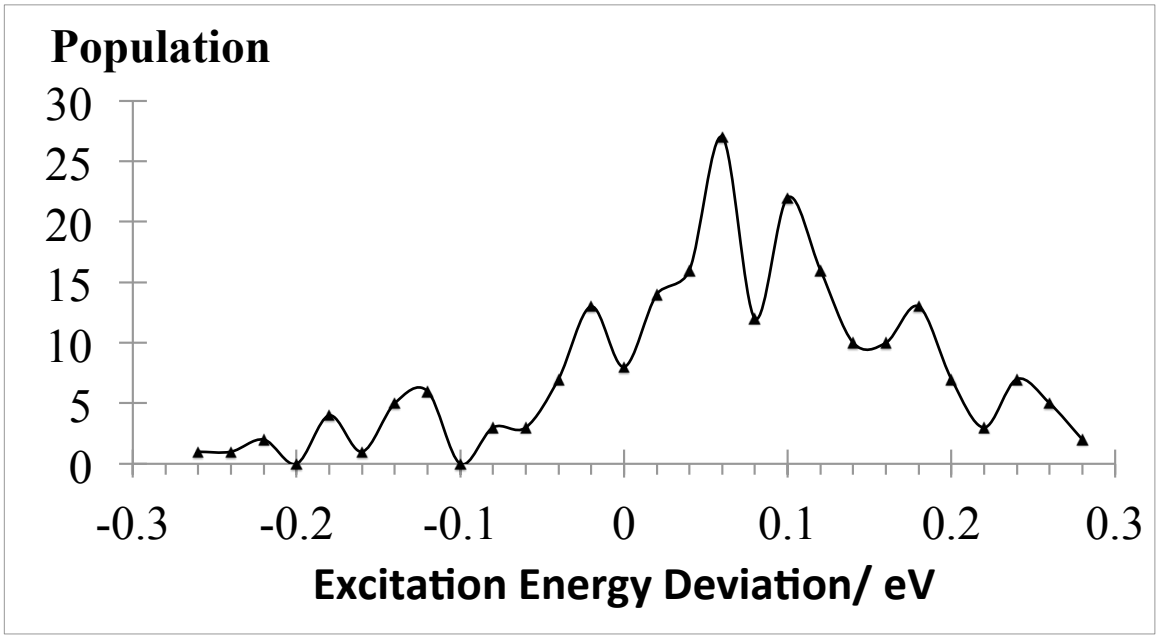

Figure 3.5a: Distribution of the benchmark set excitation energy deviations of STEOM-PT from STEOM-CC for singlet states. Bin size: 0.02.

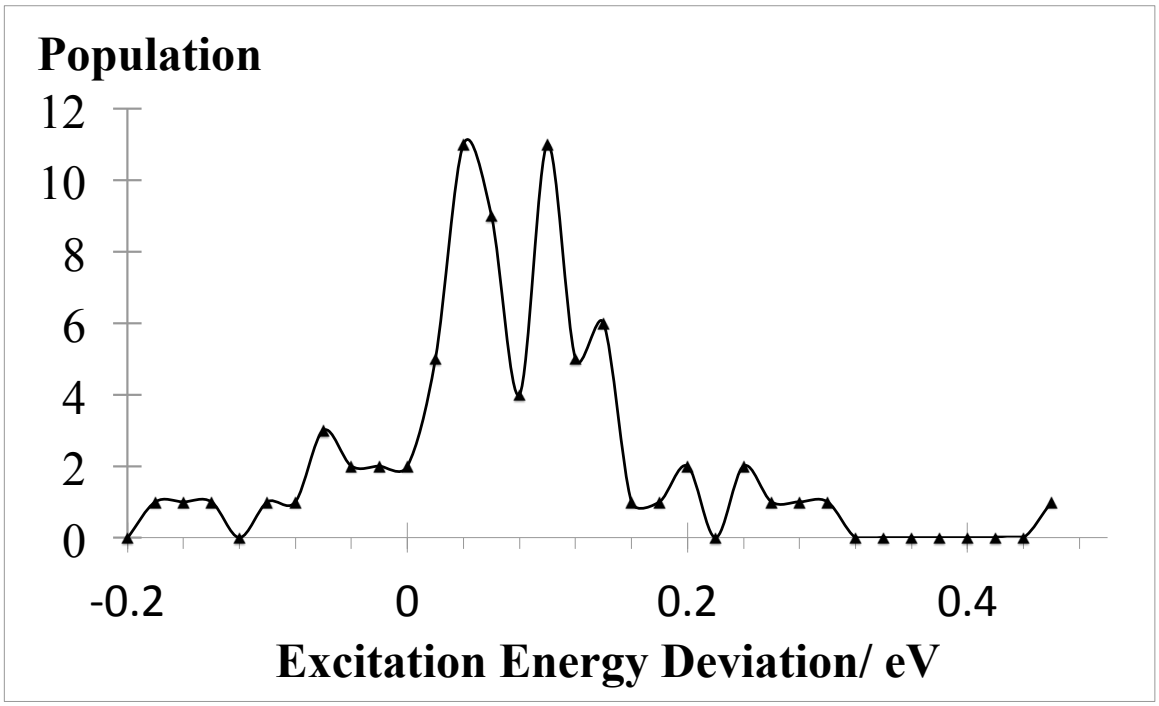

Figure 3.5b: Distribution of the benchmark set excitation energy deviations of STEOM-PT from STEOM-CC for triplet states. Bin size: 0.02.

The deviations of STEOM-PT from STEOM-CC for singlet states are rather erratic and the distribution for deviations is quite spread out with some sizeable deviations. For triplet states, the distribution of deviations is likewise rather broad. Given these results, and the fact that STEOM-CC is only about twice as demanding as STEOM-PT, the STEOM-PT approach is not all that interesting. Only if the calculation of the EA amplitudes would be approximated with a cheaper method like for example with the partitioned EOM-CC approach [108], results that might have merits should prove interesting.

III.B.5. STEOM-CC, STEOM-D and EOM-CCSD against CC3 and EOM-CCSDT-3

In this section we discuss the accuracy of STEOM-CC, STEOM-D and EOM-CCSD against CC3 and EOM-CCSDT-3. We commence by discussing results for singlet excitations and then we discuss results for triplet excitations.

III.B.5.1 Singlet Excitations

We present the results of the statistical analysis of the benchmarks of STEOM-CC, STEOM-D, EXT-STEOM and EOM-CCSD compared to CC3 and EOM-CCSDT-3 (separated by a slash) in Table 3.7 and we plot continuous distributions in Figures 3.6a and 3.6b. Again, we only include CC3 and EOM-CCSDT-3 results with T1≥87% for the reasons mentioned in section III.B.1.

Statistics	STEOM-CC	STEOM-D	EXT-STEOM	EOM-CCSD
Minimum Error	-0.219 / -0.229	-0.323 / -0.334	-0.374 / -0.384	0.009 / -0.002
Maximum Error	0.159 / 0.120	0.100 / -0.010	0.083 / -0.055	0.408 / 0.255
Mean Error	-0.019 / -0.073	-0.067 / -0.120	-0.118 / -0.161	0.198 /0.125
Mean Absolute Error	0.065 / 0.091	0.085 / 0.120	0.123 / 0.161	0.198 / 0.125
Root Mean Square Error	0.081 / 0.105	0.118 / 0.146	0.160 / 0.189	0.216 / 0.136
Standard Deviation	0.079 / 0.076	0.097 / 0.084	0.109 / 0.100	0.086 / 0.056

Table 3.7: Statistical analysis of the benchmark set excitation energy deviations in eV of STEOM-CC, STEOM-D, EXT-STEOM and EOM-CCSD from CC3 and from EOM-CCSDT-3 for singlet states. Only CC3 and EOM-CCSDT-3 states with T1≥87% are included in the analysis. A slash separates the values for the comparison against CC3 from that against EOM-CCSDT-3.

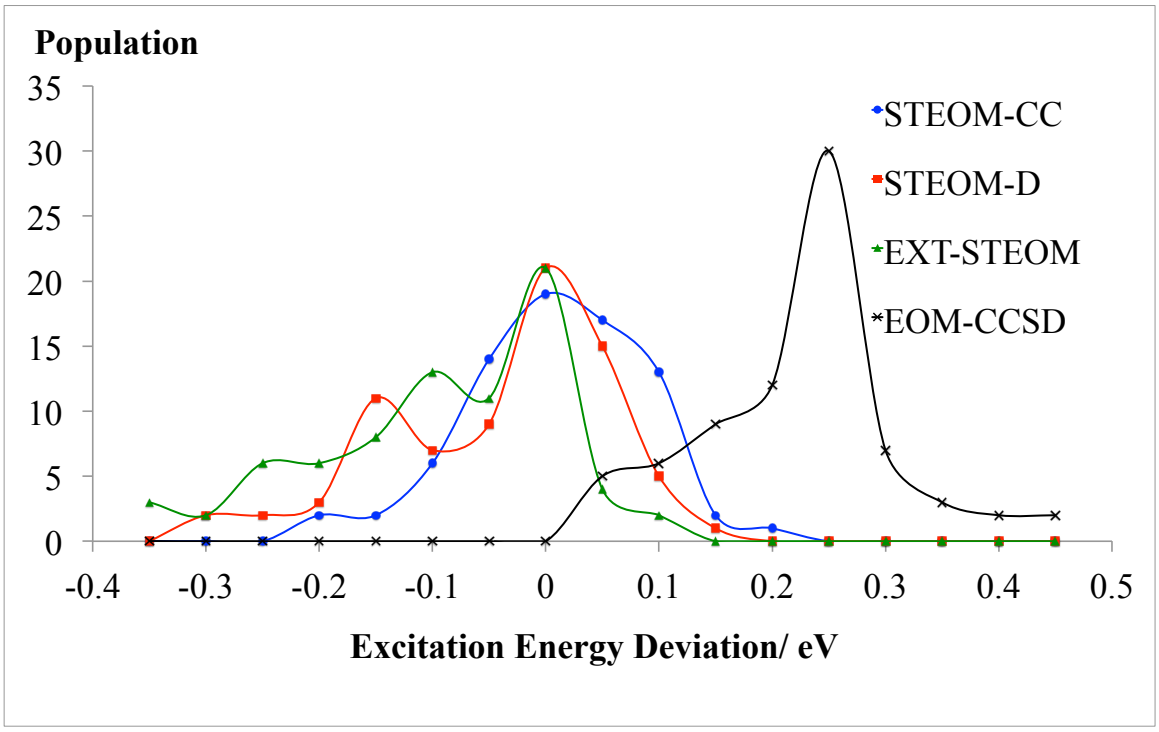

Figure 3.6a: Distribution of the benchmark set excitation energy deviations of STEOM-CC, STEOM-D, EXT-STEOM and EOM-CCSD from CC3 for singlet states. Only CC3 states with T1≥87% are included in the analysis. Bin size: 0.05.

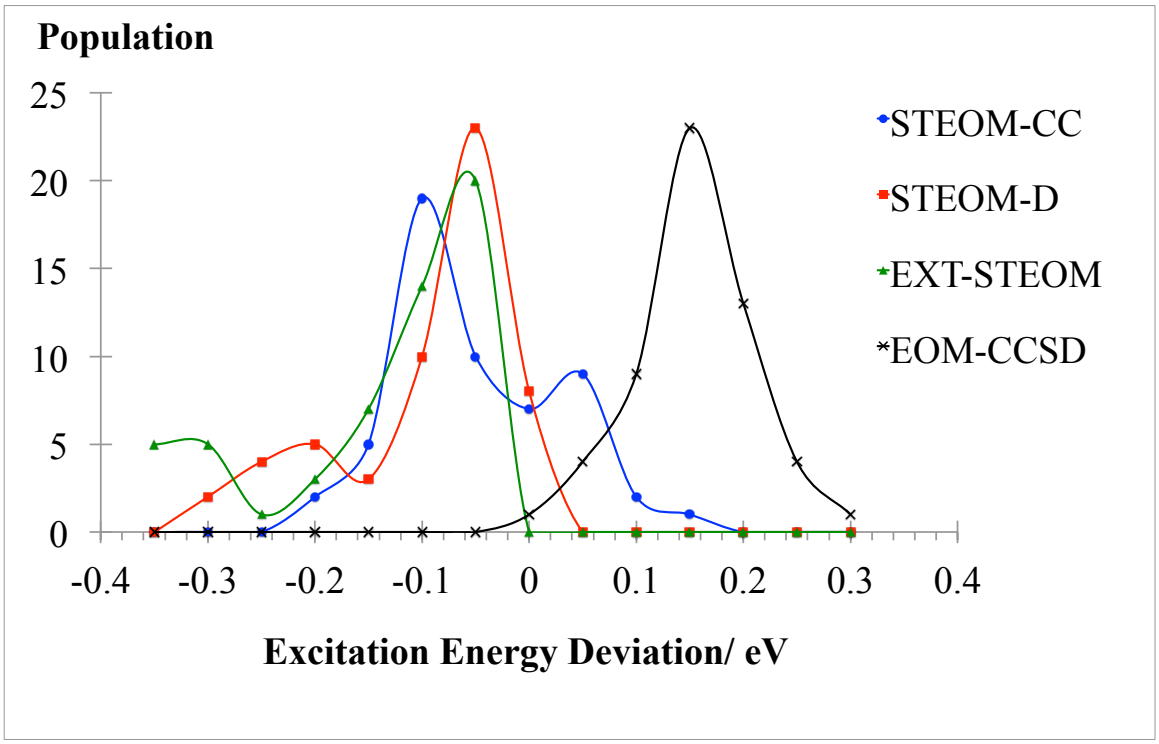

Figure 3.6b: Distribution of the benchmark set excitation energy deviations of STEOM-CC, STEOM-D, EXT-STEOM and EOM-CCSD from EOM-CCSDT-3 for singlet states. Only EOM-CCSDT-3 states with T1≥87% are included in the analysis. Bin size: 0.05.

The deviation of EOM-CCSD is very systematic in particular in comparison to EOM-CCSDT-3. This is clear from the histogram, which exhibits a sharply peaked distribution (standard deviation of 0.056 eV), centered at 0.15 eV (0.125 eV mean absolute error). The comparison with CC3 is somewhat less systematic.

For STEOM-CC the distribution is somewhat broader than for EOM-CCSD (standard deviation of 0.079 eV/ 0.076 eV). It is centered more closely to zero, in particular when compared to CC3. Overall the most relevant root mean square error is better for STEOM-CC than for EOM-CCSD.

The statistical analysis indicates that STEOM-CC is more accurate than STEOM-D. However, the histogram analysis as presented in the figures above provide additional

information, specifically that STEOM-D is quite accurate in general with the exception of some outliers. It is interesting to see that the STEOM-D has a sharper peak than STEOM-CC, in particular when compared to EOM-CCSDT-3. The distribution is shifted to about 0.05 eV lower excitation energies compared to EOM-CCSDT-3 with a wing at a deviation of around -0.2 eV. This wing corresponds to outliers, which are mostly n→π* excitations involving 'double bond O' groups found in amides, ketones and aldehydes. The only exceptions to these outliers are two σ→π* excitations.

EXT-STEOM has a broader distribution than STEOM-CC and STEOM-D. The distribution has a pronounced tail with a number of states exhibiting deviations up to about -0.4 eV. The fact that STEOM-CC and EXT-STEOM yield quite comparable results, while the size of the diagonalization manifold is greatly different, testifies to the effectiveness of the similarity transform approach. It is natural that EXT-STEOM yields lower excitation energies, as the ground state CCSD energy is the same in both approaches, while the diagonalization manifold is much larger in EXT-STEOM.

Given the low computational cost of STEOM methods and the statistical results, we can say that the STEOM approach is behaving very satisfactorily when comparing to the computationally more expensive EOM-CCSD.

III.B.5.2 Triplet Excitations

We present the results of the statistical analysis of the benchmarks of STEOM-CC, and EOM-CCSD compared to CC3 in Table 3.8 for triplet excitations and we present the distributions in Figure 3.7. First, we note that STEOM-D and EXT-STEOM methods are not implemented for triplet states, hence their absence in this section. We remind the

reader that we do not benchmark EOM-CCSDT-3 for triplet states as we expect EOM-CCSDT-3 to be very close to CC3. The reader is referred to the discussion in section III.B.1. We also note that the CC3 results for our benchmark set has a relatively high %T1 being in general above 92%. The excitation energy results are found in Table 3.2b. For this reason, we do not employ the %T1 diagnostic to filter our results and we simply include all the results in the statistical analysis.

Statistics	**STEOM-CC**	**EOM-CCSD**
Minimum Error	-0.662	-0.280
Maximum Error	0.256	0.510
Mean Error	-0.111	0.053
Mean Absolute Error	0.156	0.114
Root Mean Square Error	0.201	0.156
Standard Deviation	0.169	0.148

Table 3.8: Statistical analysis of the benchmark set excitation energy deviations in eV of STEOM-CC and EOM-CCSD from CC3 for Triplet states.

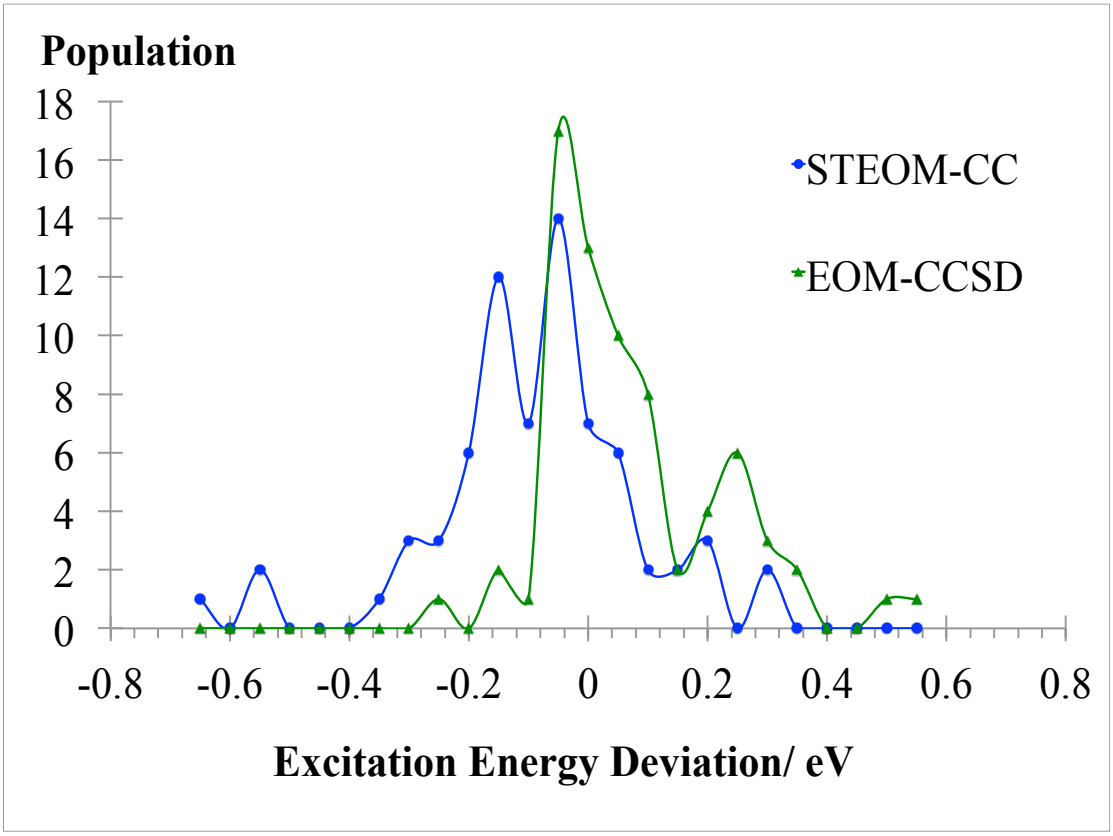

Figure 3.7: Distribution of the benchmark set excitation energy deviations of STEOM-CC and EOM-CCSD from EOM-CCSDT-3 for triplet states. Bin size: 0.05.

For triplet states STEOM-CC results show larger errors than EOM-CCSD (the root mean square error is ~ 0.20 eV for STEOM-CC compared to ~ 0.16 eV for EOM-CCSD). The difference is also evident from the plots. The error or deviation for the triplet states in STEOM-CC is even greater than in the case of singlet states. The improved accuracy of EOM-CCSD for triplet states is expected. It correlates to the larger value of %T1 in the CC3 calculations. The difficulties of STEOM to describe triplet states on the other hand are unexpected. In particular some quite large deviations (~0.66 eV) occur for low-lying triplet states. It is possible that a STEOM-D treatment would correct these errors, but this

approach has not yet been implemented. At present we do not have a good explanation for the worse behavior of STEOM for triplet states. It is surprising we think.

III.B.6. STEOM-CC, STEOM-D, NEVPT2 and CASPT2 against CC3 and EOM-CCSDT-3

In this section we compare STEOM-CC, STEOM-D to NEVPT2 and CASPT2 taking CC3 and EOM-CCSDT-3 as references for the comparison.

III.B.6.1 Singlet Excitations

We present the results of the statistical analysis of the benchmarks of STEOM-CC, STEOM-D, NEVPT2 and CASPT2 compared to CC3 and EOM-CCSDT-3 in Table 3.9. We only include states corresponding to T1≥87% in our analysis.

Statistics	STEOM-CC	STEOM-D	NEVPT2	CASPT2
Minimum Error	-0.219/ -0.229	-0.323/-0.334	-0.770/ -0.803	-0.830/ -0.654
Maximum Error	0.159/ 0.120	0.100/ -0.010	0.540/ 0.506	0.250/ 0.224
Mean Error	-0.019/ -0.073	-0.067/ -0.120	-0.066/ -0.142	-0.225/ -0.287
Mean Absolute Error	0.065/ 0.091	0.085/ 0.120	0.258/ 0.296	0.241/ 0.303
Root Mean Square Error	0.081/ 0.105	0.118/ 0.146	0.318/ 0.359	0.291/ 0.346
Standard Deviation	0.079/ 0.076	0.097/ 0.084	0.313/ 0.333	0.186/ 0.196

Table 3.9: Statistical analysis of the benchmark set excitation energy deviations in eV of STEOM-CC, STEOM-D, NEVPT2 and CASPT2 from CC3 and from EOM-CCSDT-3 for singlet states. Only CC3 and EOM-CCSDT-3 states with T1≥87% are included in the analysis.

The distributions are shown below (Figures 3.8a and 3.8b).

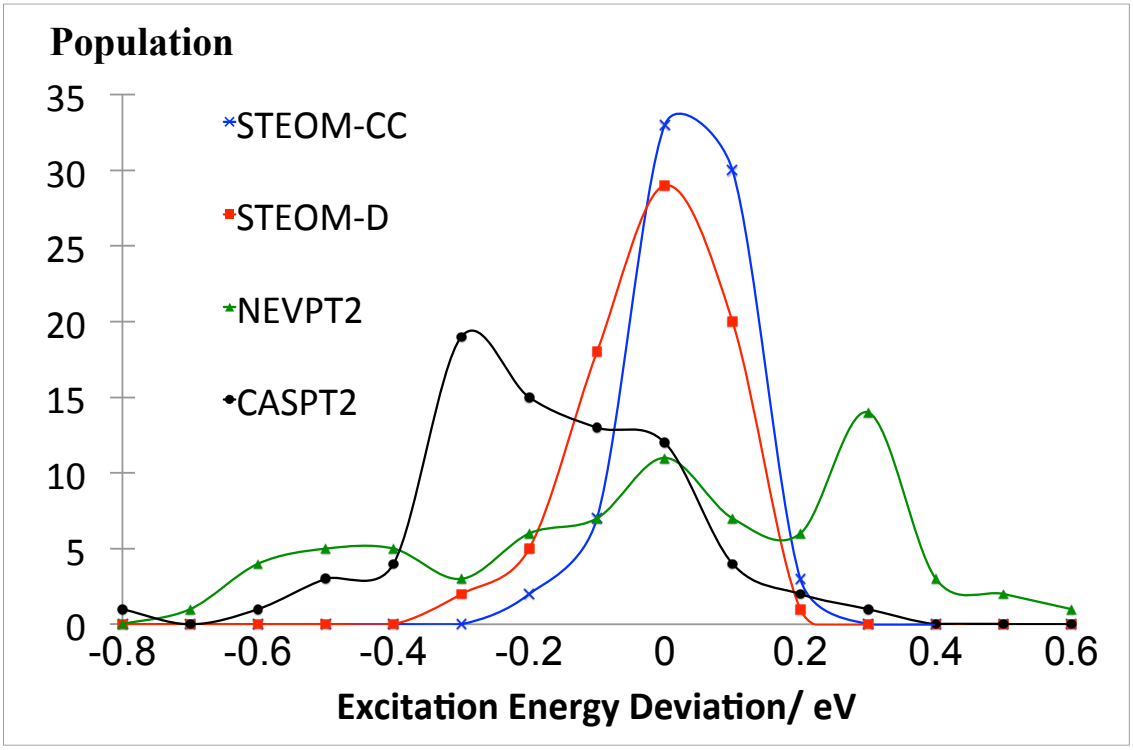

Figure 3.8a: Distribution of the benchmark set excitation energy deviations of STEOM-CC, STEOM-D, NEVPT2 and CASPT2 from CC3 for singlet states. Only CC3 states with T187% are included in the analysis. Bin size: 0.1.

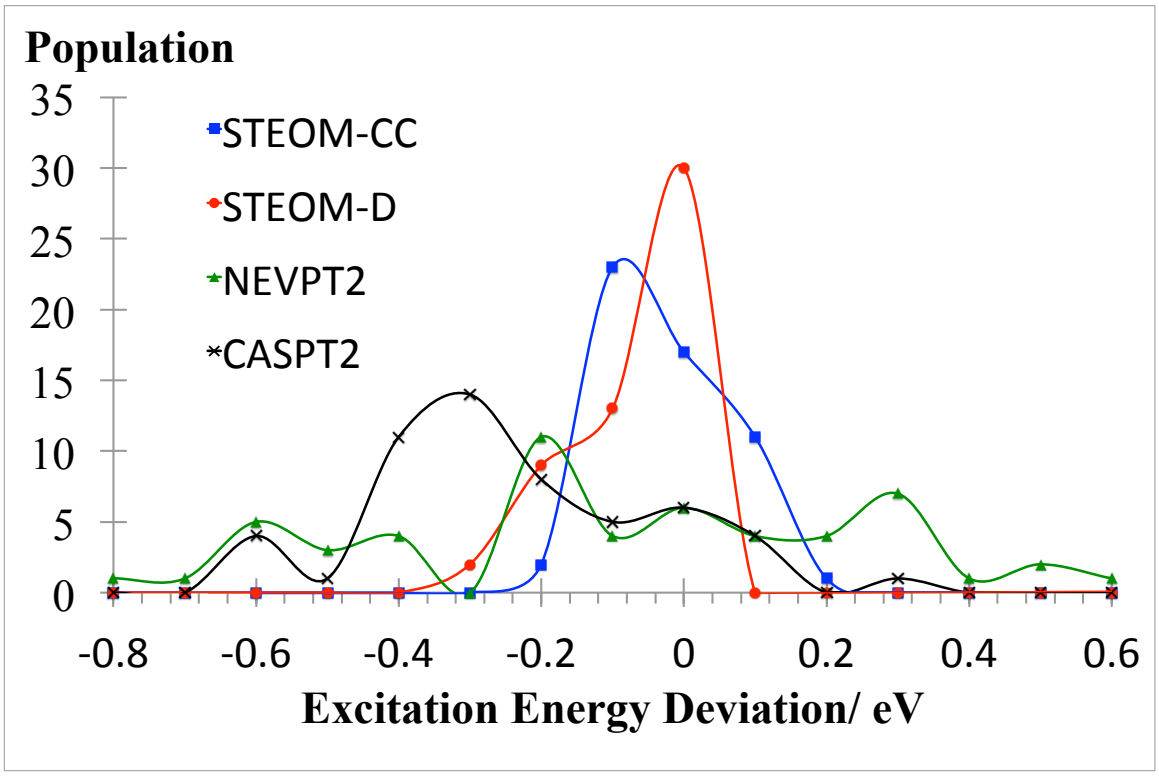

Figure 3.8b: Distribution of the benchmark set excitation energy deviations of STEOM-CC, STEOM-D, NEVPT2 and CASPT2 from EOM-CCSDT-3 for singlet states. Only EOM-CCSDT-3 states with T1≥87% are included in the analysis. Bin size: 0.1.

The plots and statistics show that STEOM-CC and STEOM-D are clearly superior to the reputable NEVPT2 and CASPT2 approaches when compared against CC3 and EOM-CCSDT-3. The statistical results show that STEOM-CC and STEOM-D are more accurate than NEVPT2 and CASPT2, while also the distributions show that there are generally less outliers for the STEOM methods compared to NEVPT2 and CASPT2.

It is not clear whether STEOM-D is an improvement over STEOM-CC.

III.B.6.2 Triplet Excitations

We present the results of the statistical analysis of the benchmarks of STEOM-CC, STEOM-D, NEVPT2 and CASPT2 compared to CC3 in Table 3.10 and plot curves for the distribution in Figure 3.9.

Statistics	STEOM-CC	EOM-CCSD	NEVPT2	CASPT2
Minimum Error	-0.662	-0.280	-0.820	-0.380
Maximum Error	0.256	0.510	0.370	0.120
Mean Error	-0.111	0.053	0.054	-0.031
Mean Absolute Error	0.156	0.114	0.170	0.075
Root Mean Square Error	0.201	0.156	0.221	0.112
Standard Deviation	0.169	0.148	0.216	0.108

Table 3.10: Statistical analysis of the benchmark set excitation energy deviations in eV of STEOM-CC, STEOM-D, NEVPT2 and CASPT2 from CC3 for triplet states.

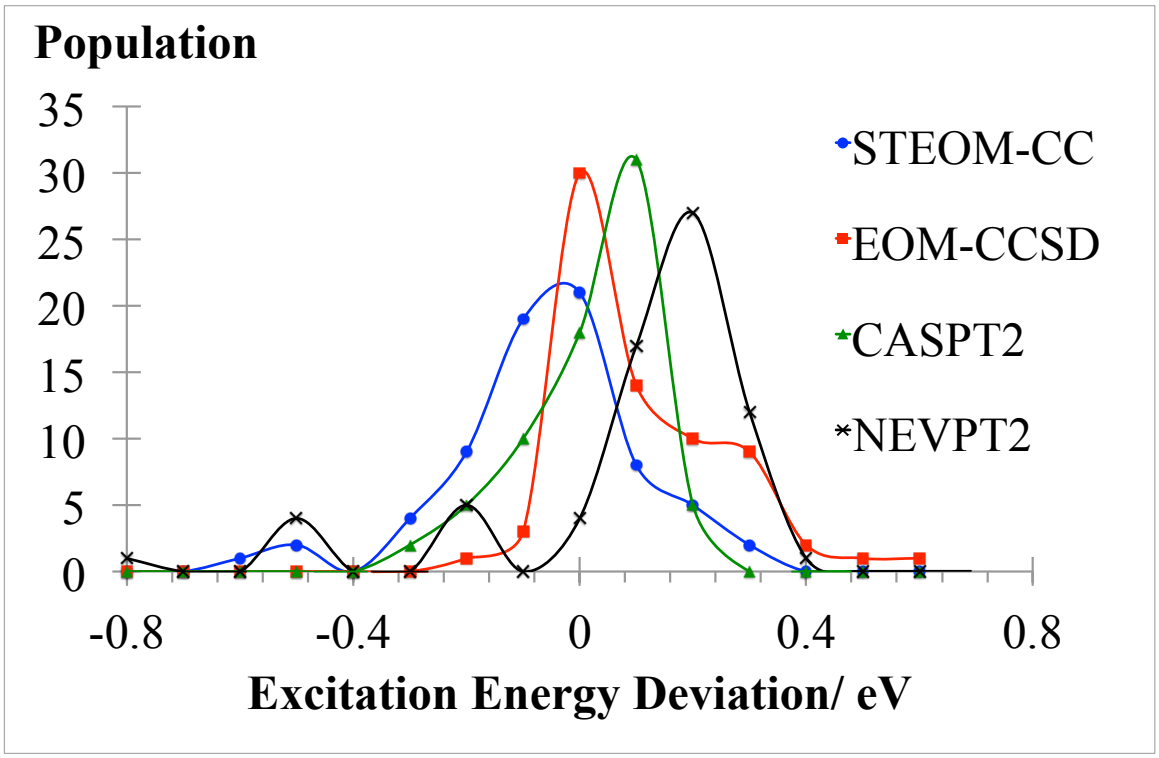

Figure 3.9: Distribution of the benchmark set excitation energy deviations of STEOM-CC, STEOM-D, NEVPT2 and CASPT2 from CC3 for triplet states. Bin size: 0.1.

The best method according to the distributions appear to be CASPT2 with all other methods in the plot slightly shifted to the right or to the left. STEOM-CC has a broader distribution, but is centered slightly below zero (around -0.1 eV). We hope that the STEOM-D approach can provide more accurate results for triplets. However, this is something we should attempt in the future.

III.B.7. Doubly Excited States

To study doubly excited states, we compare CC3 states and EOM-CCSDT-3 states with relatively low %T1 and the unbiased EXT-STEOM and NEVPT2 against CASPT2. We take the CC3 T1<80% as our diagnostic for the states that we can designate

as doubly excited and hence include in the statistical analysis. We present the results of the statistical analysis in Table 3.11.

Statistics	**CC3**	**EOM-CCSDT-3**	**EXT-STEOM**	**NEVPT2**
Minimum Error	-0.090	0.056	-0.392	-0.590
Maximum Error	0.450	0.693	0.893	0.430
Mean Error	0.206	0.403	0.299	0.136
Mean Absolute Error	0.223	0.403	0.420	0.221
Root Mean Square Error	0.255	0.439	0.476	0.261
Standard Deviation	0.155	0.179	0.380	0.229

Table 3.11: Statistical analysis of the benchmark set excitation energy deviations in eV of CC3, EOM-CCSDT-3, EXT-STEOM and NEVPT2 from CASPT2 for singlet states. Only states corresponding to T1<80% in CC3 are included in the analysis.

Below is the histogram analysis for the results represented as continuous curves (Figure 3.10).

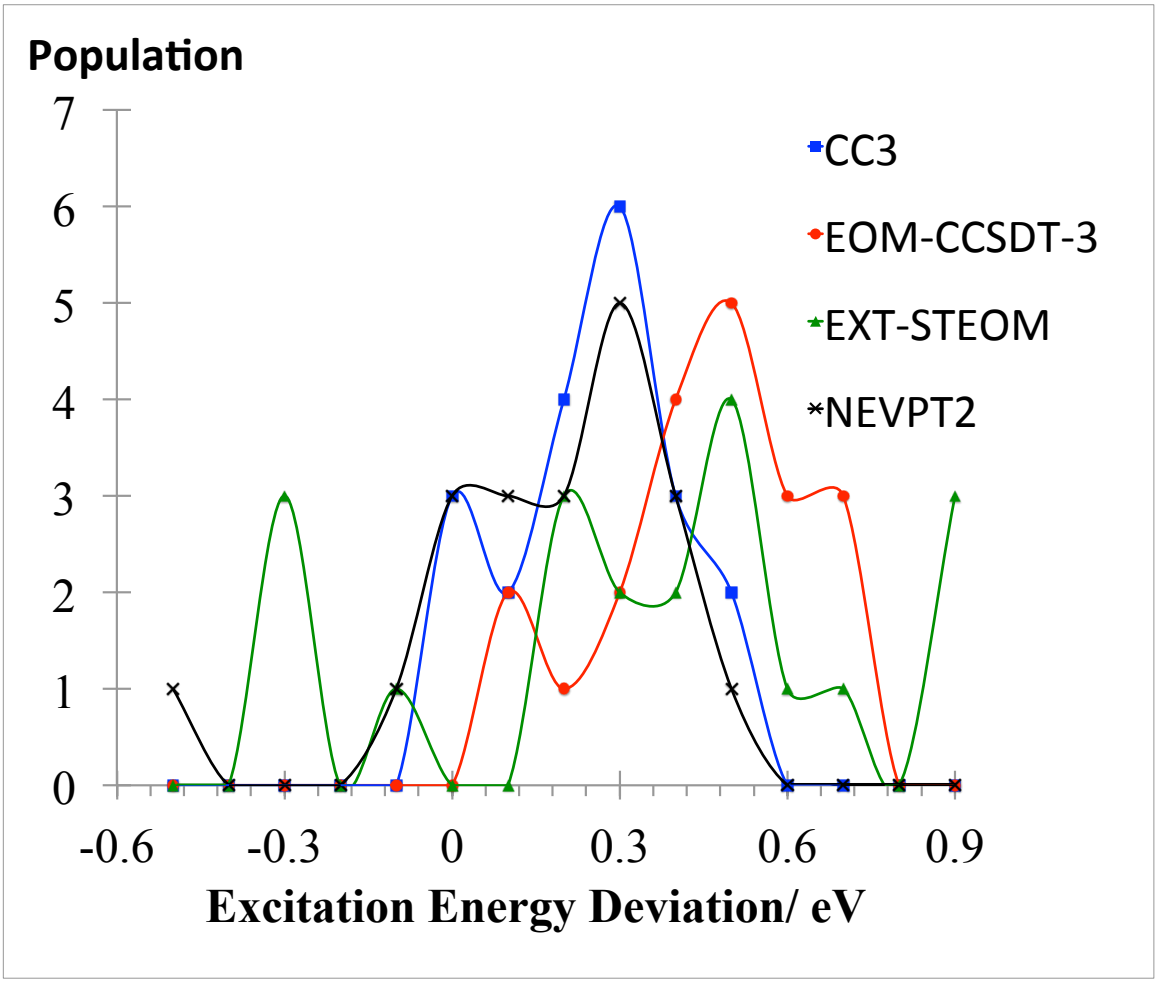

Figure 3.10: Distribution of the benchmark set excitation energy deviations of CC3, EOM-CCSDT-3, EXT-STEOM and NEVPT2 from CASPT2 for singlet states. Only states corresponding to CC3 T1<80% are included in the analysis. Bin size: 0.1.

We can see from the graph that CC3, EOM-CCSDT-3, EXT-STEOM, and NEVPT2 more or less follow a similar trend with two- or three-peaked distributions, while being increasing erratic in the order mentioned above. We should note that the CASPT2 approach itself is not a good reference for doubly excited states and therefore one of the few possible conclusions that can be drawn from the above results is that EXT-STEOM is not a much less accurate method than CC3, EOM-CCSDT-3 and NEVPT2 for doubly excited states. We realize that we should attempt a future benchmark against a method

suitable for doubly excited states to study the effectiveness of EXT-STEOM for such states.

IV. Concluding Remarks

The STEOM-CC approach and several of its variations have been applied to a large set of singly excited valence excited states of organic molecules. The STEOM-CC results for this large set of molecules demonstrates the robustness of the approach: while the approach in principle can break down for reasons discussed in section II, it has not for any of the states considered in this test set.

From the statistical analysis, it clearly transpires that STEOM-CC results are a significant improvement over EOM-CCSD, CASPT2, and NEVPT2 for singlet excited states. This conclusion does not hold for triplet excited states, however. The other approaches are clearly more accurate for triplets than for singlets, while STEOM can be more erratic for triplets and tends to be a bit less accurate for triplets than for singlets.

In this study only valence excited states are considered. For gas phase molecules Rydberg states are of considerable interest also. STEOM-CC and EOM-CCSD have an essential black box character that allows a convenient treatment of valence and Rydberg excited states. They are more cumbersome for CASPT2 and NEVPT2 as they require special selection of active spaces.

Regarding computational costs, STEOM-CC is clearly more cost-effective than EOM-CCSD. Compared to CASPT2 and NEVPT2 the comparison is more ambiguous. For

small active spaces CASPT2 and NEVPT2 are more efficient than canonical-orbital EOM-CC and STEOM-CC approaches. Recent advances in local correlation and pair natural orbital CC approaches may affect the balance. In this context STEOM-CC may have a particular advantage as the parent state CC, IP-EOM-CC and EA-EOM-CC all naturally localize. Only at the level of the final (CIS) diagonalization step does one lose localization.

In this chapter we reached some other clear conclusions. The STEOM-H (ω*) approach seems an interesting way to hermitize the transformed Hamiltonian, and is clearly superior over straightforward averaging of G and $G^{\dagger}$. It is quite satisfactory that STEOM does not sensitively depend on the precise definition of occupied and virtual orbitals as seen in section III.B.3. Replacing the CCSD step by MBPT(2) leads to significant errors, although this approach may be still of interest in practice.
The comparison between STEOM-D and STEOM-CC did not show a clear improvement due the perturbative doubles correction. This extension may not be worthwhile. The verdict is not unambiguous however. From the discussion in section III.B.5., it appears that a particular class of excitations involving 'double bond O' groups found in amides, ketones and aldehydes produce large errors (~ 0.2 eV in STEOM-D) and affects the statistics. Further investigations are desirable. Likewise the results from EXT-STEOM are disappointing. The approach provides a respectable description of doubly excited states, but is less accurate than STEOM-CC itself for states clearly dominated by singly excited states.

In the near future we plan to present a benchmarking study considering also Rydberg and charge-transfer excited states. The STEOM-CC approach is expected to describe all states about equally well, providing a balanced approach, while not being sensitive to complications due to valence-Rydberg mixing. Such a balanced description is more of a problem to EOM-CCSD, which is more accurate for Rydberg states. Likewise CASPT2 and NEVPT2 are more problematic. Therefore, STEOM-CC might be a very attractive alternative to these fully realistic molecules in the gas phase, in particular if combined with efficient local correlation approaches.

Chapter 4

The Vibronic Coupling Model: A Scheme Beyond the Born-Oppenheimer Approximation

I. Beyond the Born-Oppenheimer Approximation

The Born-Oppenheimer approximation, which makes the assumption that the relative velocity of the nuclei compared to the electrons is negligible, is a fundamental approach to predicting spectroscopy. The power of the Born-Oppenheimer approximation is that it implies that electronic and nuclear movements can be decoupled. This means that one can first solve the electronic problem for every nuclear configuration, Q (Q is a parameter), obtaining a point-wise single adiabatic potential energy surface for every electronic state and then solve for the nuclear problem. Molecular spectroscopy is often based on the Born-Oppenheimer approximation and the harmonic Franck-Condon approach, which is just using harmonic oscillators to fit excited state potential energy surfaces obtained after employing the Born-Oppenheimer approximation.

The Born-Oppenheimer approximation is sometimes inaccurate for predicting spectroscopy of polyatomic systems. The problem of polyatomics is that degeneracy of electronic states is common. This would be reflected as crossings in excited state potential energy surfaces leading to what is known as conical intersections [1]. The presence of conical intersections allows for a possibility of interesting dynamics, i.e. the system could evolve from one potential energy surface to another, thus resulting in a different chemical picture. Refer to Figure 4.1 below. In other words, the system can

undergo a rapid change in electronic character [2]. This is a result of the fact that electronic states are strongly coupled.

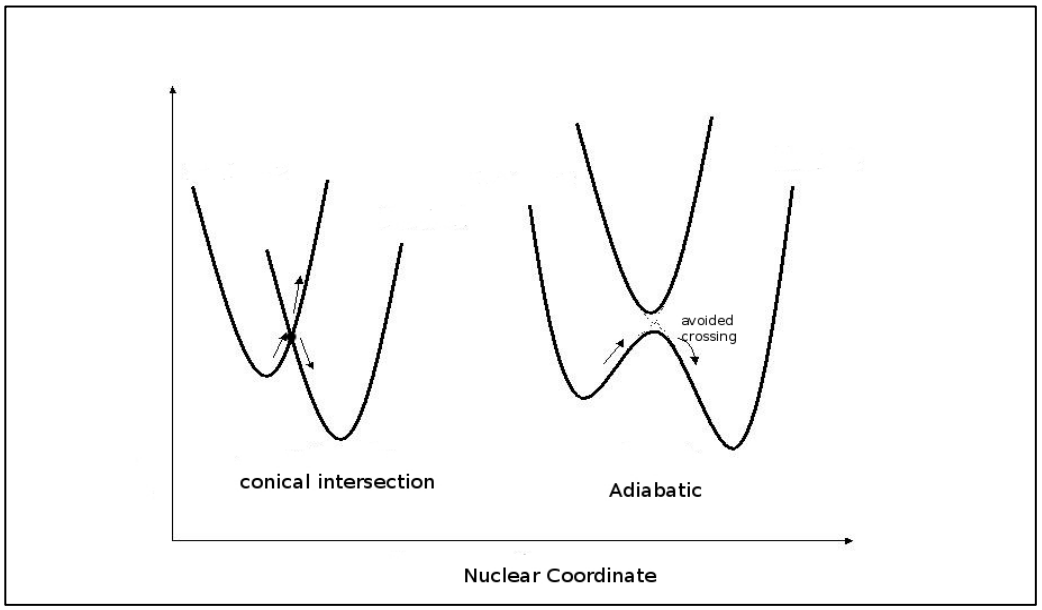

Figure 4.1: A diagrammatic representation of conical intersection and adiabatic energy surface

In the Nooijen group, spectroscopic simulations are mostly based on the vibronic (vibrational-electronic) model. This model goes beyond the Born-Oppenheimer approximation by including the coupling between different electronic states through the vibrational normal modes in the formalism of the Hamiltonian. The efficacy of the vibronic model is well established as shown by different research groups [3-5].

II. Construction of the Vibronic Model

The vibronic model Hamiltonian [6] in the adiabatic basis takes the form

$$\widehat{\mathrm{H}} = \widehat{\mathrm{T}}_{\mathrm{N}} + \mathbf{V}(\mathbf{Q}) - \widehat{\Lambda}\,, \tag{4.1}$$

where $\widehat{\mathrm{H}}$ is the full Hamiltonian, $\widehat{\mathrm{T}}_{\mathrm{N}}$ is the nuclear kinetic energy operator, $\mathbf{V}(\mathbf{Q})$ is the diagonal matrix of electronic energies i.e. $\mathbf{V}(\mathbf{Q}) = \mathrm{V_n}(\mathbf{Q})\delta_{\mathrm{nm}}$ and the nuclear displacement vector $\mathbf{Q} = (\mathcal{Q}_1, \mathcal{Q}_2, \ldots, \mathcal{Q}_{\mathrm{M}})$ in which n and m are label the adiabatic electronic states. $\widehat{\Lambda}$ is the non-adiabatic coupling operator and its matrix elements

$$\widehat{\Lambda}_{\mathrm{nm}} = \sum_{\mathrm{i}=1}^{\mathrm{M}} \mathrm{F}_{\mathrm{nm}}^{(\mathrm{i})} \frac{\partial}{\partial \mathcal{Q}_{\mathrm{i}}} - \mathrm{G}_{\mathrm{nm}}\,, \tag{4.2}$$

where the matrix $\mathbf{F}^{(\mathrm{i})}$ is anti-hermitian and the matrix $\mathbf{G}$ is hermitian. The forms of $\mathbf{F}^{(\mathrm{i})}$ and $\mathbf{G}$ will not be mentioned here for brevity. For a review of the formal derivation of the vibronic model Hamiltonian and its application in multimode molecular dynamics, an excellent review would be the one by Köppel, Domcke, and Cederbaum [6].

Without sinking in details of the forms of $\mathbf{F}^{(\mathrm{i})}$ and $\mathbf{G}$**,** it would suffice for our purpose to mention that $\widehat{\Lambda}_{\mathrm{nm}}$ contains an integral of the form $\int \phi_{\mathrm{m}}^{*}\, \nabla_{\mathbf{Q}} \phi_{\mathrm{n}} d\mathrm{r}$ where ϕ_{m} and ϕ_{n} are the electronic states m and n respectively, and r refers to electronic degrees of freedom [2]. In the adiabatic basis, for which $\widehat{\mathrm{T}}_{\mathrm{N}}$ and $\mathbf{V}(\mathbf{Q})$ diagonal but $\widehat{\Lambda}$ is not, it would be hard to evaluate $\widehat{\Lambda}_{\mathrm{nm}}$ because the adiabatic states undergo drastic changes in character near the regions of conical intersections [7] making it mathematically difficult to evaluate the partial differential with respect to $\mathbf{Q}$ with accuracy. Not only is evaluating those integrals tedious, but the solution to the nuclear Schrödinger equation also becomes considerably more complicated [6].

This motivated the quest for an adequate basis for which the partial differential with respect to $\mathbf{Q}$ tends to go to zero, thus avoiding any complications or technical difficulties. Such a basis is called a diabatic basis, denoted ψ. The diabatic states are electronic states that change little, preserve character, as a function of nuclear geometry. That is why $\int \psi_m^* \nabla_{\mathbf{Q}} \psi_n d\mathrm{r}$ is approximately zero and hence the non-adiabatic matrix elements, Λ_{nm} nearly vanish in the diabatic basis. Note that ψ refers to a diabatic state while ϕ refers to an adiabatic one. For more reading, please refer to the review by Worth and Cederbaum in which they discuss going beyond the Born-Oppenheimer approximation to solve for molecular dynamics through a conical intersection [8].

Computational schemes have been developed to solve for the diabatic states with least effort. This process is the so-called diabatization scheme [9]. In practice, one always solves for the adiabatic states and adiabatic energies at a particular $\mathbf{Q}$ in the electronic structure part of a calculation. Then, the diabatic states are defined as a linear combination of the solved adiabatic states, i.e.

$$\psi_a(\mathbf{r}, \mathbf{Q}) := \sum_n \phi_n(\mathbf{r}, \mathbf{Q}) U_{na}(\mathbf{Q}) \tag{4.3}$$

where the electronic displacement vector $\mathbf{r} = (r_1, r_2, \ldots, r_M)$, while $U_{na}(\mathbf{Q})$ defines a unitary matrix, $\mathbb{U}$. Note that a and n run over diabatic and adiabatic states, respectively. We then search for a unitary transformation, $\mathbb{U}$ such that the non-adiabatic coupling approaches zero as required. Note that we have some freedom in choosing $\mathbb{U}$ and thus the diabatic states are not unique.

If we find a particular $\mathbb{U}$, our problem reduces to the problem of solving a coupled set of differential equations for the vibrational wave functions, $\chi_a(\mathbf{Q})$. For example, for a system with two electronic states we have

$$\begin{pmatrix} T_N + V_{11}(\mathbf{Q}) & V_{12}(\mathbf{Q}) \\ V_{21}(\mathbf{Q}) & T_N + V_{22}(\mathbf{Q}) \end{pmatrix} \begin{pmatrix} \chi_1^{(\lambda)}(\mathbf{Q}) \\ \chi_2^{(\lambda)}(\mathbf{Q}) \end{pmatrix} = E_\lambda \begin{pmatrix} \chi_1^{(\lambda)}(\mathbf{Q}) \\ \chi_2^{(\lambda)}(\mathbf{Q}) \end{pmatrix} \tag{4.4}$$

Instead of a potential energy surface, we obtain a potential energy matrix $V_{ab}(\mathbf{Q})$ where a and b label the diabatic states, while λ in $\boldsymbol{\chi}^{(\lambda)}(\mathbf{Q}) = \begin{pmatrix} \chi_a^{(\lambda)}(\mathbf{Q}) \\ \chi_b^{(\lambda)}(\mathbf{Q}) \end{pmatrix}$ and E_λ, labels the final vibronic state of interest and its energy, respectively. Using $\mathbb{U}$, we relate $V_{ab}(\mathbf{Q})$ with $V_n(\mathbf{Q})$, the adiabatic potential energy surface as follows:

$$V_{ab}(\mathbf{Q}) = (\mathbb{U}^\dagger V_n(\mathbf{Q}) \mathbb{U})_{ab} \tag{4.5}$$

In practice, a Taylor series expansion of $V_{ab}(\mathbf{Q})$ along a set of normal modes [9] is employed:

$$V_{ab}(\mathbf{Q}) = V_{ab}(0) + \sum_k V_{ab}^k Q_k + \sum_{k,j} \frac{V_{ab}^{kj}}{2!} Q_k Q_j + \cdots$$
$$\forall a, b = 1, \ldots, N_e \tag{4.6}$$

where V_{ab}^k and V_{ab}^{kj} are expansion coefficients and N_e is the total number of electronic states.

In the ACES II program [10] used in the Nooijen group, solving the diabatization problem is fully automated. An outline of the parent algorithm employed in ACES II [9] is briefly discussed below:

1) Optimize the geometry of a parent state to get $\mathbf{Q}_0$, and then obtain vibrational frequencies and reference normal modes.
2) Calculate excited states at $\mathbf{Q}_0$: $|\phi_n(Q_k = 0)\rangle = |\phi_n^0\rangle$.
3) Make a small displacement along the normal mode $\mathbf{Q}_k$. Calculate the adiabatic excited states at geometry $\Delta\mathbf{Q}_k$: $|\phi_n(\Delta\mathbf{Q}_k)\rangle$. Evaluate the overlap matrix

$$S_{nm}(\Delta\mathbf{Q}_k) = \int \phi_n^0(\mathbf{r}, \mathbf{Q}_0)\phi_m(\mathbf{r}, \mathbf{Q}_0 + \Delta\mathbf{Q}_k) \tag{4.7}$$

at different geometries.

4) Find a unitary transformation for which $\sum_n S_{nm} U_{ma} \rightarrow \tilde{S}_{na}$ i.e. such that $\tilde{S}_{na}$ is diagonal.
5) This defines diabatic states $\psi_a(\mathbf{r}, \mathbf{Q}_0 + \Delta\mathbf{Q}_k) = \sum_n \phi_n(\mathbf{r}, \mathbf{Q}_0 + \Delta\mathbf{Q}_k)U_{na}$, which have maximum overlap with adiabatic states at $\mathbf{Q}_0$.
6) Use $U(\mathbf{Q}_0 + \Delta\mathbf{Q}_k)$ to obtain $\mathbb{U}^\dagger V(\mathbf{Q}_0 + \Delta\mathbf{Q}_k)\mathbb{U} = V_{ab}(\mathbf{Q}_0 + \Delta\mathbf{Q}_k)$. Take numerical derivatives $\frac{V_{ab}(\mathbf{Q}_0+\Delta\mathbf{Q}_k)-V_{ab}(\mathbf{Q}_0-\Delta\mathbf{Q}_k)}{2\Delta\mathbf{Q}_k} = V_{ab}^k$, the first order Taylor coefficient.
7) Do the same to get second and higher order coefficients.
   - Calculate: $|\phi_n(\Delta\mathbf{Q}_k)\rangle$, $S_{nm}(\Delta\mathbf{Q}_k)$.
   - Diabatize: U_{na}, $V_{ab}(\Delta\mathbf{Q}_k)$.
   - Calculate the finite difference numerical differential.

Once we calculate the Taylor series coefficients we can compute $V_{ab}(\mathbf{Q})$ at any $\mathbf{Q}$. We can then reconstruct the adiabatic potential energy surface through diagonalizing $V_{ab}(\mathbf{Q})$. The Taylor series can be truncated and thus the diabatic potentials $V_{ab}(\mathbf{Q})$ are smooth. Upon diagonalization, the Born-Oppenheimer surfaces can be very complicated, showing multiple conical intersections or avoided crossings. While the number of Taylor series coefficients is limited, complicated full potential surfaces are defined in a large dimensional space (3N-6), where N is the number of atoms in the molecule (3N-5 for linear molecules).

Based on the vibronic model Hamiltonian, we can calculate vibronic energy levels, absorption spectra and time-dependent wave functions. This is an aspect of the scheme that can be time-consuming. A number of approximations can be invoked. The most promising schemes to obtain spectra, or evolve the time-dependent Schrödinger equations, include the MultiConfiguration Time-Dependent Hartree (MCTDH) approach developed by Meyer et al. [11] and the Full Multiple Spawning (FMS) approach developed by Martinez et al. [12]. It is also interesting to use the numerically exact VIBRON approach developed in the Nooijen group for comparison with the MCTDH and FMS approaches, and to benchmark results.

Chapter 5

Derivation and Treatment of Approximate Spin-Orbit Coupling from Many-Body Relativistic Quantum Mechanics

I. Introduction

Spin–Orbit Coupling (SOC) is an effect that results from the interaction between the electron's intrinsic magnetic moment and its orbital angular momentum. SOC arises naturally as a relativistic effect in the Dirac equation [1].

SOC is a weak effect in light elements. Naively, one might therefore assume that SOC should be accounted for only if heavy elements are involved in a chemical reaction or in a spectral excitation. However, SOC turns out to be important in case of light elements too if two electronic states of different spin multiplicity are close in energy. In this case, although the coupling matrix element could be small, it serves to induce an efficient transition between the states. Such transitions are known as Intersystem Crossings (ISC) [2]. This is common in molecular processes involving electronically excited states. ISC is involved in biological processes such as photosynthesis [3]. Another effect due to SOC is observed in spectroscopy: the normally 'spin-forbidden' transitions become weakly allowed due to SOC [4]. An important example of spin-forbidden transitions due to SOC is phosphorescence [5].

Recognizing the importance of SOC in molecular applications, efforts are made to implement this effect in quantum mechanical calculations. SOC for one-electron systems can be derived from the Dirac equation. However, for many-electron systems the problem is not trivial and needs careful treatment. In this chapter, I will sketch the path to obtaining an approximate many-body quantum mechanical theory including SOC suitable for computational molecular applications. This work draws largely on the beautiful textbook "Relativistic Quantum Chemistry" written by Reiher and Wolf [6].

The structure of the chapter is as follows: first, the Dirac equation is presented and then the pathway to a many-body Dirac-like quantum mechanical theory suitable for practical calculations is drawn. Different approximation schemes like the no-pair approximation and the two-component approximation are discussed. SOC is presented in the essence of an approximate two-component many-body theory. A discussion of approximation techniques involving the use of mean-field theory to calculate SOC follows. The summary section refocuses the reader's attention on the emphasis of the whole chapter. Note that advanced concepts are mentioned in the context of the topic. An elementary discussion of such concepts is indicated whenever needed. For a more detailed discussion, please refer to the corresponding reference(s).

II. One-Electron Relativistic Quantum Mechanical Theory

As mentioned above, the most fundamental equation that accounts for SOC is the Dirac equation. The free electron Dirac equation [7] reads:

$$\underbrace{(c\vec{\boldsymbol{\alpha}}.\boldsymbol{p} + \beta m_e c^2)}_{H_{\mathrm{D}}}\Psi = i\hbar\frac{\partial}{\partial t}\Psi \tag{5.1}$$

In the above equation, H_{D} is the Dirac Hamiltonian, $\vec{\boldsymbol{\alpha}}$ and β are defined as follows: $\vec{\boldsymbol{\alpha}} = (\alpha_i) = (\alpha_1, \alpha_2, \alpha_3)$ where $\alpha_i = \begin{pmatrix} 0 & \boldsymbol{\sigma}_i \\ \boldsymbol{\sigma}_i & 0 \end{pmatrix}$ and $\beta = \begin{pmatrix} \mathbf{1} & 0 \\ 0 & -\mathbf{1} \end{pmatrix}$, while $\boldsymbol{\sigma}_i$ denote the 2×2 Pauli matrices. The wave function Ψ is a four-component spinor and all other symbols have their usual meaning.

Taking the non-relativistic limit of the Dirac equation and including higher order corrections (of order ${v^2}/{c^2}$) yields a non-relativistic Hamiltonian [8], which reads:

$$\begin{aligned} H = \frac{\boldsymbol{p}^2}{2m_e} + V(r) - \frac{\boldsymbol{p}^4}{8m_e^3c^2} + \frac{1}{2m_e^2c^2}\frac{1}{r}\frac{\mathrm{d}V}{\mathrm{d}r}\mathbf{L}\bullet\mathbf{S} \\ + \frac{\pi\hbar^2}{2m_e^2c^2}\left(\frac{Ze^2}{4\pi\varepsilon_0}\right)\delta(r) \end{aligned} \tag{5.2}$$

All symbols have their usual meaning. The third term on the right hand side of Eqn. 5.2 is the SOC term. Using that equation, one could satisfactorily account for SOC for one-electron systems.

III. Many-Electron Relativistic Quantum Mechanical Theory

The Dirac equation is a one-electron theory and hence is not directly useful to study molecular systems. There are few refinements required to the Dirac equation to make it suitable for molecular applications.

It is instructive to study two-electron systems to gain insight (see also the textbook by Bethe and Salpeter [9]). In a two-electron system, the *exact* total wave function $\Psi(ct_1, r_1, ct_2, r_2)$ can be expanded in terms of direct products $\psi_i(ct_1, r_1) \otimes \psi_j(ct_2, r_2)$. Each term in the wave function consists of '4⊗4=16' components.

If there was no interaction between the two electrons, that problem would be very easy and the Dirac Hamiltonian would be just the sum of one-electron operators, i.e. $H_{\mathrm{D}} = h_1^D + h_2^D$, where h_k^D is the one-electron Dirac operator ($k \in \{1,2\}$). Unfortunately, this is not the case as each electron generates an external electromagnetic field felt by the other electron.

To see the effect of an external field, we view the one-electron Dirac equation in an external field [6]:

$$\left[c\vec{\boldsymbol{\alpha}}.\boldsymbol{p} + \beta m_e c^2 + \underbrace{q_e\phi - q_e\vec{\boldsymbol{\alpha}}.\boldsymbol{A}}_{\equiv\hat{V}}\right]\Psi = i\hbar\frac{\partial}{\partial t}\Psi \qquad (5.3)$$

An electron in an external magnetic field would give rise to the electromagnetic interaction energy operator $\hat{V}$, which is defined as $\hat{V} \equiv q_e\phi - q_e\vec{\boldsymbol{\alpha}}.\boldsymbol{A}$, where ϕ is the scalar potential, $\boldsymbol{A}$ is the vector potential, $\boldsymbol{A} = (A^1, A^2, A^3)$ and $\nabla\times\boldsymbol{A} = \mathbf{B}$, where $\mathbf{B}$ is the magnetic field, and q_e is the electron's charge.

To solve the two-electron problem, we follow Reiher and Wolf [6] and use Eqn. 5.3 to make the following ansatz:

$$\left\{\left[-i\hbar\frac{\partial}{\partial t_1}+c\vec{\boldsymbol{\alpha}}_1.\left(\boldsymbol{p}_1-\frac{q_1}{c}\boldsymbol{A}^{(2)}\right)+\beta_1 m_e c^2+q_1\phi^{(2)}\right.\right.$$

$$\left.+V_{nuc}(r_1)\right]\otimes\mathbf{1}_4$$

$$+\mathbf{1}_4\otimes\left[-i\hbar\frac{\partial}{\partial t_2}+c\vec{\boldsymbol{\alpha}}_2.\left(\boldsymbol{p}_2-\frac{q_2}{c}\boldsymbol{A}^{(1)}\right)+\beta_2 m_e c^2+q_2\phi^{(1)}\right. \tag{5.4}$$

$$\left.\left.+V_{nuc}(r_2)\right]\right\}\Psi(ct_1,r_1,ct_2,r_2)=0$$

The external potential energy, V_{nuc} is added to the respective one-electron terms. In the above equation, vector and scalar potentials are felt by one electron and generated by the other, respectively. Note that we need not worry about relativistic effects due to nuclei as in molecular applications, we work in the clamped nuclei frame of reference and one does not need to worry about relativistic effects for slow-moving nuclei, thus the nuclear potential in that frame is simply the Coulomb potential [10].

Two problems arise and need to be addressed. First, how to deal with two time variables and, second, how are the scalar and vector potentials of the electrons to be chosen. To deal with the former problem, a single absolute time frame, $t_1, t_2 \rightarrow t$ of non-relativistic theory is adopted. This is not a well-founded approximation. It is more of an ad hoc approximation to solve the hindering problem of different time frames. The wave function now can be constructed from one-electron direct product states

$$\Psi(t,r_1,r_2)=\sum_{i,j}\psi_i(t,r_1)\otimes\psi_j(t,r_2)\,\mathrm{c}_{ij} \tag{5.5}$$

where c_{ij} are expansion coefficients. If we now use $\Psi(t, r_1, r_2)$ instead of $\Psi(ct_1, r_1, ct_2, r_2)$ in Eqn. 5.4 and adopt the absolute time frame t and rearrange, we get [6]

$$\begin{aligned}\left[c\vec{\boldsymbol{\alpha}}_1.\boldsymbol{p}_1 + c\vec{\boldsymbol{\alpha}}_2.\boldsymbol{p}_2 + \beta_1 m_e c^2 + \beta_2 m_e c^2 - q_1\vec{\boldsymbol{\alpha}}_1.\boldsymbol{A}^{(2)}\right. \\ - q_2\vec{\boldsymbol{\alpha}}_2.\boldsymbol{A}^{(1)} + q_1\phi^{(2)} + q_2\phi^{(1)} + V_{nuc}(r_1) \\ \left. + V_{nuc}(r_2)\right]\Psi(t, r_1, r_2) = i\hbar\frac{\partial}{\partial t}\Psi(t, r_1, r_2)\end{aligned} \tag{5.6}$$

The second problem was dealt with by Gaunt who derived (in an approximate fashion) an unretarded magnetic interaction operator known as the Gaunt operator [11]. He derived an operator which replaces $-q_1\vec{\boldsymbol{\alpha}}_1.\boldsymbol{A}^{(2)} - q_2\vec{\boldsymbol{\alpha}}_2.\boldsymbol{A}^{(1)} + q_1\phi^{(2)} + q_2\phi^{(1)}$ in Eqn. 5.6 by $\hat{V}_{12} = \frac{q_1 q_2}{r_{12}}(1 - \vec{\boldsymbol{\alpha}}_1\vec{\boldsymbol{\alpha}}_2)$, in which the first term is easily identified as the Coulomb operator and the second term is the Gaunt operator, $\mathrm{G}_0(1,2) = -q_1 q_2\frac{\vec{\boldsymbol{\alpha}}_1\vec{\boldsymbol{\alpha}}_2}{r_{12}}$, Eqn. 5.6 Now reads:

$$\begin{aligned}\left[c\vec{\boldsymbol{\alpha}}_1.\boldsymbol{p}_1 + c\vec{\boldsymbol{\alpha}}_2.\boldsymbol{p}_2 + \beta_1 m_e c^2 + \beta_2 m_e c^2 + \hat{V}_{12} + V_{nuc}(r_1)\right. \\ \left. + V_{nuc}(r_2)\right]\Psi(t, r_1, r_2) = i\hbar\frac{\partial}{\partial t}\Psi(t, r_1, r_2)\end{aligned} \tag{5.7}$$

Eqn. 5.7 includes relativistic effects due to unretarded instantaneous electromagnetic interactions. The interaction energy of two moving charges is, however, affected by the retarded electromagnetic fields due to finite speed of transmission. Breit derived a retardation term [12] that accounts for this problem. The retardation term is referred to as the retardation operator, $B_{\mathrm{ret.}}(1,2)$. It defines the Breit operator, $B_0(1,2) \equiv \mathrm{G}_0(1,2) + B_{\mathrm{ret.}}(1,2)$, which is explicitly

$$B_0(1,2) \equiv -\frac{q_1 q_2}{2}\left[\frac{\vec{\boldsymbol{\alpha}}_1 \vec{\boldsymbol{\alpha}}_2}{r_{12}} + \frac{(\vec{\boldsymbol{r}}_{12}.\vec{\boldsymbol{\alpha}}_1)(\vec{\boldsymbol{r}}_{12}.\vec{\boldsymbol{\alpha}}_2)}{r_{12}^3}\right] \tag{5.8}$$

The interaction energy $\hat{V}_{12}$, after this approximation, becomes: $\hat{V}_{12} \approx \frac{q_1 q_2}{r_{12}} - B_0(1,2)$.

Employing the Breit operator, the stationary quantum mechanical equation for two electrons in the central field of an atomic nucleus reads

$$\begin{aligned} &\Bigg\{ \underbrace{c(\vec{\boldsymbol{\alpha}}.\boldsymbol{p})_1 + \beta_1 m_e c^2 + V_{nuc}(r_1)}_{\equiv \hat{h}_1^D} \\ &+ \underbrace{c(\vec{\boldsymbol{\alpha}}.\boldsymbol{p})_2 + \beta_2 m_e + V_{nuc}(r_2)}_{\equiv \hat{h}_2^D} \\ &+ \underbrace{\frac{q_1 q_2}{r_{12}} - \frac{q_1 q_2}{2}\left[\frac{\vec{\boldsymbol{\alpha}}_1 \vec{\boldsymbol{\alpha}}_2}{r_{12}} + \frac{(\vec{\boldsymbol{r}}_{12}.\vec{\boldsymbol{\alpha}}_1)(\vec{\boldsymbol{r}}_{12}.\vec{\boldsymbol{\alpha}}_2)}{r_{12}^3}\right]}_{\approx \hat{V}_{12}} \Bigg\} \Psi(r_1, r_2) \\ &= E\Psi(r_1, r_2) \end{aligned} \tag{5.9}$$

It is important to highlight that the operator pair, $\vec{\boldsymbol{\alpha}}_1 \vec{\boldsymbol{\alpha}}_2$ represents a sum over tensor products:

$$\vec{\boldsymbol{\alpha}}_1 \vec{\boldsymbol{\alpha}}_2 = \sum_{i=1}^{3} \alpha_{1,i} \otimes \alpha_{2,i} \tag{5.10}$$

where the 4×4 matrices $\alpha_{1,i}$ and $\alpha_{2,i}$ must not be multiplied according to the rules of matrix multiplication, which is the reason why the central dot of the scalar product has been omitted. Instead, these operators act on the corresponding one-electron spinor functions (to see an example, refer to section 9.3.3 of reference [6]).

Despite these efforts, we still don't have a complete relativistically covariant theory as both the Coulomb and the Coulomb–Breit terms are not strictly Lorentz invariant. This problem is solved by a time-dependent perturbation theory approach in quantum electrodynamics to obtain a Lorentz invariant expression for the electron-electron interaction [13]. The resulting expression contains terms that depend on the frequency of the virtual photon or likewise on the one-particle energies of the electrons. Every two-electron integral has a different photon frequency. This makes the calculation of molecular integrals computationally expensive scaling with n^8 where n is the number of basis functions [10]. Thus, one can abandon the requirement for strict Lorentz invariance for the sake of computational efficiency and seek instead the use of approximate many-particle Hamiltonians like the one employed in Eqn. 5.9. Generalizing Eqn. 5.9, we get a Dirac-like equation for many-electron systems. Of course, quantum field theory seems to be the most rigorous approach to the many-body problem. However, there are problems associated with the use of quantum field theory for molecular systems. A brief discussion comes later in the context of the next section.

IV. No-Pair Approximation

A principle difficulty of using a Dirac-like equation for many-electron systems is the presence of negative energy one-particle spinors in the basis. Solving the problem numerically for atoms, for which relativistic effects are more prominent for example, $^{238}U^{2+}$, yields continuum solutions. The full solution never converges and we do not get bound states. This is referred to as the Brown-Ravenhall disease [14, 15]. This means that

there is a solution to each energy value and we don't get discrete excitations. The problem here is that the negative energy solutions mix in with the positive energy solutions giving a continuum. This implies that Eqn. 5.9 is not a correct physical equation because it does not give rise to physical solutions.

The reason for the failure of Eqn. 5.9 might be the ad hoc approximation of assuming a single absolute time frame, t of non-relativistic theory. The rigorous solution to this problem would be quantum field theory. However, this proves to be not very practical for computational purposes [16]. Another problem that arises when using quantum field theory is that the number of particles is not fixed which makes it cumbersome for studying molecular systems. We will thus refrain from working in two different time frames and will proceed in the single absolute time frame aiming to find other solutions to the Brown-Ravenhall disease.

A practical solution to this problem turns out to be the no-pair approximation [17], which is projecting the many-electron Dirac-like equation onto the positive energy states. To arrive at this approximation, we use a wave function ansatz:

$$\Psi(r_1, r_2, \dots, r_N) = |\psi_1(r_1)\psi_2(r_2) \dots \psi_N(r_N)| \tag{5.11}$$

Note that $|\psi_1(r_1)\psi_2(r_2) \dots \psi_N(r_N)|$ is shorthand notation for a single Slater determinant, which in the case of Eqn. 5.11, is a Slater determinant of spinors.

Our aim is to find a solution that satisfies our ansatz. To do so, we variationally optimize the energy expression

$$\left\langle \Psi(r_1, r_2, \dots, r_N) \middle| \left(\sum_i h_i^D + \sum_{j>i} \hat{V}_{ij} \right) \middle| \Psi(r_1, r_2, \dots, r_N) \right\rangle \tag{5.12}$$

In the above expression, $\left(\sum_i h_i^D + \sum_{j>i} \hat{V}_{ij}\right)$ comprises the many-electron Hamiltonian obtained by generalizing Eqn. 5.9 to many-electron systems, where h_i^D is the one-electron operator given by $h_i^D = \underbrace{c(\vec{\boldsymbol{\alpha}}.\boldsymbol{p})_i + \beta_i m_e c^2}_{\hat{T}_D} + V_{nuc}(r_i)$, in which $\hat{T}_D$ is the Dirac kinetic energy operator, and $\hat{V}_{ij}$ is the two-electron operator given by $\hat{V}_{ij} = \frac{q_i q_j}{r_{ij}} - \frac{q_i q_j}{2}\left[\frac{\vec{\alpha}_i \vec{\alpha}_j}{r_{ij}} + \frac{(\vec{r}_{ij}.\vec{\alpha}_i)(\vec{r}_{ij}.\vec{\alpha}_j)}{r_{ij}^3}\right]$. The Roman indices i, j are electron labels which run from 1 to N, i.e. $i, j \in \{1,2, \dots, N\}; j > i$.

This energy optimization problem could be dealt with using the Hartree-Fock self-consistent field approach, in which one introduces the so-called Fock operator that defines one-electron spinors [18], which at convergence satisfies

$$\hat{F}\psi_i(r_i) = \varepsilon_i \psi_i(r_i) \tag{5.13}$$

where $\hat{F}$ is the one-electron Fock operator, which has eigenfunctions $\psi_i(r_i)$, the one-electron spinors and eigenvalues ε_i with $i \in \{1,2, \dots, N\}$. Solving for the Dirac-like many-electron equation at the Hartree-Fock level of theory is referred to as the Dirac-Hartree-Fock procedure [6]. The goal of the Dirac-Hartree-Fock procedure is to produce a suitable set of one-electron spinors, which define a unique wave function, $\Psi(r_1, r_2, \dots, r_N)$.

The Hartree-Fock method is a powerful approximation method used to solve for the ground state energy and the ground state wave function of many-electron systems.

Realize however that the ansatz used in expression 5.11 is an approximation. The *exact* wave function is an expansion of direct products of spinors not a single Slater determinant. This is why we need to go beyond Hartree-Fock by including the so-called electron correlation effects [18], which are further corrections to the Hartree-Fock solutions.

In the electron correlation treatment to the Dirac-Hartree-Fock procedure, only spinors corresponding to positive energy solutions are retained and a second quantized Hamiltonian [18] is defined as follows:

$$\widehat{H}_{\text{no-pair}} = \sum_{i,j} \underbrace{\langle i|h^D(1)|j\rangle}_{h_{ij}^D(1)} \hat{a}_i{}^\dagger \hat{a}_j + \frac{1}{4} \sum_{i,j,k,l} \underbrace{\langle ij|V(2)|kl\rangle}_{V_{ijkl}(2)} \hat{a}_i{}^\dagger \hat{a}_j{}^\dagger \hat{a}_k \hat{a}_l \tag{5.14}$$

This Hamiltonian $\widehat{H}_{\text{no-pair}}$ is the no-pair Hamiltonian. It is the sum of one-electron terms, $\sum_{i,j} h_{ij}^D(1)$ and two-electron terms, $\sum_{i,j,k,l} V_{ijkl}(2)$. Note that $\hat{a}_i{}^\dagger$, $\hat{a}_j{}^\dagger$ are creation operators and $\hat{a}_k$, $\hat{a}_l$ are annihilation operators; i, j, k and l run over the one-particle spinors corresponding to positive energy solutions, produced from the Dirac-Hartree-Fock procedure. For our purposes it suffices to introduce Eqn. 5.14 without going through its derivation (for a complete derivation, in the non-relativistic case, please refer to reference [18]). We point out the fact that spin-orbit interaction effects are implicit in the no-pair formalism.

If instead of the no-pair Hamiltonian, one would retain a summation in Eqn. 5.14 over all spinors corresponding to positive and negative energy solutions, one would obtain the second quantized version of the many-body Hamiltonian analogue of Eqn. 5.9. This would give rise to the Brown-Ravenhall disease. The restriction to positive energy solutions resolves this problem. This is the no-pair approximation. It is a practical observation that the no-pair Hamiltonian yields excellent results in the context of molecular physics [17].

Note that the restriction to positive energy solutions is in principle a projection of the Fock space on the subspace corresponding to positive energy solutions. The subspace corresponding to negative energy solutions is orthogonal to the subspace corresponding to positive energy solutions and such projection will only retain the subspace corresponding to positive energy solutions. Note also that the inclusion of creation and annihilation operators in the formalism automatically ensures the antisymmetry of the wave function, as this is evident from the anti-commutation relations of annihilation operators.

The relativistic treatment of many-body systems using the mean-field approach simplifies the problem as the mean-field equation (Eqn. 5.14) turns out to be analogous to the mean-field equation for the non-relativistic many-body problem [6]. In conventional quantum mechanical programs, various approximations based on the no-pair Hamiltonian can be employed. It is also possible, for small systems, to employ exact diagonalization techniques. Solving using the mean-field approach (Eqn. 5.14) is computationally

expensive (not prohibitive), yet yields very good results [19]. A more computationally attractive approximation technique for solving the many-body problem is the two-component approximation.

V. Two-Component Approximation

One of the most computationally efficient techniques to solve for the relativistic many-body problem is employing a two-component formalism. This is usually done by applying the Foldy-Wouthuysen transformation [20] on the Breit equation (Eqn. 5.9). The derivation is quite tedious and is left out for brevity.

The Foldy-Wouthuysen transformation truncated at order $\frac{1}{c^2}$ leads to the following Breit-Pauli Hamiltonian, H_{BP} [21]:

$$H_{\mathrm{BP}} = \sum_i \left[\frac{\boldsymbol{p}_i{}^2}{2m_e} + V_{nuc}(i)\right] + \sum_i \sum_j \frac{e^2}{r_{ij}} - \sum_i \frac{\boldsymbol{p}_i{}^4}{8m_e^3c^2}$$
$$+ \frac{1}{2m^2c^2}\left[\sum_i \sum_\alpha \frac{Z_\alpha e^2}{r_{i\alpha}^3} \mathrm{l}_{i\alpha}.\hat{\mathbf{s}}_i \right. \tag{5.15}$$
$$\left. - \sum_i \sum_{j\neq i} \frac{e^2}{r_{ij}^3} \hat{\mathbf{l}}_{ij}.\left(\hat{\mathbf{s}}_i + 2\hat{\mathbf{s}}_j\right)\right]$$

In the above formula, $\hat{\mathbf{l}}$ and $\hat{\mathbf{s}}$ are spatial and spin angular momentum operators; $\hat{\mathbf{l}}_{i\alpha} \equiv (\mathbf{r}_i - \mathbf{R}_\alpha)\times\mathbf{p}_i$ and $\hat{\mathbf{l}}_{ij} \equiv \left(\mathbf{r}_i - \mathbf{r}_j\right)\times\mathbf{p}_i$, Roman and Greek subscripts refer to electrons and nuclei respectively and the other symbols have their usual meanings.

Recognize that SOC is explicit in the Breit-Pauli Hamiltonian, H_{BP}. The third term in Eqn. 5.15 is known as the Breit-Pauli spin-orbit Hamiltonian, H_{BP}^{SO}:

$$H_{\mathrm{BP}}^{SO} = \frac{1}{2m^2c^2}\left[\sum_i \sum_\alpha \frac{Z_\alpha e^2}{r_{i\alpha}^3} \mathrm{l}_{i\alpha}.\hat{\mathbf{s}}_i - \sum_i \sum_{j\neq i} \frac{e^2}{r_{ij}^3} \hat{\mathbf{l}}_{ij}.\left(\hat{\mathbf{s}}_i + 2\hat{\mathbf{s}}_j\right)\right] \equiv \sum_i H^{SO}(i) + \sum_{j\neq i} H^{SO}(i,j) \tag{5.16}$$

where, $H^{SO}(i)$ and $H^{SO}(i,j)$ refer to one- and two-electron operators respectively.

Comparing the two-component many-electron equation (Eqn. 5.15) with the two-component one-electron equation (Eqn. 5.2) is very instructive. We highlight one special issue: $\frac{1}{r}\frac{\mathrm{d}V}{\mathrm{d}r}$ in the SOC term of Eqn. 5.2 would give rise to a $\frac{1}{r^3}$ term for a Coulomb potential. This gives some intuition of the $\frac{1}{r_{i\alpha}^3}$ and $\frac{1}{r_{ij}^3}$ present in the Breit-Pauli spin-orbit Hamiltonian, H_{BP}^{SO} (Eqn. 5.16).

The advantage of adopting the two-component Breit-Pauli Hamiltonian, H_{BP}, is that it is easier to incorporate in existing electronic structure codes. Typically, the Breit-Pauli spin-orbit Hamiltonian, H_{BP}^{SO}, is treated as a perturbation and first-order degenerate perturbation theory is employed.

Note that in Eqn. 5.16, unlike the two-electron operator, $H^{SO}(i,j)$, the one-electron operator, $H^{SO}(i)$, has an explicit dependence on the nuclear charges, Z_α. This means that $H^{SO}(i)$ grows faster with nuclear charges than $H^{SO}(i,j)$, which only grows as a result of the increase in the electron density in the region close to the nuclei. Accordingly, one can approximate the two-electron terms. This is more convenient especially since evaluating them exactly is computationally expensive. An effective one-electron approach is often employed.

VI. **Atomic Mean-Field Integral (AMFI) Method**

Heß et al. [22] developed an approximation method for calculating the spin-orbit contribution. They define an effective one-electron approach by means of a mean-field approximation to the Breit-Pauli spin-orbit operator, H_{BP}^{SO}.

We follow the order in the paper by Heß et al. [22] by introducing the matrix element of the spin-orbit operator, $\mathcal{H}_{ij}^{SO}$, between a pair of Slater determinants differing by a single valence spin orbital excitation $i \to j$

$$\mathcal{H}_{ij}^{SO} = \langle i|H^{SO}(1)|j\rangle + \frac{1}{2}\sum_k n_k \{\langle ik|H^{SO}(1,2)|jk\rangle - \langle ik|H^{SO}(1,2)|kj\rangle - \langle ki|H^{SO}(1,2)|jk\rangle\} \tag{5.17}$$

where, $H^{SO}(1)$ and $H^{SO}(1,2)$ are taken in the Breit-Pauli form, i.e. $H^{SO}(i)$ and $H^{SO}(i,j)$. The occupation numbers n_k denote the occupancy of orbitals common to the

determinants in the bra and the ket. The derivation of Eqn. 5.17 involves the use of Slater rules (for a review on Slater rules, please refer to reference [18]).

More generally, suppose we have a determinant optimized in a mean-field calculation, and characterized by a one-particle density matrix D_{kl}, given by

$$D_{lk} = \sum_{a\ \mathrm{occ}} \mathrm{c}_{la}^{*}\mathrm{c}_{ka} \tag{5.18}$$

Where, c_{ka} is the expansion coefficient of orbital ψ_a in the basis $|k\rangle$, i.e. $|\psi_a\rangle = \sum_k |k\rangle \mathrm{c}_{ka}$. The density matrix is an ingredient in the Hartree-Fock equations (for details of the derivation of the density matrix in the Hartree-Fock equations, please refer to reference [18]).

The mean-field spin-orbit contribution then reads

$$\begin{aligned}\mathcal{H}_{ij}^{\text{mean-field}} = \langle i|H^{SO}(1)|j\rangle + \frac{1}{2}\sum_k\sum_l \{\langle ik|H^{SO}(1,2)|jl\rangle \\ -\langle ik|H^{SO}(1,2)|lj\rangle - \langle ki|H^{SO}(1,2)|jl\rangle\} D_{lk}\end{aligned} \tag{5.19}$$

This expression is reminiscent of the usual expression for the mean-field Hamiltonian (or Fock matrix) in the Hartree-Fock theory:

$$\begin{aligned}F_{ij}^{\text{mean-field}} = \langle i|H(1)|j\rangle \\ + \sum_k\sum_l \{\langle ik|H(1,2)|jl\rangle - \langle ik|H(1,2)|lj\rangle\} D_{lk}\end{aligned} \tag{5.20}$$

Note that the two-electron term in Eqn. 5.19 has one more term in the summation than the corresponding one in Eqn. 5.20. This stems from the fact that $H^{SO}(1,2)$ taken in the

Breit-Pauli form is not symmetric under the permutation of electron labels as follows from Eqn. 5.16.

An important feature of the mean-field approach is that the matrix elements of the two-electron term, along with the density matrix, are more or less the same for different excited states. Thus, the two-electron contribution can be considered to be a constant perturbation (which needs to be evaluated once), hence defining an effective one-electron operator.

Eliminating the two-electron contribution simplifies the exact diagonalization calculation significantly. However, to evaluate the mean-field contribution, one still has to evaluate all multi-center spin-orbit integrals. Owing to the presence of $\frac{1}{r^3}$ terms in H_{BP}^{SO}, one can-to a good approximation-set the multi-center integrals to zero and retain only one-center integrals centered on one atom. The exclusion of multi-center integrals in the calculation of the mean-field contribution is referred to as the Atomic Mean-Field Integral (AMFI) Method.

In the AMFI code, used in the computational framework, one replaces the density matrix D_{lk} by approximate atomic occupation numbers

$$D_{lk} = \bar{n}_k \delta_{lk} \tag{5.21}$$

reflecting spherical density around each atom and thus restricting the calculation to one-center integrals centered on one atom. Note that δ_{lk} is the Kronecker delta. This expression is more or less correct for the inner shell electrons in a molecule, which provide the largest contribution to the spin-orbit operator. At first sight, the

approximation appears to be severe. However, extensive testing of these methods for many molecular systems springs confidence that they serve as an adequate treatment of spin-orbit effects [23, 24].

VII. **Summary**

The Dirac equation (Eqn. 5.1) is a fundamental equation of nature describing the relativistic quantum mechanics of a one-particle system. Spin-orbit coupling is implicit in that equation and can be easily recognized by taking the non-relativistic limit of the Dirac equation (Eqn. 5.2).

For many-body systems, the fundamental theory of nature is quantum field theory. However, for molecular physics application, quantum field theory proves to be troublesome. A generalization of the one-particle Dirac equation to many-body systems is the alternative. For many-body systems, the presence of interaction energy between particle pairs makes the problem non-trivial. Gaunt and Breit contributed to this problem by deriving interaction energy terms that approximate relativistic electromagnetic effects, including retardation.

The use of the many-body relativistic Breit Hamiltonian (Eqn. 5.9), in which spin-orbit interaction effects are implicit, turns out to be problematic as it gives rise to the Brown-Ravenhall disease. Overcoming that difficulty is achieved by another approximation, the

no-pair approximation, which is accomplished by adopting second quantization after the Dirac-Hartree-Fock treatment and projecting onto the positive energy states.

Although successful, the no-pair approximation turns out to be computationally demanding and other computationally cost-effective approaches are pursued. A two-component approach is adopted and the Breit-Pauli Hamiltonian obtained by the Foldy-Wouthuysen transformation of the Breit Hamiltonian (Eqn. 5.9) is exploited. Spin-orbit coupling is explicit in the Breit-Pauli Hamiltonian and is referred to as the Breit-Pauli spin-orbit Hamiltonian (Eqn. 5.16), which can be treated as a perturbation. The two-component formalism is more convenient for electronic structure calculations as it is easier to incorporate in existing electronic structure codes.

The Breit-Pauli spin-orbit Hamiltonian contains one- and two-electron terms. The two-electron terms can be approximated by effective one-electron operators, which are defined by means of a mean-field approach (Eqn. 5.19). An additional approximation of computational effectiveness is the AMFI method (see Eqn. 5.21). The AMFI method relieves the burden of evaluating multi-centre two-electron spin-orbit integrals and one has to worry only about one-centre integrals, which can be easily evaluated. This technique proves to be successful for many molecular systems.
Developing methodologies to evaluate relativistic spin-orbit coupling effects is an active area of research in chemical physics. It will be fascinating to see what physical, mathematical and computational insights this may lead to.

Chapter 6

The Full Picture: Combining Electronic Structure with Vibronic Coupling and Spin-Orbit Coupling

In this chapter, the connection between electronic structure, vibronic coupling, and spin-orbit coupling is outlined. The intention is to motivate the reader to appreciate the usefulness of the three theoretical approaches in combining together a computational scheme that can investigate dynamics and spectroscopy of interesting molecular systems.

By calculating excited states in a set of displaced geometries and a suitable diabatization scheme, we can develop vibronic coupling models. This is "routinely" done in the Nooijen group. In this work one uses the various versions of EOM-CC and the interesting STEOM-CC to develop vibronic models for singlet and triplet (and maybe doublet) manifolds. In the near future, members of the group will include spin-orbit perturbation into the Hamiltonian, such that one can diagonalize

$$\langle \nu | \overline{H} + e^{-\hat{T}} H^{SO} e^{\hat{T}} | \chi \rangle, \tag{6.1}$$

where ν and χ run over both singlet and triplet states and H^{SO} is the Breit-Pauli SO operator (discussed in the chapter 5). The above matrix is for example of the size $10^6 \times 10^6$.

We can envision two versions of a vibronic Hamiltonian including, spin-orbit interaction:

a) $\mathbf{H}(\mathbf{Q}) = \hat{T}_N \mathbf{1} + \mathbf{V}(\mathbf{Q}) + \mathbf{H}^{SO}(\mathbf{Q} = 0)$

b) $\mathbf{H}(\mathbf{Q}) = \hat{T}_N \mathbf{1} + \mathbf{V}_{(H+SO)}(\mathbf{Q})$

In the above equations: $\mathbf{H}(\mathbf{Q})$ is the Hamiltonian evaluated within the diabatic states and $\mathbf{H}^{\mathrm{SO}}(\mathbf{Q}=0)$ is the Breit-Pauli SO operator evaluated within the EOM-CC framework at the equilibrium geometry $\mathbf{Q}=0$. The $\mathbf{H}^{\mathrm{SO}}(\mathbf{Q}=0)$ matrix is expected to be a good approximation for the $\mathbf{H}^{\mathrm{SO}}(\mathbf{Q})$ at different geometries, because the diabatic states change little. In contrast, $\mathbf{V}_{(\mathrm{H+SO})}(\mathbf{Q})$ is the matrix evaluated explicitly at all displacements $\mathbf{Q}$. Fine details of these models are yet to be worked out and tested.

Having obtained vibronic models at the EOM-CC level, and including spin-orbit coupling, we need to interface these models to VIBRON, MCTDH and FMS programs. This is to be followed by the final time-dependent simulations, which will describe the quantities of interest: for example the transition probability to move from the first singlet excited state, S_1, to the first triplet excited state, T_1. Such a transition is an example of Intersystem Crossing (ISC). For an illustration of ISC we refer the reader to Figure 6.1 below. Also using this scheme, one can simulate spin-forbidden transitions.

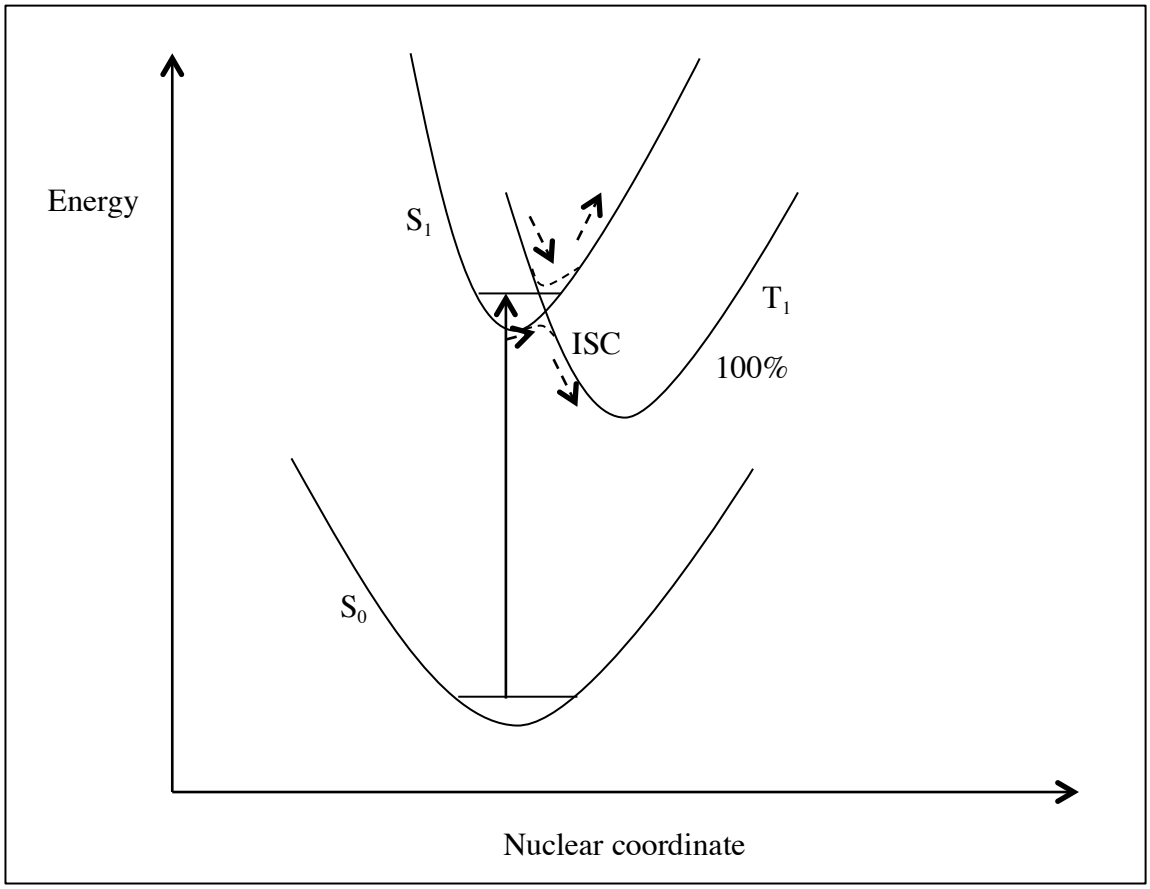

Figure 6.1: An excitation from S_0 to S_1, followed by transition from S_1 to T_1.
S_0 refers to the singlet ground state.
Dotted lines refer to intersystem crossings between S_1 and T_1.

References

Chapter 1

[1] L.M. Brown, in *Companion Encyclopedia of the History and Philosophy of the Mathematical Sciences*, edited by I Grattan-Guinness (Routledge, London, 1994), pp. 1252-1260.

[2] N. Taylor, *LASER: The inventor, the Nobel laureate, and the thirty-year patent war* (Simon & Schuster, New York, 2000).

[3] *November 17 – December 23, 1947: Invention of the First Transistor*, American Physical Society News (Volume 9, Number 10, November 2000).

[4] P. Kapitza, Nature **141**, 74 (1938).

[5] J.F. Allen and A.D. Misener, Nature **142**, 643 (1938).

[6] P.F. Dahl, *Superconductivity, Its Historical Roots and Development from Mercury to the Ceramic Oxides* (American Institute of Physics, New York, 1992).

Chapter 2

[1] J. Čížek, J. Chem. Phys. **45**, 4256 (1966).

[2] I. Shavitt and R.J. Bartlett, *Many Body Methods in Chemistry and Physics: MBPT and Coupled-Cluster Theory*, Cambridge Molecular Science (Cambridge University Press, New York, 2009).

[3] R.J. Bartlett and M. Musial, Rev. Mod. Phys. **79**, 291 (2007).

[4] T.D. Crawford and H.F. Schaefer III, in *An Introduction to Coupled Cluster Theory for Computational Chemists*, edited by B. Lipkowitz and D.B. Boyd (Wiley-VCH, New York, 2000), Vol. 14, pp. 33–136.

[5] R.M. Dreizler and E.K.U Gross, *Density Functional Theory: An Approach to the Quantum Many-Body Problem* (Springer-Verlag, Berlin, 1990).

[6] R.G. Parr and W. Yang, *Density Functional Theory of Atoms and Molecules* (Oxford University Press, New York, 1989).

[7] M. Nooijen, Adv. Quantum Chem. **56**, 181 (2009).

[8] A.C. Hurley, *Electron Correltation in Small Molecules* (Academic Press, London, 1976).

[9] J.A. Pople, R. Krishnan, H.B. Schlegel, and J.S. Binkley, Int. J. Quantum Chem. Symp. **14**, 545 (1978).

[10] R.J. Bartlett and G.D. Purvis, Int. J. Quantum Chem. **14**, 561 (1978).

[11] A. Szabo and N.S. Ostlund, *Modern Quantum Chemistry: Introduction to Advanced Electronic Structure Theory* (Dover Publications, New York, 1996).

[12] K. Raghavachari, G.W. Trucks, J.A. Pople, and M. Head-Gordon, Chem. Phys. Lett. **157**, 479 (1989)

[13] K. Emrich, Nucl. Phys. A **351**, 379 (1981).

[14] H. Sekino and R.J. Bartlett, Int. J. Quantum Chem., Quantum Chem. Symp. **18**, 255 (1984).

[15] D.C. Comeau and R.J. Bartlett, Chem. Phys. Lett. **207**, 414 (1993).

[16] J.F. Stanton and R.J. Bartlett, J. Chem. Phys. **98**, 7029 (1993).

[17] E. R. Davidson, J. Comput. Phys. **17**, 87 (1975).

[18] P. Pulay, Chem. Phys. Lett. **100**, 151 (1983).

[19] S. Saebo and P. Pulay, Chem. Phys. Lett. **113**, 13 (1985).

[20] C. Hampel and H.-J. Werner, J. Chem. Phys. **104**, 6286 (1996).

[21] M. Schütz and H.-J.Werner, J. Chem. Phys. **114**, 661 (2001).

[22] G. Rauhut and H.-J.Werner, Phys. Chem. Chem. Phys. **3**, 4853 (2001).

[23] P.E. Maslen, A.D. Dutoi, M.S. Lee, Y.H. Shao, and M. Head-Gordon, Mol. Phys. **103**, 425 (2005).

[24] J.E. Subotnik, A. Sodt, and M. Head-Gordon, J. Chem. Phys. **128**, 034103 (2008).

[25] W. Klopper, F.R. Manby, S. Ten-No, and E.F. Valeev, Int. Rev. Phys. Chem. **25**, 427 (2006).

[26] T. Shiozaki, S. Hirata, and E.F. Valeev, Ann. Rev. Comput. Chem. **5**, 131 (2010).

[27] D.P. Tew, C. Hättig, R.A. Bachorz and W. Klopper, in *Recent Progress in Coupled Cluster Methods*, edited by P. Čársky, J. Paldus and J. Pittner (Springer-Verlag, Berlin, 2010), pp. 535-572.

[28] H.-J. Werner, T.B. Adler, G. Knizia and F.R. Manby, in *Recent Progress in Coupled Cluster Methods*, edited by P. Čársky, J. Paldus and J. Pittner, Eds.; (Springer-Verlag, Berlin, 2010), pp. 573-620.

[29] L. Kong , F.A. Bischoff, and E.F. Valeev, Chem. Rev. **112** (1),75 (2012).

[30] F. Neese, F. Wennmohs, and A. Hansen, J. Chem. Phys. **130**, 114108 (2009).

[31] F. Neese, A. Hansen, and D.G. Liakos, J. Chem. Phys. **131**, 064103 (2009).

[32] C. Riplinger and F. Neese, J. Chem. Phys. **138**, 034106 (2013).

[33] J. Yang, Y. Kurashige, F.R. Manby, G.K.-L. Chan, J. Chem. Phys. **134**, 044123 (2011).

Chapter 3

[1] I. Shavitt and R.J. Bartlett, *Many Body Methods in Chemistry and Physics: MBPT and Coupled-Cluster Theory*, Cambridge Molecular Science (Cambridge University Press, New York, 2009).

[2] R.J. Bartlett and M. Musial, Rev. Mod. Phys. **79**, 291 (2007).

[3] T.D. Crawford and H.F. Schaefer III, in *An Introduction to Coupled Cluster Theory for Computational Chemists*, edited by B. Lipkowitz and D.B. Boyd (Wiley-VCH, New York, 2000), Vol. 14, pp. 33–136.

[4] A. Tajti, P.G. Szalay, A.G. Csaszar, M. Kallay, J. Gauss, E.F. Valeev, B.A. Flowers, J. Vazquez, and J.F. Stanton, J. Chem. Phys. **121**, 11599 (2004).

[5] F. Pawlowski, A. Halkier, P. Jørgensen, K.L. Bak, T. Helgaker, and W. Klopper, J. Chem. Phys. **118**, 2539 (2003).

[6] Y. Alexeev, T.L. Windus, C.G. Zhan, and D.A. Dixon, Int. J. Quantum Chem. **104**, 379 (2005).

[7] K. Raghavachari, G.W. Trucks, J.A. Pople, and M. Head-Gordon, Chem. Phys. Lett. **157**, 479 (1989)

[8] P. Pulay, Chem. Phys. Lett. **100**, 151 (1983).

[9] S. Saebo and P. Pulay, Chem. Phys. Lett. **113**, 13 (1985).

[10] C. Hampel and H.-J. Werner, J. Chem. Phys. **104**, 6286 (1996).

[11] M. Schütz and H.-J.Werner, J. Chem. Phys. **114**, 661 (2001).

[12] G. Rauhut and H.-J.Werner, Phys. Chem. Chem. Phys. **3**, 4853 (2001).

[13] P.E. Maslen, A.D. Dutoi, M.S. Lee, Y.H. Shao, and M. Head-Gordon, Mol. Phys. **103**, 425 (2005).

[14] J.E. Subotnik, A. Sodt, and M. Head-Gordon, J. Chem. Phys. **128**, 034103 (2008).

[15] W. Klopper, F.R. Manby, S. Ten-No, and E.F. Valeev, Int. Rev. Phys. Chem. **25**, 427 (2006).

[16] T. Shiozaki, S. Hirata, and E.F. Valeev, Ann. Rev. Comput. Chem. **5**, 131 (2010).

[17] D.P. Tew, C. Hättig, R.A. Bachorz and W. Klopper, in *Recent Progress in Coupled Cluster Methods*, edited by P. Čársky, J. Paldus and J. Pittner (Springer-Verlag, Berlin, 2010), pp. 535-572.

[18] H.-J. Werner, T.B. Adler, G. Knizia and F.R. Manby, in *Recent Progress in Coupled Cluster Methods*, edited by P. Čársky, J. Paldus and J. Pittner, Eds.; (Springer-Verlag, Berlin, 2010), pp. 573-620.

[19] L. Kong , F.A. Bischoff, and E.F. Valeev, Chem. Rev. **112** (1),75 (2012).

[20] F. Neese, F. Wennmohs, and A. Hansen, J. Chem. Phys. **130**, 114108 (2009).

[21] F. Neese, A. Hansen, and D.G. Liakos, J. Chem. Phys. **131**, 064103 (2009).

[22] C. Riplinger and F. Neese, J. Chem. Phys. **138**, 034106 (2013).

[23] J. Yang, Y. Kurashige, F.R. Manby, and G.K.-L. Chan, J. Chem. Phys. **134**, 044123 (2011).

[24] J. Geertsen, M. Rittby, and R.J. Bartlett, Chem. Phys. Lett. **164**, 57 (1989).

[25] M. Nooijen and R.J. Bartlett, J. Chem. Phys. **102**, 6735 (1995).

[26] D. Mukhopadhyay, S. Mukhopadhyay, R. Chaudhuri, and D. Mukherjee, Theor. Chim. Acta **80**, 441 (1991).

[27] J.F. Stanton and R.J. Bartlett, J. Chem. Phys. **98**, 7029 (1993).

[28] M. Nooijen and R.J. Bartlett, J. Chem. Phys. **102**, 3629 (1995).

[29] K.W. Sattelmeyer, H.F. Schaefer III, and J.F. Stanton, Chem. Phys. Lett. **378**, 42 (2003).

[30] H.J. Monkhorst, Int. J. Quantum Chem. **S 11**, 421 (1977).

[31] D. Mukherjee and P.K. Mukherjee, Chem. Phys. **39**, 325 (1979).

[32] H. Koch and P. Jørgensen, J. Chem. Phys. **93**, 3333 (1990).

[33] H. Nakatsuji and K. Hirao, J. Chem. Phys. **68**, 2053 (1978).

[34] H. Nakatsuji, Chem. Phys. Lett. **67**, 329 (1979).

[35] H. Koch, O. Christiansen, P. Jørgensen, A.M. Sanchez de Mers, and T. Helgaker, J. Chem. Phys. **106**, 1808 (1997).

[36] J.D. Watts and R.J. Bartlett, Chem. Phys. Lett. **258**, 581 (1996).

[37] J.D. Watts and R.J. Bartlett, Chem. Phys. Lett. **233**, 81 (1995).

[38] T. Watson, V. Lotrich, P. Szalay, A. Perera, and R.J. Bartlett, J. Phys. Chem. A **117** (12), 2569 (2013).

[39] J. Shen and P. Piecuch, Chem. Phys. **401**, 180 (2012).

[40] J. Shen and P. Piecuch, J. Chem. Phys. **136**, 144104 (2012).

[41] K. Kowalski and P. Piecuch, J. Chem. Phys. **113**, 18 (2000).

[42] J.R. Gour, P. Piecuch, and M. Włoch, J. Chem. Phys. **123**,134113 (2005).

[43] M. Valiev, E.J. Bylaska, N. Govind, K. Kowalski, T.P. Straatsma, H.J.J. Van Dam, D. Wang, J. Nieplocha, E. Apra, T.L. Windus, W.A. de Jong, "NWChem: a comprehensive and scalable open-source solution for large scale molecular simulations" Comput. Phys. Commun. **181**, 1477 (2010).

[44] V. Lotrich, N. Flocke, M. Ponton, A. Yau, A. Perera, E. Deumens, and R.J. Bartlett, J. Chem. Phys. **128**, 194104 (2008).

[45] D.P. Tew and C. Hättig, Int. J. Quantum Chem.**113**, 224 (2013).

[46] D.P. Tew, B. Helmich, and C. Hättig, J. Chem. Phys. **135**, 074107 (2011).

[47] M. Nooijen and R.J. Bartlett, J. Chem. Phys. **106**, 6441 (1997).

[48] M. Nooijen and R.J. Bartlett, J. Chem. Phys. **106**, 6449 (1997).

[49] M. Nooijen and R.J. Bartlett, J. Chem. Phys. **107**, 6812 (1997).

[50] M. Nooijen, Spectrochimica Acta A **55**, 539 (1999).

[51] I. Lindgren, Int. J. Quantum Chem., Symp. **12**, 33 (1978).

[52] I. Lindgren and D. Mukherjee, Phys. Rep. **151**, 93 (1987).

[53] D. Mukherjee and S. Pal, Adv. Quantum Chem. **20**, 291 (1989).

[54] B. Jeziorski and J. Paldus, J. Chem. Phys. **90**, 2714 (1989).

[55] K. Jankowski, J. Paldus, I. Grabowski, and K. Kowalski, J. Chem. Phys. **97**, 7600 (1992).

[56] U. Kaldor, Theor. Chim. Acta **80**, 427 (1991).

[57] K. Jankowski and P. Malinowski, J. Phys. B **27**, 829 (1994).

[58] L.Z. Stolarczyk and H.J. Monkhorst, Phys. Rev. A **32**, 725 (1985).

[59] G.C. Wick, Phys. Rev. **80**, 268 (1950).

[60] D. Mukherjee, Chem. Phys. Lett. **274**, 561 (1997).

[61] W. Kutzelnigg and D. Mukherjee, J. Chem. Phys. **107**, 432 (1997).

[62] L.G. Kong, M. Nooijen, and D. Mukherjee, J. Chem. Phys. **132**, 234107 (2010).

[63] D. Sinha, R. Maitra, and D. Mukherjee, Computational and Theoretical Chemistry, **1003**, 62 (2013).

[64] T. Yanai and G.K.-L. Chan, J. Chem. Phys. **124**, 194106 (2006).

[65] T. Yanai and G.K.-L. Chan, J. Chem. Phys. **127**, 104107 (2007).

[66] E. Neuscamman, T. Yanai, and G.K.-L. Chan, J. Chem. Phys. **132**, 024106 (2010).

[67] D.A. Mazziotti, Phys. Rev. Lett. **97**, 143002 (2006).

[68] D.A. Mazziotti, Phys. Rev. A **75**, 022505 (2007).

[69] M. Hanauer and A. Köhn, J. Chem. Phys. **134**, 204111 (2011).

[70] M. Hanauer and A. Köhn J. Chem. Phys. **136**, 204107 (2012).

[71] D. Datta, L. Kong, and M. Nooijen, J. Chem. Phys. **134**, 214116 (2011).

[72] O. Demel, D. Datta, and M. Nooijen, J. Chem. Phys. **138**, 134108 (2013).

[73] M. Nooijen and R.J. Bartlett, J. Chem. Phys. **104**, 2652 (1996).

[74] M. Wladyslawski and M. Nooijen, Adv. Quantum Chem. **49**, 1 (2005).

[75] M. Nooijen, K.R. Shamasundar, and D. Mukherjee, Mol. Phys. **103**, 2277 (2005).

[76] K. Andersson, P.-Å. Malmqvist, B.O. Roos, A.J. Sadlej, and K. Wolinski, J. Phys. Chem. **94**, 5483 (1990).

[77] K. Andersson, P.-Å. Malmqvist, and B.O. Roos, J. Chem. Phys. **96**, 1218 (1992).

[78] B.O. Roos, K. Andersson, M.P. Fülscher, P.-Å. Malmqvist, L. Serrano-Andrés, K. Pierloot and M. Merchán, in *Advances in Chemical Physics: New Methods in Computational Quantum Mechanics*, edited by I. Prigogine and S.A. Rice (Wiley, New York, 1996), Vol. XCIII, pp. 219–331.

[79] C. Angeli, R. Cimiraglia, S. Evangelisti, T. Leininger, and J.P. Malrieu, J. Chem. Phys. **114**, 10252 (2001).

[80] C. Angeli, R. Cimiraglia, and J.P. Malrieu, Chem. Phys. Lett. **350**, 297 (2001).

[81] C. Angeli and R. Cimiraglia, Theor. Chem. Acc. **107**, 313 (2002).

[82] C. Angeli, R. Cimiraglia, and J.P. Malrieu, J. Chem. Phys. **117**, 9138 (2002).

[83] J.F. Stanton, J. Gauss, J.D. Watts, W. Lauderdale, and R.J. Bartlett (1996) ACES II, an ab initio program system, incorporating the MOLECULE vectorized molecular integral program by Almlöf, J., and Taylor, P.R., and a modified version of the ABACUS integral derivative package by T. Helgaker, H.J.Aa. Jensen, P. Jørgensen, J. Olsen, and P.R. Taylor.

[84] M.E. Casida, *Recent Developments and Applications of Modern Density Functional Theory, Theoretical and Computational Chemistry*, edited by J. M. Seminario (Elsevier, Amsterdam, 1996), pp. 391–439.

[85] M.E. Casida, J. Mol. Struct. (THEOCHEM) **914**, 3 (2009).

[86] A.A. Korkin, M. Nooijen, and R.J. Bartlett, J. Phys. Chem. A **102** 1837 (1998).

[87] D.S. Peterka, M. Ahmed, A.G. Suits, K.J. Wilson, A. Korkin, N. Nooijen, and R.J. Bartlett, J. Chem. Phys. **110**, 6095 (1999).

[88] M. Wladyslawski and M. Nooijen, The photoelectron spectrum of the NO3 radical revisited: A theoretical investigation of potential energy surfaces and conical intersections, *ACS Symposium Series*, Vol. 828 (2002), pp. 65–92.

[89] M. Tobita, S.S. Perera, M. Musiał, R.J. Bartlett, M. Nooijen, and J.S. Lee, J. Chem. Phys. **119**, 10713 (2003).

[90] M. Nooijen and V. Lotrich, J. Chem. Phys. **113**, 494 (2000).

[91] M. Nooijen, J. Phys. Chem. A **104**, 4553 (2000).

[92] S.R. Gwaltney, R.J. Bartlett, and M. Nooijen, J. Chem. Phys. **111**, 58 (1999).

[93] M. Schreiber, M.R. Silva-Junior, S.P. Sauer, and W. Thiel, J. Chem. Phys. **128**, 134110 (2008).

[94] M.R. Silva-Junior, M. Schreiber, S.P. Sauer, and W. Thiel, J. Chem. Phys. **129**, 104103 (2008).

[95] M.R. Silva-Junior, M. Schreiber, S.P. Sauer, and W. Thiel, J. Chem. Phys. **133**, 174318 (2010).

[96] I. Schapiro , K. Sivalingam , and F. Neese, J. Chem. Theory Comput. DOI: 10.1021/ct400136y.

[97] M. Nooijen, J. Chem. Phys. **104**, 2638 (1996).

[98] L. Meissner, J. Chem. Phys. **108**, 9227 (1998).

[99] M. Musial and R.J. Bartlett, J. Chem. Phys. **129**, 044101 (2008).

[100] M. Musial and R.J. Bartlett, J. Chem. Phys. **135**, 044121 (2011).

[101] W.J. Hehre, L. Radom, P.v.R. Schleyer and J.A. Pople, *Ab Initio Molecular Orbital Theory* (Wiley, New York, 1986).

[102] M.J. Frisch et al., Gaussian 03, Revision C.02, (Gaussian, Inc., Wallingford, CT, 2004).

[103] A. Schäfer, H. Horn, and R. Ahlrichs, J. Chem. Phys. **97**, 2571 (1992).

[104] CFOUR, a quantum chemical program package written by J.F. Stanton, J. Gauss, M.E. Harding, P.G. Szalay with contributions from A.A. Auer, R.J. Bartlett, U. Benedikt, C. Berger, D.E. Bernholdt, Y.J. Bomble, L. Cheng, O. Christiansen, M. Heckert, O. Heun, C. Huber, T.-C. Jagau, D. Jonsson, J. Jusélius, K. Klein, W.J. Lauderdale, D.A. Matthews, T. Metzroth, L.A. Mück, D.P. O'Neill, D.R. Price, E. Prochnow, C. Puzzarini, K. Ruud, F. Schiffmann, W. Schwalbach, S. Stopkowicz, A. Tajti, J. Vázquez, F. Wang, J.D. Watts and the integral packages MOLECULE (J. Almlöf and P.R. Taylor), PROPS

(P.R. Taylor), ABACUS (T. Helgaker, H.J. Aa. Jensen, P. Jørgensen, and J. Olsen), and ECP routines by A.V. Mitin and C. van Wüllen.

[105] O. Christiansen, H. Koch, and P. Jørgensen, J. Chem. Phys. **103**, 7429 (1995).

[106] K. Kowalski and P. Piecuch, J. Chem. Phys. **115**, 643 (2001).

[107] S.A. Kucharski, M. Włoch, M. Musiał, and R.J. Bartlett, J. Chem. Phys. **115** 8263 (2001).

[108] S.R. Gwaltney, M. Nooijen, and R.J. Bartlett, Chem. Phys. Lett. **248**, 189 (1996).

Chapter 4

[1] D.R. Yarkony, Rev. Mod. Phys. **68**, 985 (1996).

[2] H.H. Chang, Undergraduate Thesis: *From Electronic Structure Theory to Molecular Spectroscopy* (2003).

[3] L.S. Cederbaum, W. Domcke, H. Köppel, and W. Von Niessen, Chem. Phys. **26**, 169 (1977).

[4] A.H. Schroeder and S. Mazur, J. Am. Chem. Soc. **100**, 7339 (1978).

[5] A. Hjortsberg, B. Nygren, J. Vallin, and F.S. Ham, Phys. Rev. Lett. **39**, 1233 (1977).

[6] H. Köppel, W. Domcke, and L.S. Cederbaum, Adv. Chem. Phys. **57**, 59 (1984).

[7] E. Teller, J. Phys. Chem. **41**, 109 (1937).

[8] G.A. Worth and L.S. Cederbaum, Ann. Rev. Phys. Chem. **55**, 127 (2004).

[9] M. Nooijen, Int. J. Quantum Chem. 95, 768 (2003).

[10] J.F. Stanton, J. Gauss, J.D. Watts, W. Lauderdale, and R.J. Bartlett (1996) ACES II, an ab initio program system, incorporating the MOLECULE vectorized molecular

integral program by Almlöf, J., and Taylor, P.R., and a modified version of the ABACUS integral derivative package by T. Helgaker, H.J.Aa. Jensen, P. Jørgensen, J. Olsen, and P.R. Taylor.

[11] H.-D. Meyer, U. Manthe, and L.S. Cederbaum, Chem. Phys. Lett. **165**, 73 (1990).

[12] T.J. Martinez, M. Ben-Nun, and R.D. Levine, J. Phys. Chem. **100**, 7884 (1996).

Chapter 5

[1] C. Cohen-Tannoudji, B. Diu and F. Laloë, *Quantum Mechanics*, Volume II (John Wiley & Sons, New York, 2006).

[2] C.M. Marian, Comput. Mol. Sci. **2**, 187 (2012).

[3] M.K. Brown, Chem. Phys. Lett. **48**, 17 (1977).

[4] N.J. Turro, *Modern Molecular Photochemistry* (University Science Books, Sausalito, 1991).

[5] T. Engel and P. Reid, *Thermodynamics, Statistical Thermodynamics & Kinetics* (Pearson, Essex, 2013).

[6] M. Reiher and A. Wolf, *Relativistic Quantum Chemistry* (Wiley-VCH, Weinheim, 2009).

[7] P.A.M. Dirac, Proc. Roy. Soc. A **117**, 610 (1928).

[8] B.H. Brandsen and C.J. Joachain, *Quantum Mechanics* (Prentice Hall, Essex, 2000).

[9] H.A. Bethe and E.E. Salpeter, *Quantum Mechanics of One- and Two- Electron Atoms* (Dover Publications, New York, 2008).

[10] K.G. Dyal and K. Fægri Jr., *Introduction to Relativistic Quantum Chemistry* (Oxford University Press, New York, 2007).

[11] A. Gaunt, Phil. Trans. R. Soc. A **228**, 151 (1929).

[12] G. Breit, Phys. Rev. **34**, 553 (1929).

[13] V.B. Beresteskii, E.M. Lifshitz and L.P. Pitaevski, *Quantum Electrodynamics* (Pergamon Press, Oxford, 1982).

[14] G.E. Brown, D.G. Ravenhall, Proc. R. Soc. Lond. A **208**, 552 (1951).

[15] M. Nooijen, Can. J. Chem. **87**, 1499 (2009).

[16] I. Lindgren, *Relativistic Many-Body Theory: A New-Field Theoretical Approach* (Springer, New York, 2011).

[17] J. Sucher, Phys. Rev. A **22**, 348 (1980).

[18] A. Szabo and N.S. Ostlund, *Modern Quantum Chemistry: Introduction to Advanced Electronic Structure Theory* (Dover Publications, New York, 1996).

[19] L. Visscher, E. Eliav, and U. Kaldor, J. Chem. Phys. **115**, 9720 (2001).

[20] L.L. Foldy and S.A. Wouthuysen, Phys. Rev. **78**, 29 (1950).

[21] R.E. Moss, *Advanced Molecular Quantum Mechanics* (Chapman & Hall, London, 1973).

[22] B.A. Heß, C.M. Marian, U. Wahlgren, and O. Gropen, Chem. Phys. Lett. **251**, 365 (1996).

[23] B. Schimmelpfennig, L. Maron, U. Wahlgren, C. Teichteil, H. Fagerli, and O. Gropen, Chem. Phys. Lett. **286**, 261 (1998).

[24] F. Neese, J. Chem. Phys. **122**, 034107 (2005).